The Dissertation Committee for Xianzhe Wang Certifies that this is the approved version of the following dissertation:

The adenylate cyclase toxin as a target for antibody therapeutics and vaccination against whooping cough

Committee:

Jennifer A. Maynard, Supervisor

George Georgiou

Shelley M. Payne

Adrian T. Keatinge-Clay

Lauren I. R. Ehrlich

The adenylate cyclase toxin as a target for antibody therapeutics and vaccination against whooping cough

by

Xianzhe Wang, B.S.

Dissertation

Presented to the Faculty of the Graduate School of

The University of Texas at Austin

in Partial Fulfillment

of the Requirements

for the Degree of

Doctor of Philosophy

The University of Texas at Austin

August 2015

Dedication

I dedicate this work to my parents who have always been caring and supportive throughout my life and during my graduate studies.

Acknowledgements

I would like to thank my advisor Dr. Jennifer Maynard who has always been supportive, encouraging, enlightening, and optimistic during my graduate study.

I thank my committee members Dr. George Georgiou, Dr. Shelley Payne, Dr. Adrian Keatinge-Clay, and Dr. Lauren Ehrlich for their helpful comments and suggestions. I also thank past and current lab members for help in various ways. Special thanks to Dr. Kevin Entzminger for discussion on various lab techniques, Dr. Zach Frye for help with structural and bioinformatic analysis, Dr. Annalee Nguyen for discussion of techniques and ideas, and undergraduate researcher Brennan Hodgson for data collection.

The adenylate cyclase toxin as a target for antibody therapeutics and vaccination against whooping cough

Xianzhe Wang, Ph.D

The University of Texas at Austin, 2015

Supervisor: Jennifer A. Maynard

Whooping cough, also known as pertussis, is caused by the bacterium *Bordetella pertussis*. Since widespread vaccination with heat-killed whole cell vaccines (wP) in the 1950s, the number of cases dropped dramatically. However, there has been a consistent resurgence in the past two decades, coinciding with the switch from wP vaccines to acellular vaccines (aP). US CDC estimates 16 million cases and 195,000 deaths worldwide per year. Accumulating evidence show that aP vaccines provide short protection against the symptoms but not against subclinical infection and transmission of the disease. Changing the adjuvant to induce more protective immunity or inclusion of additional protective antigens are some of the strategies to improve the efficacy of aP vaccines.

Adenylate cyclase toxin (ACT) is a 177 kDa protein produced by *B. pertussis* and related species. ACT mainly targets leukocytes through $\alpha_M\beta_2$ integrin and translocates its N-terminal cyclase domain into the cytosol, generating supraphysiological level of cAMP. Studies have shown that ACT-deficient stains are less pathogenic and passive immunization with polyclonal antibodies or active immunization with ACT protected mice against bacterial challenges. However, ACT is not included in any of the current aP

vaccines, due to a lack of understanding of its protective epitopes and its poor solubility and stability.

We aimed to identify potent neutralizing antibodies (nAbs) as therapeutic candidates, and map their epitopes to guide the design of vaccine antigen overcoming the solubility and stability issues. Two nAbs, M2B10 and M1H5, were discovered from antibody phage display libraries from ACT-immunized mice. They bind non-overlapping conformational epitopes in the C-terminal RTX domain of ACT. Our data suggest their mode of action is interrupting the interaction between the toxin and its cellular receptor.

On the other hand, individual domains of ACT were expressed in *E. coli* and purified. The catalytic and RTX domains retained antigenicity but are biophysically superior to full-length ACT. We further showed that the RTX domain elicited similar level of neutralizing antibody response to ACT in mice.

These antibodies, together with those neutralizing other major *B. pertussis* toxins, may constitute a therapy for severe pertussis infection, and the epitopes provide the basis for structure-based antigen design for superior stability and immunogenicity.

Table of Contents

List of Tables

List of Figures

Chapter 1: Introduction and background

1.1 WHOOPING COUGH

Whooping cough is a highly infectious disease caused primarily by the bacterium *Bordetella pertussis*, which is a Gram-negative, fastidious aerobic coccobacillus of the genus *Bordetella*. *B. pertussis* only infects human, especially infants and children, and remains one of the leading causes of death in children [1]. Three classical symptoms are paroxysmal cough, post-cough vomiting, and inspiratory whoop. In recent years, more and more adolescents and adults have been reported to be infected, but their symptoms are much less severe and sometimes even asymptomatic. They might serve as carriers and transmit the disease to children who are more susceptible with potentially fatal consequences [2].

One strain of *Bordetella parapertussis* also causes whooping cough in human, while another strain infects sheep only, with no transmission between the two hosts. *Bordetella bronchiseptica* infects a wide range of mammals, and rarely human. Genomic analysis of the three species indicates that *B. pertussis* and *B. parapertussis* independently evolved from a common *B. bronchiseptica*-like ancestor through large-scale gene loss and inactivation [3, 4]. Whole-cell or acellular pertussis vaccines confer little protection against *B. bronchiseptica* infection [5].

While whooping cough incidence has dropped dramatically since the initiation of widespread vaccination programs using killed *B. pertussis* bacteria in the 1950s, in recent years rates have rebounded dramatically, reaching a 60-year high in the US in 2012 (Figure 1.1) [6-8]. This trend is especially troubling for unimmunized infants, who are most susceptible to the disease and exhibit the highest rates of morbidity and mortality. Modified vaccination strategies, including booster immunization of adolescents, adults

Chapter 1 is based on previous publication: **Wang, X.**, V.W. Coljee, and J.A. Maynard, *Back to the future: recombinant polyclonal antibody therapeutics.* **Curr Opin Chem Eng**, 2013. **2**(4): p. 405-415. All authors contributed to writing and editing of the manuscript

and pregnant women, have been implemented to reduce transmission to neonates.

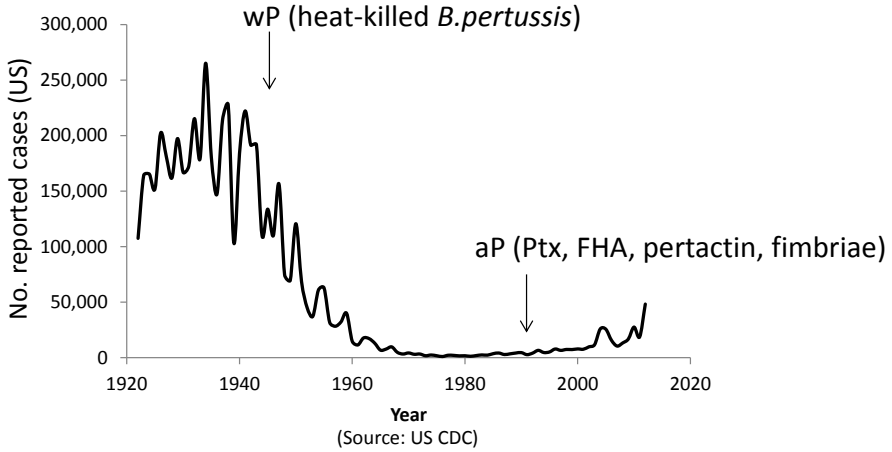

Figure 1.1: Resurgence of pertussis.

After the widespread vaccinations with heat- killed *B. pertussis* whole cell vaccines (wP) in the 1950s, pertussis cases dropped dramatically. In the 1990s, acellular vaccines, consisting of one to four protein antigens, replaced the reactogenic wP vaccines. Since then, there is a consistent resurgence of pertussis.

This increase in disease incidence coincides with the switch from whole cell to acellular vaccines in the 1990s, and has been attributed to several factors, including increased awareness, mismatch between vaccine and circulating strains, a Th1/ Th2 immune response instead of the more effective Th1 response and a shorter duration of protection conferred by acellular vaccines [9]. Recently, Warfel *et al.* demonstrated that acellular vaccines protect against disease symptoms but not subclinical infection and transmission in a novel non-human primate model [10]. Taken together, these data provide a compelling argument for modification of the current vaccine.

B. pertussis produces a number of adhesins, including filamentous hemagglutinin (FHA), pertactin (PRN), fimbriae; and toxins, including pertussis toxin (PT), adenylate cyclase toxin (ACT), tracheal cytotoxin (TCT), heat-labile toxin, and lipopolysaccharide

(LPS) or lipooligosaccharid (LOS) [8]. The adhesins and toxins help the bacteria to adhere to host cells and intoxicate the immune cells, leading to successful colonization in the host and evasion of the host innate and adaptive immune responses. The symptoms of whooping cough are caused by the toxins instead of bacterial invasion. Therefore, treatment with antibiotics after the catarrhal phase does not change the course of the disease. It is still not clear which toxin(s) contribute(s) to the cough symptom, and there is no serological correlation of protection (e.g. antibody titers for specific antigens or epitopes) [11-13].

Currently licensed acellular vaccines contain chemically detoxified pertussis toxin (PT) and up to four surface adhesins, including filamentous hemagglutinin, pertactin and fimbriae 2/3. Exciting approaches in development to enhance vaccine-mediated protective immunity include a genetically attenuated *B. pertussis* for intranasal delivery [14], nanoparticle formulations including purified antigens and novel adjuvant formulations [15], as well as inclusion of additional highly conserved protective antigens in the current vaccine [16, 17].

1.2 ADENYLATE CYCLASE TOXIN

A strong candidate for inclusion in the acellular vaccines is the adenylate cyclase toxin (ACT), which aids in immune evasion and is produced by three closely related *Bordetella* species, including *B. pertussis*, *B. parapertussis*, and *B. bronchiseptica*.

ACT-deficient *Bordetella* strains have shown significantly compromised colonization and reduced persistence in various mouse models [18-20], while some hypervirulent strains express higher ACT levels [21]. Moreover, active or passive immunization with polyclonal anti-ACT antibodies protected mice against lethal respiratory challenges by *B. pertussis* and *B. parapertussis* [21] and shortened the period

of bacterial colonization in the respiratory tract [22]. Finally, natural infection of humans results in a strong anti-ACT antibody response [23].

ACT is a large ~177 kDa protein consisting of two functionally discrete regions: the catalytic domain (residues 1-385), and a pore-forming or hemolysin region which is part of the larger repeat in toxin (RTX) family, represented in >250 bacterial strains (Figure 1.2). After translocation into the cytosol, the catalytic domain binds eukaryotic calmodulin with low nanomolar affinity [24] and rapidly converts available ATP to cAMP via its adenylate cyclase activity [25]. The resulting supraphysiological cAMP levels disrupt signaling and bactericidal activities in phagocytic cells [26-28]. The C-terminal ~1300 residues exhibit homology to the *E. coli* α-hemolysin. This region consists of a hydrophobic domain capable of forming a cation-selective transmembrane channel (residues 525-715) [29], a modification region bearing two acylation sites at residues Lys860 and Lys983 [30], the RTX domain (residues 1006-1600), consisting of ~40 calcium binding sites formed by glycine- and aspartate-rich nonapeptide repeats and finally, a C-terminal secretion signal (1600-1706). The RTX region also harbors the receptor-binding site, with specificity for the $\alpha_M\beta_2$ integrin (also called CR3, Mac-1 and CD11b/CD18) present on phagocytic leukocytes [31, 32]. Both post-translational acylation by the co-expressed enzyme CyaC and calcium ion-mediated structural changes are essential for receptor binding, cAMP intoxication and pore-forming activities [30, 33].

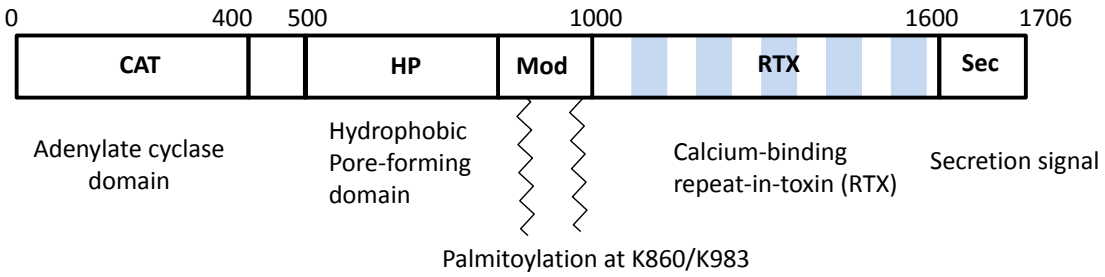

Figure 1.2: Adenylate cyclase toxin domain architecture.

ACT is a 177kDa protein toxin, consisting of five sequential domains: the catalytically active N-terminal adenylate cyclase (CAT) domain, the central hydrophobic (HP) domain, modification (Mod) region carrying two acylation sites K860 and K983, the C-terminal repeat-in-toxin (RTX) domain and finally a C-terminal secretion signal (Sec). The five shaded blocks in the RTX region represent tandem Gly-Asp rich repeats.

ACT is secreted through a type I secretion pathway formed by the CyaB, CyaD, and CyaE proteins. Most of the secreted ACT is associated with filamentous hemagglutinin (FHA), the major adhesin on the cell surface, and does not actively intoxicate the host cells [34]. Instead of acting as a direct adhesin, ACT interacts with FHA, and enhances FHA-mediated adhesion to epithelial cells [35]. It is the newly synthesized and secreted soluble ACT, instead of cell-associated ACT, that actively intoxicates host cells in close proximity [36].

The C-terminal RTX domain of ACT is intrinsically disordered in the absence of calcium, but undergoes large conformational change into compact β-roll structure upon binding of calcium (Figure 1.3) [37]. This feature is thought to have an evolutionary advantage: the low calcium concentration in the bacterial cytosol keeps ACT in a random coil state which facilitates its secretion from C-terminus through type I secretion machinery; once the C-terminus is secreted and encounters millimolar calcium in the host respiratory tract, it starts to fold into receptor binding conformation.

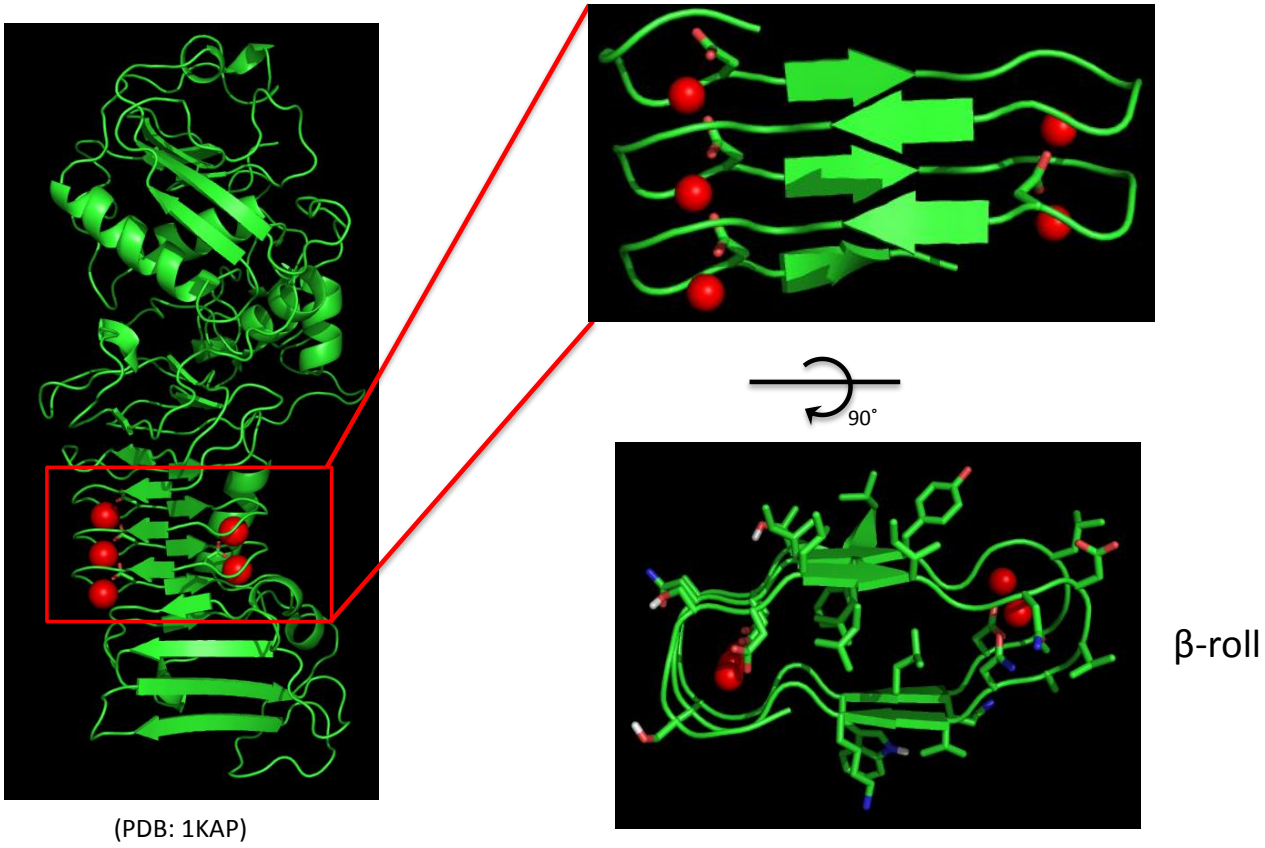

Figure 1.3: Crystal structure of *Pseudomonas aeruginosa* alkaline protease and sequence alignment with RTX domain of ACT.

Crystal structure of *Pseudomonas aeruginosa* alkaline protease, containing a new type of calcium binding motif rich in glycine and aspartic acid residues (PDB code: 1KAP) [38]. The calcium ions are shown as red globules, and the interacting Asp residues are shown as sticks. The segment of alkaline protease containing the four Asp residues is highly homologous with a stretch of sequence within the block III of ACT RTX domain. All four Asp residues involved in calcium binding are conserved between the two proteins, as indicated by arrows in the alignment. The shaded boxes indicate the 9-residue repeat motifs.

ACT mainly targets phagocytic leukocytes (*e.g.* neutrophils, macrophages, dendritic cells, and natural killer cells), but can also intoxicate other cell types with an order of magnitude lower efficiency in the absence of CD11b/CD18 receptor (e.g. erythrocytes, epithelium cells [39]). In a recent model of receptor-mediated translocation: the RTX domain binds CD11b/CD18 receptor and insert into the membrane with concomitant influx of calcium, which activates calpain to cleave the talin tether. This liberates the ACT-receptor complex to mobilize into cholesterol-rich lipid rafts, which facilitates the translocation of the catalytic domain, followed by cleavage by endogenous protease [40, 41]. The mechanism to deliver the catalytic domain into cells without specific receptors has not been elucidated yet.

At μg/mL concentration, ACT forms small cation-selective pores in host cell membrane, resulting in efflux of K^+ and colloid-osmotic lysis of erythrocytes, known as hemolysis [42]. Studies with lipid bilayers showed that the pore formation is dependent on the presence of mM calcium, pH, electrical potential, and lipid composition of the membrane [43-45]. Sheep erythrocytes are prone to both cAMP intoxication and hemolysis, but human red blood cells are resistant to hemolysis by ACT, and are intoxicated to a lesser extent. These suggest that cAMP intoxication and K^+ efflux are two independent processes, and the different responses to ACT were hypothesized to be due to the differences in membrane lipid compositions [46, 47].

ACT is unique in that its catalytic domain directly translocates across the membrane of various cell types, not requiring receptor-mediated endocytosis [48]. Although this process requires the hemolytic moiety, it is independent of the pore formation activity. An ACT mutant with E570Q+K860R substitutions lacked pore formation activity, but retained the ability to translocate the catalytic domain across cytoplasmic membrane into cytosol to catalyze cAMP formation [49]. A model proposed

that the translocation and pore formation are the results of two different pathways by ACT molecules in different conformations (Figure 1.4): ACT molecules inserted into the cell membrane are in equilibrium between the translocation and pore-formation precursors. The translocation precursor undergoes conformational change to deliver the catalytic domain into the cytosol; while the pore-formation precursor causes K^+ efflux, and can oligomerize to form larger pores leading to cell lysis [47, 50]. The presence of dimer and higher-order oligomers on toxin-treated erythrocytes was detected by immune-gold labeling, and the hemolytic activity was correlated with the formation of oligomers [51]. The two pathways seemed to be competitive: a monoclonal antibody 3D1, which was known to block the translocation of catalytic domain, increased the hemolytic activity of ACT, suggesting the equilibrium being driven toward the pore-formation precursor [52].

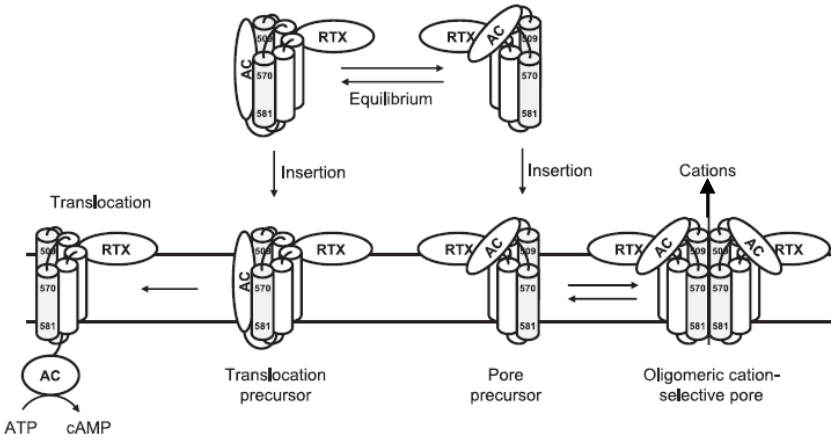

Figure 1.4: The model of ACT translocation and pore formation processes.

Two conformational states of ACT are in equilibrium in solution, which formed translocation and pore-formation precursors upon insertion into the host cell membrane. The translocation precursor undergoes conformational change to deliver the catalytic domain into the cytosol; while the pore-formation precursor causes K^+ efflux, and can oligomerize to form larger pores leading to cell lysis [50].

Due to its unique delivery mechanism and invasiveness into a wide range of cell types, ACT has been exploited as a vehicle to deliver polypeptides into eukaryotic cells. Extensive peptide insertions ranging from 2-9 residues spanning the entire ACT sequence revealed permissive sites within the catalytic domain, tolerating insertion of up to 206 amino acids without severely affecting the translocation process. The translocation requires the unfolding of the passenger protein, and is also dependent on the charge state of the passenger protein [53, 54]. $CD8^+$ [55-57] and $CD4^+$ [58] T cell epitopes have been successfully delivered into major histocompatibility complex (MHC) class I and class II pathways to induce CTL response and CD4+ T-cell response *in vivo*. Immunization with recombinant ACT containing a HPV16-$E7_{\Delta 30\text{-}42}$ oncoprotein fragment, which was optimized for translocation efficiency, induced Th1 and CTL responses and resulted in complete remission of grafted tumor in mice [59].

Despite evidence indicating ACT is a protective antigen, few neutralizing antibodies have been described and the location of neutralizing epitopes remains unclear. Moreover, ACT is prone to aggregation and degradation when produced by *Bordetella* or recombinantly by *E. coli*, precluding its inclusion in current acellular vaccine formulations [36]. Therefore, we aimed to identify neutralizing antibodies and their domain specificity and determine whether any single domain, possessing desirable expression and protein stability characteristics, can recapitulate the antibody responses induced by the holo-toxin.

1.3 CURRENT TRENDS OF ANTIBODY THERAPEUTICS

Antibodies now represent the largest fraction of the biologics market, currently >$20 billion annually, with 28 antibodies commercially available to treat cancer and inflammatory and infectious diseases [60]. Their appeal is due in large part to good safety

profiles, clear development paths and robust manufacturing processes. Improvements in cell culture engineering have led to yields of > 10 g IgG per liter culture [61], while protein engineering has allowed tailoring of key characteristics such as ligand binding affinity, in vivo half-life and immunogenicity [62]. Nevertheless, engineering of a single antibody does not always result in improved clinical efficacy, as was seen with Motavizumab, a highly engineered Palivizumab variant with 70-fold improved affinity for the respiratory syncytial virus F protein that conferred no additional clinical benefit [63].

In contrast to therapeutics, the native immune response does not generate a single antibody in response to disease, but instead a complex polyclonal response, comprised of multiple antibodies binding multiple epitopes with the ability to mediate a variety of effector functions.

Polyclonal anti-serum was first used as an immunotherapy in 1891 by Emil von Behring and Shibasaburo Kitasato and is still used to treat numerous diseases, including those caused by viruses, venoms and toxins. Targeting multiple epitopes offers broad strain protection and greatly decreases the selective pressure for resistant strains, as antigens with one or a few mutations are still effectively targeted [64]. Indeed, development of resistance to hyperimmune immunoglobulin by a previously sensitive pathogen has, to our knowledge, never been described, while escape variants to individual antibodies are readily generated in lab settings [65]. However, as blood-derived products, intravenous immunoglobulin (IVIG) is subject to batch-to-batch variability, limited availability, and carries the risk of blood-borne disease transmission [64]. More critically, even in high-titer immunoglobulin preparations isolated from immunized volunteers, only a small fraction of antibodies bind the target of interest and

of these, only a fraction will exert the desired effect (Figure 1.5). This results in a low specific activity and relatively high doses to observe a clinical effect.

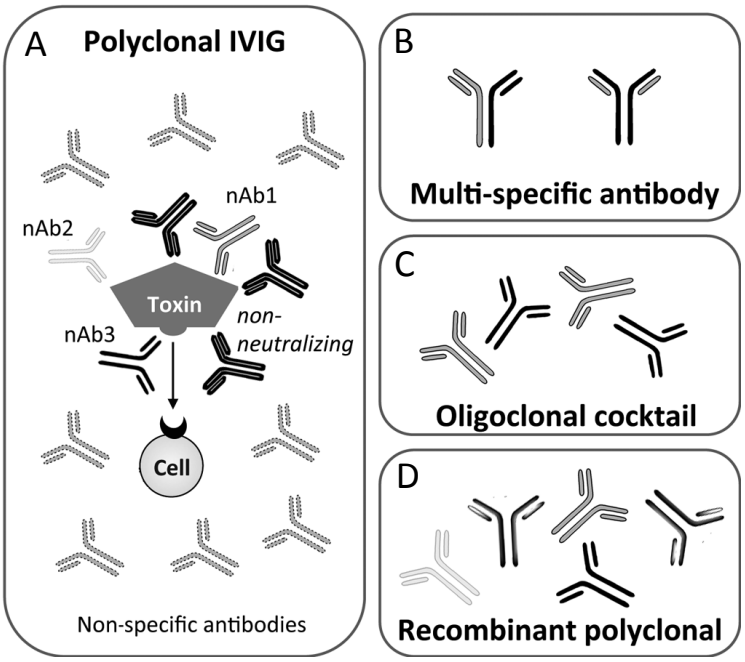

Figure 1.5: Polyclonal antibody therapeutics.

(A) While a traditional IVIG product contains a large number of antibodies binding a variety of antigens, only a fraction bind the antigen of interest (*e.g.,* a bacterial toxin) and of those, only a fraction are clinically relevant protective antibodies (*e.g.,* those that competitively inhibit a toxin-receptor interaction, block toxin endocytosis or catalysis). IVIG thus requires large doses for efficacy. **(B)** Multi-specific antibodies yield a single molecular entity able to bind two distinct epitopes, thereby combining the ease of monoclonal antibody manufacturing with broader antigen specificity. **(C)** Oligoclonal antibody cocktails are a combination of several monoclonal antibodies, each grown, purified and characterized in parallel before combining. **(D)** Recombinant polyclonal antibodies are comprised of multiple (two to 26) molecular entities, each binding clinically relevant epitopes. These are produced and purified *en masse* from a single cell line (Crucell/ Merus) or a polyclonal master cell bank (Symphogen).

In recent years, evidence has accumulated supporting the idea that mixtures of antibodies binding multiple non-overlapping epitopes combine the benefits of an engineered monoclonal antibody with the broad-spectrum activity of a polyclonal

therapeutic. Moreover, since the component antibodies can be produced individually, they can be selected on the basis of affinity, epitope specificity and protective mechanism to ensure that each member of the mixture contributes to the overall pharmacological effect.

In the simplest case, monoclonal antibodies already approved for use in humans are being tested in new combinations with other approved or investigational monoclonal antibodies [66]. For instance, disregulation of the epidermal growth factor receptor (EGFR) is involved in many cancers. Two approved anti-EGFR monoclonal antibodies (Cetuximab and Panitumumab) bind EGFR domain III, blocking ligand-receptor activation and downstream signaling. Recent studies have demonstrated that combinations of antibodies binding non-overlapping epitopes are more effective than a single antibody at inhibiting tumor growth by triggering EGFR internalization and degradation [67]. Antibody combinations may also access other mechanisms, such as complement-dependent cytotoxicity and potentiate otherwise non-protective antibodies [68]. A recently approved biclonal combination consisting of the monoclonal antibodies Trastuzumab and Pertuzumab, which target different epitopes on the HER-2 growth factor receptor, was effective in reducing progression rates in breast cancer patients who had shown progression with Trastuzumab treatment alone [69, 70]. In a remarkable feat of protein engineering, a single antibody binding site was engineered to bind both VEGF and HER2 with high affinity (Kds of 3 and 0.2 nM, respectively) and enhanced in vivo efficacy, creating a new type of bispecific antibody in which each binding site can bind one of two distinct antigens [71].

To create the novel anti-EGFR cocktail Sym004, Pedersen et al. [72, 73] systematically tested combinations of two or three antibodies from a pool of 88 murine anti-EGFR antibodies for tumor inhibition activity. The most potent mixture, a 1:1

combination of antibodies 992 and 1024, showed maximal tumor inhibition, which correlated with EGFR down-regulation. The antibodies bind non-overlapping epitopes on EGFR domain III; indeed antibody 992 exhibited synergistic growth inhibition with all antibodies tested that bind non-overlapping epitopes. Suggesting this may be a common strategy, Spangler *et al.* examined pairwise combinations of six murine anti-EGFR antibodies, with the pair most potently reducing surface EGFR levels binding non-overlapping domain III epitopes, leading to reduced receptor recycling [74]. Treatment with 50mg/kg of Sym004 led to complete tumor regression in all mice, while Cetuximab alone or the individual antibodies exhibited only partial suppression. Sym004 performed well in pre-clinical studies and is currently in Phase II trials [75].

Development of antibody therapeutics to treat infectious diseases has lagged behind those for cancer, with only a single monoclonal antibody available (Palivizumab, MedImmune), in part due to the difficulties associated with multiple antigens and naturally occurring strain variation. These therapeutics may be more viable as combinations of antibodies binding potently neutralizing epitopes and triggering appropriate effector functions. Since polyclonal antibodies were first used to treat toxin-mediated diseases, early efforts to deconvolute the polyclonal response into a mixture of specific monoclonal antibodies centered on these pathogens. One study showed that antibodies elicited by murine immunization bound 20 distinct epitopes on the tetanus toxoid heavy chain [76], while in humans 17 unique epitopes were observed [77]. Quaternary combinations of the murine antibodies were 200-fold more protective in a mouse model than the individual antibodies [76]. In another study, two human anti-tetanus toxin antibodies provided similar protection in mouse model as a polyclonal preparation at >100-fold lower dose (0.7 mg versus 100 mgs) [78].

Similar studies with botulinum toxin A (BoNT/A) showed that while no single antibody significantly neutralized the toxin, a combination of three antibodies binding non-overlapping epitopes on the heavy chain exhibited a potency 90 times greater than human hyperimmune globulin and 20,000-fold greater than any single antibody [79]. Analysis of the detailed pharmacokinetics of BoNT/A in the presence of a similar set of antibodies identified therapeutic windows for passive immunization post-intoxication [80]. The antibodies are thought to block receptor binding and toxin internalization, followed by Fc-dependent hepatic clearance of antibody-toxin complexes [81]. Engineered, human versions of these antibodies are in development as Xoma 3AB, an equimolar mixture of three antibodies, which is over 500-times more potent in mouse potency tests than the equine IVIG. While this product can treat only one of the seven BoNT serotypes (encompassing sub-types A1, A2 and A3) [81], analogous cocktails are in development for other serotypes. In another protein engineering feat, individual antibodies have been engineered to bind the same epitope as presented by multiple sub-types or even multiple serotypes with high affinity and specificity and could potentially be combined to create a single cocktail with broaden strain coverage [82, 83].

A second cocktail in development neutralizes rabies virus, for which high titer human or equine polyclonal immunoglobulin remains the standard of care. Crucell Holland BV identified two human antibodies, CR57 and CR4098 from immunized humans that bind non-overlapping epitopes on the rabies glycoprotein with high affinity (2.4 and 4.5 nM, respectively) [84]. While most antibodies neutralizing rabies virus bind conformational epitopes in antigenic site II, CR57 binds a linear epitope in site I (residues 226-231) and CR4098 binds a conformational epitope within site III. Each monoclonal antibody alone was shown to neutralize 24 of 26 street isolates, similar to rabies IVIG. However, the binary combination neutralized all 26 strains and was at least as potent as

IVIG in a hamster model [85]. Critically, escape variants with mutations in the CR57 epitope are neutralized by CR4098 and vice versa, while *in vitro* selection for variants escaping both antibodies was unsuccessful [65]. This binary cocktail is safe in humans [86], can be administered in conjunction with the rabies vaccine and is now in Phase II clinical trials as CL184.

Additional antibody cocktails are in development to treat infectious diseases, although their effectiveness has yet to be demonstrated in clinical trials. Medarex has recently presented promising clinical data showing that a biclonal therapeutic targeting *C. difficile* toxins A and B was able to lower the incidence of recurrence in patients when administered in combination with vancomycin or metronidazole [87]. Crucell is pursuing a biclonal cocktail against SARS coronavirus [88]. Preclinical data has also been presented demonstrating the effectiveness of biclonals against Hepatitis C virus [89, 90] *in vitro* and in animal models. A triclonal mixture of broadly neutralizing anti-HIV antibodies binding the fusogenic gp120 (2G12) and conformational epitopes within the membrane proximal region of gp41 (4E10, 2F5) has been assessed in a Phase II trial, with six of fourteen volunteers showing partial or complete control of viremia [91, 92]. A binary mixture of antibodies binding the non-overlapping CD4 binding site (VRC01) and a glycan-dependent epitope in the V1V2 region of the viral spike trimer (PG9) demonstrated neutralization of 98% of 208 HIV strains *in vitro* [93].

Biclonal and triclonal antibodies function synergistically to neutralize a target pathogen and can target more than one epitope, yet they are still vulnerable to mutations of their target epitopes. Jim Marks and his group at UCSF have observed, targeting BoNT/A, that a minimum of three antibodies is required for effective neutralization, and that through point mutation or epitope shift of any of these three antibodies could cause the antibody cocktail to become ineffective, events that are less likely to occur for this

particular target antigen but could be a hazard for more mutable pathogens [79]. Thus, in many cases more complex polyclonal mixtures may be required to confer adequate protection. While not all activities may be relevant for each clinical case, in aggregate the drug would enable protection against a complex disease, while reducing the potential immunogenicity of each individual component [94].

Excelimmune employed a set of five human antibodies recognizing *S. aureus*, including methicillin-resistance *S. aureus* (MRSA) strains, in *in vivo* studies. These showed protection exceeding that conferred by any monoclonal antibody, fully protecting mice against a lethal dose of bacteria at a 1 mg/kg dose [95, 96]. Of these five antibodies, only a single antibody binds an identified antigen, while the others bind either cell surface or soluble proteins. Many *S. aureus* toxins are encoded by phages, resulting in considerable diversity between strains. When a case of acute sepsis presents, the optimal clinical outcome may be obtained by treatment with a single therapeutic with broad strain coverage, rather than first identifying the specific strain before treating with a more specialized drug.

Finally, an excellent test case for recombinant polyclonal antibody therapy may be disease caused by *Bordetella*, primarily *B. pertussis*. *Bordetella* genomic sequences are highly conserved, with over 20 known virulence factors and, critically, no single serological correlate of protection. Currently available acellular vaccines include between two and five antigens known to induce strong humoral immune responses. In spite of broad vaccine coverage, disease persists and incidence has increased dramatically in recent years, with high infant morbidity and mortality rates. However, treatment with high-titer anti-pertussis toxin IVIG has been shown to reverse disease symptoms up to seven days after infection in mice [97] and in Phase II trials with infants, shown to reduce the number of whoops [98-100]. There are also several examples in the literature of

synergistic antibody combinations with potencies surpassing that of polyclonal antisera in mice [101]. Since the key antigens are well-characterized with, in most cases, neutralizing antibodies and protective epitopes already identified [101-103], antibodies could be rationally combined to identify a potently protective cocktail. The antibodies could be individually engineered for traits likely to correlate with protection, including high affinity, recognition of all circulating clinical strains and their protective mechanisms characterized [102, 104].

A key question during development of recombinant cocktails or polyclonal antibody therapeutics is which antibodies should be combined? What minimal collection will be synergistic and potently protective yet robust against antigenic variation? The answer may lie in defining antibody repertoires responding to the different epitopes present on an antigen; from this comprehensive collection, protective antibodies binding different epitopes can be selected for further characterization and engineering. Older work used phage libraries generated from donor PBMCs, but this approach suffers from loss of native light-heavy chain pairing and heterologous expression constraints [105]. Exciting newer technologies have been developed to isolate and sequence the variable regions present in antigen-specific plasmablasts [106-109], which correlate with serum antibodies observed proteomically [110, 111].

The overall serum response recognizing a single antigen appears to be oligoclonal with a discrete number of clades resulting from an initial VDJ recombination event followed by somatic hypermutation. In the circulating repertoire, multiple clade members - not just highest affinity or most highly mutated - persist, perhaps to provide the plasticity to respond to antigenic variants [112]. Antibodies present in the circulating repertoire exhibit affinities between 10 – 0.1 nM [113, 114], consistent with expectations based on the limits of B cell receptor signaling [115] and competition for limited antigen

[116]. While the naïve/ germline repertoire can encode antibodies with high affinity for large, antigenically complex antigens, within a clade 10-100-fold increases in affinity are observed as the genes are progressively altered via somatic hypermutation [112]. An analysis of plasma cells after tetanus toxin immunization observed 32 and 41 unique Vh and Vl rearrangements, respectively, while one donor immunized with the 2003 influenza vaccine yielded 17 unique Vh rearrangements; overall the affinities ranged from 250 to 0.3 nM [117].

A single antigen can present multiple antigenic sites, which include neutralizing and non-neutralizing, immunodominant and weakly immunogenic epitopes. The native polyclonal response will include antibodies recognizing all of these, including "decoy" epitopes that are highly immunogenic and dominate the polyclonal response but are only weakly or non-protective. The key advantage of recombinant polyclonal therapeutics is that it can be comprised exclusively of high affinity antibodies binding potently neutralizing epitopes with characterized protective mechanisms to not just recapitulate but exceed the potency of the natural response.

The manufacture of individual monoclonal antibodies is well-developed, primarily using stably transfected CHO cells in fed-batch culture, followed by downstream purification and product characterization according to standards set by Center for Drug Evaluation and Research (CDER) at the FDA [119]. These steps typically involve protein A affinity and size exclusion chromatography followed by analyses of structural integrity (SDS-PAGE, peptide mapping, free sulfhydryl and mono- and oligosaccharide analyses). A simple approach to generation of antibody cocktails, especially those which have already received approval as a monoclonal therapeutic, is to process the molecules in parallel, combining them after purification or at the point of

administration [91]. This may be favored from a regulatory perspective, considering the FDA combination drug rule.

Bi- and triclonal therapeutics comprised of novel antibodies are currently generated in a similar manner, with master cell banks prepared for each antibody, which are then expanded, expressed and purified separately before combining in defined ratios [91, 120]. As these mixtures are relatively simple, manufacturing them as monoclonals avoids retooling established manufacturing platforms with the main concern being undesirable interactions between the component antibodies. For instance, the XOMA 3AB anti-BoNT triclonal cocktail is produced in this way, with the presence and integrity of each component antibody monitored by HPLC chromatography (hydrophobic interaction and reverse phase) and ELISA, using toxin domains specifically engineered to bind a single antibody in the mixture [120]. This cocktail can be stored at 2-8 °C for two years and is robust to lyophilization, retaining full-antigen-reactivity after five months at 50 °C [121]. However, as the number of unique molecules increases above two or three, the manufacturing costs rise precipitously, since each molecule sequentially monopolizes facilities and requires individual characterization. Moreover, as each batch is subject to failure, producing multiple small batches eliminates the savings achieved by economies of scale in larger recombinant protein production facilities [122].

To constrain costs, strategies have been developed to produce recombinant polyclonal antibodies in a single pot, several of which have subsequently entered clinical trials. This process-as-product strategy bypasses the manufacturing hurdles associated with individual antibody production but introduces new challenges to demonstrate reproducible cell growth, genomic stability, constant antibody ratios and integrity of the component antibodies. Detailed strategies to tackle these challenges and routes for regulatory approval are reviewed in [123].

1.4 ANTIBODY DISCOVERY AND ENGINEERING TECHNOLOGIES

1.4.1 Hybridoma

Hybridoma technology was invented by Georges J.F. Köhler and César Milstein in 1975 [124], and was awarded Nobel Prize in Physiology or Medicine for 1984 because it opened up new fields for biomedical research and biological therapeutics.

The procedure starts with mouse immunization, followed by fusion of B cells with immortal myeloma cells. The supernatants from individual fusion cells are screened for secreted antibodies binding the target antigen. Each confirmed cell line can be cultured indefinitely to produce unlimited amount of monoclonal antibody with predetermined specificity. However, this procedure is labor intensive, inefficient, and requires mouse immunization for each different target. Other limitations include the immunogenicity associated with the mouse origin for human use [125], inability to control the isotypes of the antibodies [126], and difficulty to generate antibodies against poorly immunogenic antigens [127].

1.4.2 Recombinant antibody

The invention of recombinant DNA technologies, such as PCR and DNA sequencing, allowed the amplification and identification of antibody variable region residues from hybridomas, and also enables antibodies to be produced recombinantly in bacteria, yeast, plants, or mammalian cells [128-130]. This brings several advantages: first, immunization is not strictly required to generate antibodies with desired specificity. Instead, large non-immune or synthetic antibody libraries can be screened for antibodies against essentially any target [131, 132]. Second, antibodies can be engineered for desired properties, such as improved affinity or enhanced stability [133]. Third, to avoid immunogenicity problem when used as therapeutics, fully human antibodies can be

isolated from nonimmune libraries constructed from human peripheral mononuclear cells or immune libraries from immunized transgenic mice that possess human antibody repertoires [134, 135].

1.4.3 Phage display

Display of proteins on the surface of filamentous phage was first developed around 1990 [136, 137], and has become a widely used tool in the field of antibody discovery and engineering. Starting from animal immunization, the light chain variable regions (VL) and heavy chain variable regions (VH) are amplified from spleen cells *en masse*, and spliced together with a flexible linker (e.g.$(Gly\text{-}Gly\text{-}Gly\text{-}Gly\text{-}Ser)_2$) in between, by overlap extension PCR (SOE-PCR). The resulting fragments encoding single chain antibody fragments (scFv) are then cloned into phagemid, upstream of M13 phage minor coat protein – PIII (5 copies per phage). The phagemids are transformed into *E. coli* cells expressing the F pilus and then rescued by infection of helper phage to provide the rest of the coat proteins for assembly of new phage. The single-stranded phagemid DNA are preferentially packaged into the newly assembled phage, and the pIII-scFv fusion protein competes with the wild-type pIII encoded by helper phage for assembly. The secreted phage mostly carry 0~2 copies of scFv on the tip. With the scFv displayed on phage surface and the DNA encoding the scFv packaged inside, phage display provides a direct link between the phenotype (binding) and genotype (DNA sequence). Alternatively, phage libraries can be generated from parent libraries via mutagenesis or synthetically.

Nowadays, phage libraries with up to 10^{11} clones can be routinely prepared [138]. The library is then "panned" on an ELISA plates with the immobilized target antigen or in solution with antigen-coated magnetic beads. Weakly bound phage is removed by

washing; the bound phage can be eluted with extreme pH, amplified by infecting log-phase *E. coli* expressing F pilus, and rescued with helper phage to produce more phage for successive rounds of selection. Specific binders are typically enriched after 2~5 rounds of selection depending on a number of factors, including the frequency of binders in the starting library, stringency of the washing step, etc. Individual phage clones are then tested for binding with the antigen (Figure 1.6). Confirmed binders can be further characterized or engineered as phage-displayed or soluble antibody fragments.

Phage display is high-throughput and convenient, generating antigen-specific antibody fragments in weeks instead of months comparing to hybridoma technology. However, with eukaryotic origin, some antibodies do not fold properly on phage surface, or express poorly in *E. coli* [139, 140].

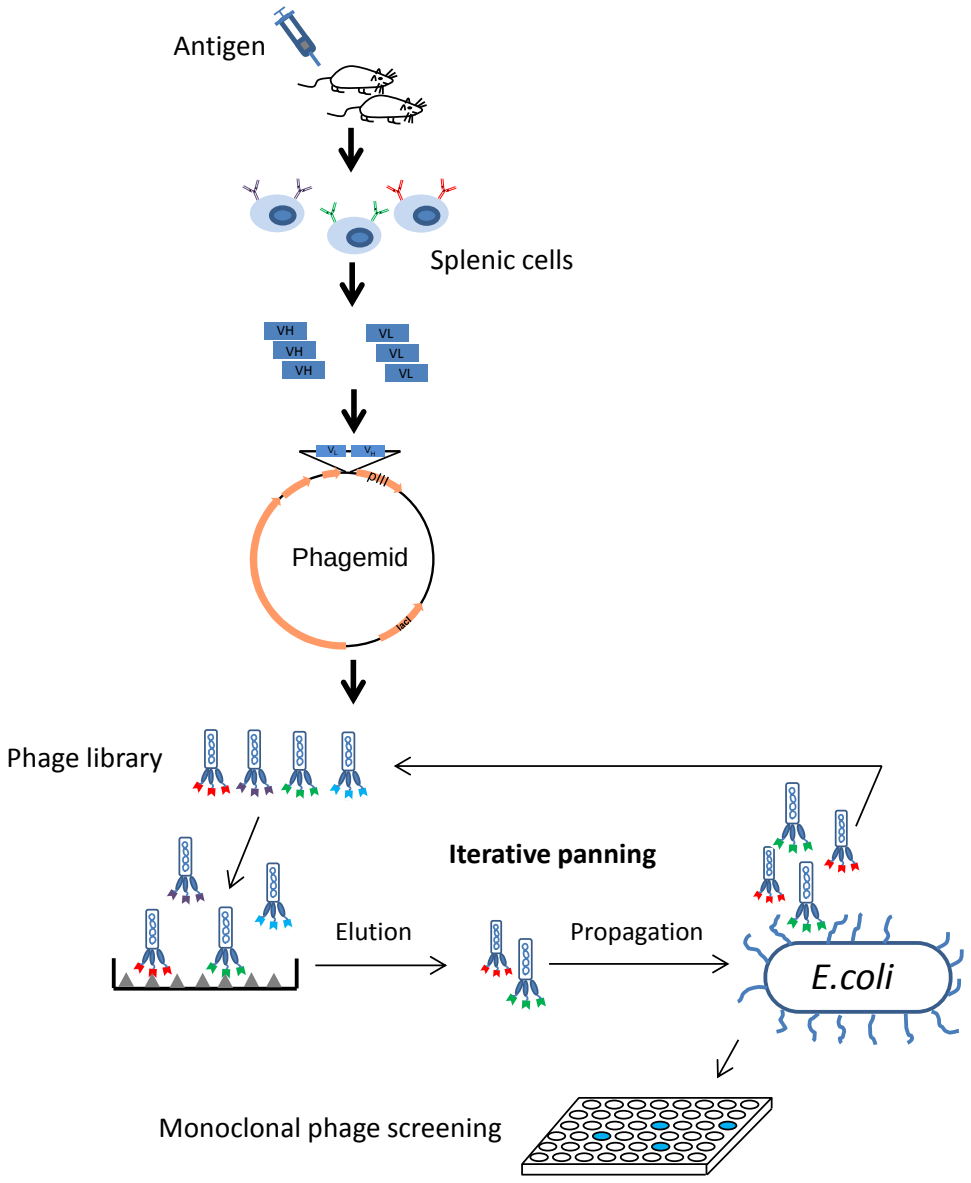
Antigen
Splenic cells
VH
VH
VH
VL
VL
VL
pIII
Phagemid
lacI
Phage library
Iterative panning
Elution
Propagation
E.coli
Monoclonal phage screening

Figure 1.6

Figure 1.6: General antibody discovery process using phage display technology.

Mice are immunized with the antigen of interest with adjuvants. The spleens are harvested, from which mRNA or total RNA is extracted. Then cDNA is synthesized via reverse transcription. Genes encoding antibody light and heavy chain fragments are amplified from cDNA using predefined primer sets. Then the light and heavy chain gene fragments are spliced together by SOE-PCR. The resulting single-chain antibody genes are cloned into the phagemid vector and transformed into *E. coli* competent cells, forming the starting library. The cells are grown and infected with helper phage to produce the phage-displayed antibody library, which is panned against the target antigen. Unbound phage is washed away, while bound phage is eluted and re-infected into *E. coli* with F pilus to be amplified for the next round of selection. After several rounds of selection, hundreds of individual *E. coli* colonies harboring phage clones are inoculated into 96-well plates and grown for phage production, followed by detection of binding with the immunizing antigen via ELISA.

1.4.4 Yeast display

Comparing to phage display, yeast display is advantageous in that it is better suited for display of eukaryotic proteins that don't fold correctly in *E. coli* or proteins that require posttranslational modification. The yeast endoplasmic reticulum ensures only properly folded proteins are secreted [141]. Moreover, the larger size of yeast allows fluorescence-activated cell sorting (FACS) of the library, providing real time and quantitative control over the desired properties. For example, a state-of-art cell sorter can sort up to $2.5X10^8$ cells per hour. Cells can be stained for surface display level and binding affinity; and the populations of cells with desired properties can be collected.

The protein of interest can be display either by fusing it to a protein that will be localized on the cell surface or by expressing a surface-anchored capture protein that will recognize it. The most commonly used is the Aga1p-Aga2p system [142]: the Aga1p protein is stably integrated in the yeast chromosome and is anchored in the cell surface when secreted, while the Aga2p protein forms two disulfide bonds with Aga1p when secreted to the cell surface, thereby displaying the fusion partner (Figure 1.7). Both Aga1p and Aga2p are under the control of the galactose promoter.

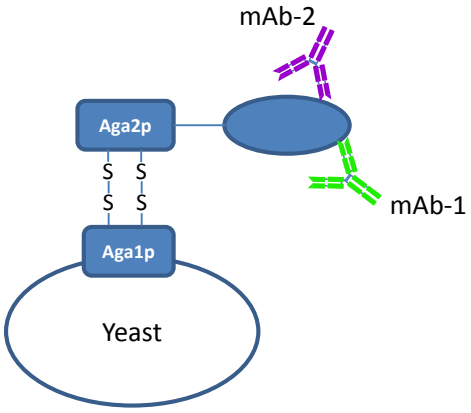

Figure 1.7: Yeast surface display.

Target protein is fused to Aga2p protein and displayed on yeast surface through two disulfide bonds between Aga1p and Aga2p.

Chapter 2: Discovery and characterization of neutralizing antibodies against *Bordetella* adenylate cyclase toxin

2.1 INTRODUCTION

Adenylate cyclase toxin (ACT) is one of the most important virulent factors produced by the three major species of *Bordetella*. Ample evidence suggests that it induces protective immunity *in vivo*. ACT was first noticed as a 43kD protein fragment exhibiting adenylate cyclase activity in the supernatant of *B. pertussis* culture [143], but the full-length ACT was not identified until the discovery of the *cyaABDE* operon in 1989 [144], after the development of the acellular vaccines. Since then, ACT has not received enough attention as a protective antigen. Also, few monoclonal neutralizing antibodies have been discovered and characterized; little is known about the protective epitopes on ACT.

ACT primarily intoxicates phagocytes by binding to the $\alpha_M\beta_2$ integrin and translocating the adenylate cyclase domain into the host cytosol, generating supraphysiological cAMP levels at ng/mL concentration. At higher concentration (μg/mL), ACT forms pores on cell membrane leading to cell lysis. Based on the recent finding of *in vivo* ACT concentration at the bacterium-host cell interface [145], the cAMP intoxication process is likely more important and relevant for the disease than the pore formation activity.

Previously, Lee *et al.* reported 12 monoclonal antibodies identified from immunized mice using hybridoma technology. The mAbs bind epitopes across different regions of ACT, with six targeting the C-terminal RTX domain, two targeting the hydrophobic domain, two targeting the acylation bearing region, and two targeting the distal end of catalytic domain. Although the C-terminal region of ACT was suggested to

Chapter 2 is based on previous publication: **Wang, X**, Gray MC, Hewlett EL, and J.A. Maynard, *The Bordetella Adenylate Cyclase Repeat-in-Toxin (RTX) Domain Is Immunodominant and Elicits Neutralizing Antibodies.* **J Biol Chem**, 2015. **290**(6): p. 3576-91. XW and JAM conceived the study. XW performed and analyzed the experiments. MG and EH provided critical reagents. EH provided suggestions. XW and JAM wrote the manuscript.

carry protective epitopes [146], only one of the six mAbs could inhibit hemolytic activity and none could potently inhibit the cAMP intoxication process; one of two mAbs targeting the hydrophobic domain inhibits invasive cyclase activity and partially hemolytic activity [147]; two mAbs 3D1/5D1 targeting the distal end of the catalytic domain (residues 373-399) inhibit cAMP intoxication, by preventing the delivery of catalytic domain into host cells [52].

Here we set out to analyze the antibody repertoire upon mouse immunization with ACT, using phage display which has higher throughput than the hybridoma technology. In accordance with previous report that the C-terminal RTX domain is immunodominant, we found that most of the binders recovered from the phage display antibody libraries bound the RTX domain. We then expressed unique binders as soluble single-chain antibodies (scAb) and used a cell-based assay with J774A.1, a murine macrophage cell line that expresses the receptor for ACT—$\alpha_M\beta_2$ integrin (also known as CD11b/CD18 or CR3), to screen for antibodies that could neutralize the cAMP intoxication of the macrophage cells. Nine out of 21 antibodies were neutralizing and bound two non-overlapping epitopes as determined by competition ELISA. Then, we converted the representative neutralizing antibodies, M2B10 and M1H5, into full length chimeric IgG format, with mouse variable region and human constant region. Competition ELISA with previous anti-ACT monoclonal antibodies showed no competition, indicating that M2B10 and M1H5 bound novel epitopes on the RTX domain. This is the first report of anti-ACT neutralizing antibody binding the RTX region. The affinities of the neutralizing antibodies were measured by kinetic exclusion assay (KinExA).

J774A.1 cells express $\alpha_M\beta_2$ integrin, while CHO-K1 cells do not. Interestingly, our neutralizing antibodies inhibited the cAMP intoxication of CHO-K1 cells much less efficiently than that of J774A.1 cells. This led to our hypothesis that the mechanism of

action of the neutralizing antibodies was to block the receptor binding. Our hypothesis was supported by flow cytometric measurement of the association of ACT to J774A.1 cells and ELISA data comparing ACT binding to purified $\alpha_M\beta_2$ integrin, in the absence or presence of neutralizing antibodies. Finally, we showed that M2B10 and M1H5 could neutralize the newly synthesized ACT secreted by live *B. pertussis*, and bound *B. pertussis* cells probably via the surface-associated ACT.

2.2 MATERIALS AND METHODS

2.2.1 Murine immunization

All protocols were approved by the University of Texas at Austin IACUC (protocol #2012-00068) and all mice were handled in accordance with IACUC guidelines. As a source for antibody libraries, two 6-week BALB/c mice were primed intraperitoneally (*i.p.*) with 17 μg of ACT (dialyzed against PBS to remove urea) in complete Freud's adjuvant (CFA). Four weeks later, the mice were bled through tail vein, and boosted subcutaneously with the same amount of PBS-dialyzed ACT in incomplete Freund's adjuvant (IFA). Two weeks later, the mice were sacrificed and blood collected by cardiac puncture. Spleens were removed sterilely, sliced into pieces and immediately immersed in 1ml of cold RNALater solution. After soaking overnight at 4 °C, the solution was removed and the spleens were stored at -80 °C.

Anti-ACT antibody titers in the sera were determined by ELISA. Neutralizing activities in the sera were determined with CHO-K1cells at 400-fold dilutions.

2.2.2 Phage display antibody library construction

Total RNA was extracted from frozen spleens with TRIZol (Invitrogen) and the RNeasy Mini Kit (QIAgen) or PureLink RNA kit (Invitrogen) according to the manufacturers' instructions. The quality and concentration of total RNA was assessed by

agarose gel electrophoresis and $A_{230:260:280}$ ratio (approximately 1:2:1 for pure RNA) measured by NanoDrop 2000 (Thermo Scientific). For first-strand cDNA synthesis, 5 µg of total RNA was used. To maximize diversity, two separate reactions were performed using combinations of Superscript II + $d(T)_{23}$ VN primer or Superscript III (Invitrogen)+ random hexamer (Thermo Scientific), following manufacturers' instructions. The two sets of cDNA were pooled as template for amplification of the V_L and V_H repertoires using the primer sets and PCR conditions described by Krebber *et al*. [148]. The PCR products were gel purified, with 10ng each of V_L and V_H used as template in an overlap PCR to generate V_L-linker-V_H fragments (scFv). This product was gel purified and digested overnight with *Sfi*I prior to directional ligation with similarly *Sfi*I-digested pMopac24 vector [149]. Ten individual electroporations were performed to transform XL1-Blue cells. The transformants were pooled and an aliquot was 10-fold serially diluted and plated to count library size; the rest were plated on eight 150mm 2xYT agar plates (10 µg/mL tetracycline, 200 µg/mL ampicillin, and 2% glucose). After incubation overnight at 37˚C, the bacterial lawns were scraped off in 2xYT medium and pooled to form the master library.

2.2.3 Phage production, purification, and panning

Aliquots of the master library was used to inoculate 250 mL 2xYT medium with 10 µg/mL tetracycline, 200 µg/mL ampicillin, and 2% glucose in 1 L flasks to an OD_{600} of ~ 0.1. The cultures were grown at 37˚C for 2-3 hours until the OD_{600} reached ~0.6, induced and rescued by adding 1mM IPTG and M13KO7 helper phage (MOI ~ 20), incubated for 30min without shaking at 37˚C, and then returned to a shaking incubator at room temperature. Three hours after adding helper phage, the culture was supplemented with 50 µg/mL kanamycin prior to overnight incubation with shaking. Phage was then

purified by double precipitation with 1/5 volume of precipitation solution (2.5M NaCl, 20% PEG-8000). The concentration of viable phage was assessed as colony forming units (cfu), with serially diluted phage added to log-phase XL1-Blue cells, followed by plating on 2xYT agar plate with 200 μg/mL ampicillin, and enumeration of colonies after overnight incubation.

Two rounds of panning were performed using ACT as bait. Eight ELISA plate wells (Costar) were coated with 50 μL of 2 μg/mL and 1 μg/mL ACT in PBS at 4˚C overnight for the first and second round respectively. Input phage (100 ul) were diluted into 900 μL of 5% non-fat milk in PBST (PBS, 0.05% Tween-20) and incubated for 1 h before transferring 100 μL to each of the 8 wells. After a 1 hour incubation at room temperature, followed by five (or ten for round 2) washes with PBST, bound phage was eluted with 100 μL per well of 0.1 N HCl for 10min at RT. The eluted phage was pooled and immediately neutralized with 48μL of 2M Tris base. Half of the output phages were added into 5ml of log-phase XL1-Blue culture grown with 10μg/mL tetracycline at 37˚C to retain the F plasmid, incubated for 30min without shaking and 1hr with shaking at 225rpm in 37˚C, then spun down and plated on six 150mm 2YT agar plate (200μg/mL ampicillin, 10μg/mL tetracycline, and 2% glucose). After overnight incubation at 37˚C, colonies or lawn were scraped, pooled, mixed thoroughly, and aliquots used for second round of panning as described above.

Input and output phage titers (colony forming unit, cfu) were determined by infecting and plating *E. coli* on selection plates as described above. Sequence diversity was monitored throughout all steps by performing colony PCR with primers 5'-GCCATGGCGGACTACAAAG-3' and 5'-GGAATTCGGCCCCCGAG-3' to amplify the VL-VH region of random colonies on the phage titration plates, followed by *BstN*I

digestion and agarose gel electrophoresis. Clones with unique fingerprints were confirmed by DNA sequencing.

To produce monoclonal phage clones from panning outputs, single colonies from output plates were inoculated into sterile 96-well plates containing 100 µL 2YT medium (2% glucose, 200 µg/mL ampicillin, and 10 µg/mL tetracycline), and grown at 37˚C overnight with shaking. The next morning, 10 µL of the overnight culture was inoculated into another plate with 90 µL per well of fresh medium containing 0.25% glucose and antibiotics, grown at 37˚C for 3hr, then 50 µL 2YT (200µg/mL Amp, 3mM IPTG, and M13KO7 helper phage) was added and let shaking at room temperature for 3 hours, before adding 50µL of 2YT (200µg/mL ampicillin, 1mM IPTG, 200µg/mL kanamycin). The plate was then shaken at room temperature overnight. The supernatant was used for phage ELISA as described below. The V_L-V_H genes of positive clones were amplified and fingerprinted with *Bst*NI. Phagemids of the unique ones were extracted and confirmed by DNA sequencing.

2.2.4 Antibody expression and purification

To convert phage-displayed scFvs to soluble single chain antibody fragments (scAbs), consisting of a variable light chain domain (V_L) connected via a flexible $(Gly_4Ser)_2$ to a variable heavy chain domain (V_H) followed by a human kappa constant domain to enhance expression and solubility, the scFv region was removed from pMopac24 phagemid vector by *Sfi*I digestion, and directionally ligated into *Sfi*I-digested pMopac54 plasmid [150]. For scAb production, 100ml of TB supplemented with 200µg/mL ampicillin and 1% glucose were inoculated at OD_{600} = 0.02, grown overnight at room temperature. The next morning, cells were pelleted at 5000g for 10min at room temperature, resuspended in 100ml of TB medium with ampicillin but no glucose, and

grown at room temperature for 1h before induction with 1mM IPTG. After another 4 hours, cells were harvested by centrifugation at 5000g, 10min, 4˚C. Osmotic shock was performed as described [150]. ScAbs in the dialyzed shockates were purified by IMAC resin followed by size exclusion chromatography with a Superdex 200 column on FPLC (GE Healthcare). Protein concentrations were measured by BCA assays (Pierce) using a BSA standard with purity assessed by SDS-PAGE.

To convert scAbs into full-length IgG with enhanced stabilities and *in vivo* half-lives, the V_L and V_H genes were subcloned onto Igκ-Abvec and IgG-Abvec vectors as described by Smith *et al*. [108]. For IgG production, paired Igκ-Abvec and IgG-Abvec plasmids were transiently transfected into CHO-K1 cells using Lipofectamine 2000 (Life Technologies) according to manufacturer's instructions. Culture media were collected at 1-2 day intervals, neutralized with 1M Tris pH 8.0, pooled, and IgG purified by ammonium sulfate precipitation followed by HiTrap Protein A column. The purity and presence of aggregates were assessed by SDS-PAGE and size-exclusion chromatography using a Superdex S200 column. The concentration was determined by A_{280} using extinction coefficients calculated from deduced amino acid sequences [151].

2.2.5 Analysis of antibody binding by ELISA

For monoclonal phage screening, the 96-well phage production plates described above were spun at 3000g for 20min, with 40 µL of supernatant transferred to a coated (2 µg/ml ACT in PBS) and blocked (5% nonfat milk in PBST, M-PBST) ELISA plate containing 60 µL M-PBST per well, and incubated at room temperature for 1hr. After 4 washes with PBST, 50 µL of 1:2000 HRP-conjugated anti-M13 antibody (GE Healthcare) was added, and incubated 1hr at room temperature. The plate was washed 4 times, 50 µL/ well TMB substrate added and incubated at room temperature. The reaction

was quenched by adding 50 μL/well 1M HCl, and the absorbance at 450 nm recorded with a SpectraMax M5 (Molecular Devices). Wells with absorbance higher than 2-fold of background were identified for further characterization.

Binding assays to assess domain specificity and relative affinity of soluble scAb or IgG proteins were performed in a similar manner. Purified ACT (1 μg/mL) or domains (equimolar with ACT) were coated on ELISA plates, followed by blocking and serial dilutions of purified antibodies, and finally detection with goat anti-mouse IgG HRP-conjugated antibody (to detect murine antibodies), goat anti-human κ chain HRP-conjugated antibody (to detect scAbs) or goat anti-human IgG (Fc-specific) HRP-conjugated antibody (to detect recombinant IgG). For competition ELISA, the antibody of interest was used at a fixed concentration determined to yield 70-80% of the maximal signal, and mixed with an equal volume of serially diluted competitor antibody, followed by detection as above.

To test the effect of calcium on antibody binding to ACT or domains, ACT or domains were coated in PBS as normal. HBST (50mM Hepes, 150mM NaCl, 0.05% Tween-20, pH 7.5) -5% milk or HBST-1% BSA supplemented with 0.2 mM $CaCl_2$, 2 mM $CaCl_2$, 20 mM $CaCl_2$, or 5 mM EDTA were used as blocking solution and diluent. The antibodies were titrated in diluents with different calcium concentrations and the detection antibody was diluted in the same conditions as the antibody to be detected.

2.2.6 *In vitro* cAMP intoxication & neutralization assay

CHO-K1 cells were grown in DMEM (Sigma) supplemented with 10% fetal bovine serum and penicillin/streptomycin. J774A.1 cells (ATCC #TIB-67) were grown in DMEM supplemented with 10% fetal bovine serum, 1mM sodium pyruvate, and penicillin/streptomycin. To measure the cAMP intoxication of J774A.1 cells by ACT or

antibody neutralization, J774A.1 cells were seeded at $4\times10^4/cm^2$ in 24-well plates (Costar) one day before the assay. ACT alone or with antibodies was diluted in DMEM without supplements in a final volume of 1 mL; base DMEM media contains 1.8 mM $CaCl_2$. ACT was used at 125 ng/mL in all assays unless otherwise specified; antibodies were present at 160-fold molar excess. While ACT and antibody mixtures incubated at room temperature for 30 min, cells were washed twice with plain DMEM prior to addition of 480 µL of antibody-ACT solution to duplicate wells. The plate was incubated at 37˚C for 30 min in a CO_2 incubator, followed by two washes with cold PBS. Lysis solution (500µL; 0.1N HCl, 0.1% Triton X-100) was added into each well, and plate was rocked on ice for 10min. The lysates were transferred into 1.5ml tubes and boiled for 10min to inactivate ACT and cAMP hydrolyzing enzymes. To assess cAMP intoxication or antibody neutralization in CHO-K1 cells, ACT was used at 250 ng/mL, with all other assay conditions held constant.

The resulting cellular lysates were clarified by centrifugation at 13,000 g for 5min. The supernatant was diluted 6-fold with 200mM Hepes, 150mM NaCl, 0.05% Tween, pH 8.0 prior to cAMP measurement using a competition ELISA as described by Karimova *et al*. [152]. All assays were performed at least in duplicate, with cAMP concentrations normalized to total protein concentration in the lysates as measured by BCA assay (Pierce).

2.2.7 J774A.1 cell lysis assay

Cell lysis was monitored by enzymatic activity of lactate dehydrogenase released into the medium upon cell lysis. J774A.1 cells were seeded at 10^5 cells/well in 96-well round-bottom plates one day before the assay. 100 µL each of ACT alone (0.25 µg/mL) or ACT pre-incubated with scAbs (10 µg/mL, 160-fold molar excess) in plain DMEM

were added to triplicate wells and incubated for 2 hrs at 37 ˚C. Then the plate was centrifuged at 250 g for 5min and LDH activity in the supernatants was measured by a colorimetric assay with the CytoTox 96 kit (Promega, WI, USA). After subtracting the background signal from control wells without ACT, the sample absorbance at 490 nm was normalized to ACT-only controls as follows: 100% * [$A_{490\ (ACT+antibody)}$–$A_{490\ (no\ ACT)}$]/[$A_{490\ (ACT\ \ only)}$- $A_{490\ (no\ ACT)}$].

2.2.8 Analysis of ACT-integrin binding by ELISA

Recombinant murine $\alpha_M\beta_2$ integrin (R&D Systems) was coated at 1μg/mL in PBS at 4˚C overnight, and blocked with M-PBST. ACT or purified domains were serially diluted and incubated for 1h at room temperature, followed by detection with polyclonal rabbit anti-ACT antibody and HRP-conjugated goat anti-rabbit antibody. To assess the effect of antibodies on ACT binding to integrin, ACT (1 μg/mL) was mixed with equal volume of serially diluted antibody (5, 1.6, 0.5 and 0-fold molar excess) and incubated for 1h at room temperature before transferring to blocked $\alpha_M\beta_2$ ELISA plate. The bound ACT was detected as described above.

2.2.9 Protein conjugation and flow cytometry

ACT was dialyzed against HBSC (50mM Hepes, 150mM NaCl, 2mM $CaCl_2$ pH 8.0) to remove urea, and then biotinylated with 100-fold molar excess of EZ-Link Sulfo-NHS-LC-Biotin (Thermo Scientific) at room temperature for 2-3 h before quenching with 1M Tris (pH 8.0) and dialysis against HBSC overnight in 4 ˚C. Biotinylated ACT (B-ACT; 210 μL of 0.8 μg/mL) was incubated with equal volume containing 120 μg/mL purified scAb (M2B10, M1H5, M1F11, and M1C12) in DMEM + 1% BSA at room temperature for 30min. Then, 200μL of the incubated mixtures was added to 4×10^5 washed J774A.1 cells in duplicate, and incubated on ice for 30min to allow ACT binding

but not internalization. After two washes with FACS buffer (HBSC + 2%FBS), 200μL of 1:500 phycoerythrin (PE)-conjugated Streptavidin (BioLegend) was used to detect cell-associated biotinylated ACT. After 20min incubation on ice and three washes, the cells were finally resuspended in 600μL FACS buffer and analyzed on an LSR Fortessa II. Data analysis was performed with Flowjo software (V10).

2.2.10 *Bordetella* culture

To evaluate ACT neutralization in the context of the whole bacterium, *B. pertussis* Tohama I was grown on Bordet Gengou agar plate supplemented with 15% defibrinated sheep blood (BD) at 37°C for 4 to 5 days. Bacteria were then inoculated into modified synthetic Stainer-Scholte medium (SSM) and grown at 37°C with shaking at 225 rpm for 20~24 h, to an OD600 of 0.7~1.0. Bacteria were pelleted by centrifugation at 5,000 g for 10 min, resuspended in PBS, and diluted to an OD_{600} of 0.4 in DMEM + 10% heat-inactivated (HI) FBS; then mixed with equal volume of serially diluted neutralizing or control IgGs in DMEM+10% HI-FBS, and incubated at room temperature for 20min before addition to adherent J774A.1 cells and incubation of 1hr at 37˚C. Intracellular cAMP level was then measured as previously described.

To see if neutralizing antibodies bind the whole bacteria, ~10 fresh *B. pertussis* and *B. parapertussis* colonies on Bordet Gengou agar plates were scraped off using disposable inoculation loops, dislodged into FACS buffer (HBSC-1%BSA, filtered through 0.22 μm filter) in microfuge tubes and washed 3 times (6,000g, 4min). The OD_{600} was measured and adjusted to 1.0. Then 10 μL each of the bacteria were added into 100 μL of antibodies (10 μg/mL for anti-LOS antibody (D26E, Life Technologies); 100 μg/mL for M2B10, M1H5, irrelevant mAb, and anti-ACT rabbit polyclonal antibody). After 30 min incubation on ice, the samples were washed twice before

detection with 1:50 fluorescent antibodies (Alexa647 anti-human Fc for M2B10, M1H5, and irrelevant mAb; Alexa647 anti-mouse Fc for D26E; FTIC anti-rabbit IgG for rabbit polyclonal antibody). After 30min incubation on ice, the samples were washed twice before resuspension in 700 μL FACS buffer and analyzed on an LSR Fortessa II. The threshold rates were 100~500 events/sec when running at the highest flow rate.

2.2.11 Affinity measurement of the neutralizing antibodies by KinExA

Aliquots of 200 mg polymethylmethacrylate (PMMA) beads (Sapidyne Instruments) were coated with 1mL of 10 or 20 μg/mL of RTX_{751} diluted in HBSC at 4˚C overnight on a rotator. The beads were washed by settling for 1min at room temperature and removal of the supernatant. Beads were blocked with HBST + 1% BSA for 1hr at room temperature on a rocker. After washing, the beads were resuspended in 1mL of blocking solution and transferred to 40mL glass reservoir containing 27mL of running buffer (50 mM Hepes, 150mM NaCl, 0.05% Tween-20, 2 mM $CaCl_2$, 1mg/mL BSA, 0.02% sodium azide, pH 7.5). The amount of beads to charge the sample line to the appropriate height was determined empirically. Then, M1H5 or M2B10 IgG (concentrations near estimated K_d) was passed through the packed beads, followed by detection of bound antibody with Alexa647 anti-human Fc antibody. Concentrations of 2nM for M1H5 and 3nM for M2B10 generated signal intensities of 0.5~1.5V. Next, different concentrations of RTX_{751} was pre-incubated with 2nM M1H5 or 3nM M2B10 for 1hr at room temperature before flowing through packed beads to determine the concentrations of antigen to yield 0 or 100% maximal signal. Finally, RTX_{751} at a full range of concentrations were pre-incubated with the fixed concentrations of M1H5 or M2B10 before measuring the amount of antibody bound to the RTX_{751}-coated beads. The beads were discharged after each run and re-packed using fresh beads from the reservoir.

Each concentration of antigen was performed in duplicates. The experiments were carried out on a KinExA 3000 (Sapidyne Instruments). And data was analyzed using KinExA Pro software based on equations described by Ohmura *et al.* [153].

2.3 RESULTS

2.3.1 Mouse immunization and antibody phage display library construction and panning

To determine whether a single ACT domain dominates the immune response and to identify neutralizing antibodies, we used phage display to analyze murine antibody repertoires after ACT immunization. Two mice were immunized intraperitoneally with 17μg of ACT in complete Freund's adjuvant and four weeks later boosted subcutaneously once with incomplete Freund's adjuvant. Anti-ACT titers in sera were determined by ELISA (Figure 2.1A). Both mouse #1(M1) and #2 (M2) showed satisfactory serum antibody response toward ACT, with M2 having ~10 fold higher titers than M1 at week 4 (4 weeks after the first immunization) and week 6 (2 weeks after the second immunization). Both 6-week sera neutralized the cAMP intoxication of CHO-K1 cells by ACT at a 1:400 dilution (Figure 2.1B), indicating the presence of neutralizing antibodies.

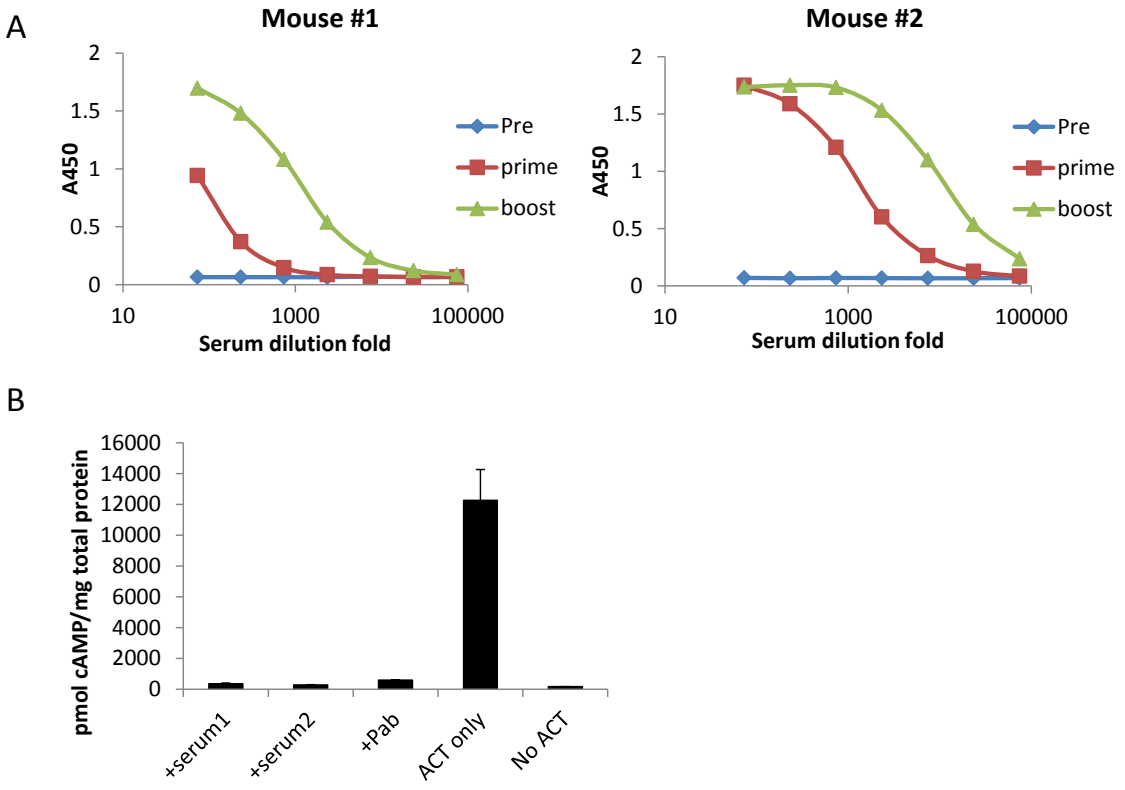

Figure 2.1: Mouse immunization with full-length ACT.

Two mice were immunized intraperitoneally with 17 µg of ACT in complete Freund's adjuvant and boosted subcutaneously once with incomplete Freund's adjuvant. (A) Blood samples were collected before immunization, 4 weeks after the first immunization, and 2 weeks after the second immunization. Sera were serially diluted starting from 100-fold dilution on ELISA plates coated with 1 µg/mL ACT. (B) 250 ng/mL ACT was incubated with 400-fold diluted sera or 10 µg/mL rabbit anti-ACT polyclonal antibody (Pab) before adding to CHO-K1 cells. After incubation for 30 min at 37˚C, the intracellular cAMP levels were measured by ELISA and normalized to total protein concentrations in the lysates.

The spleens were harvested, and each was used to construct an antibody phage-display library as described by Krebber *et al.* [148], containing ~10^7 total transformants. The resulting libraries (input1) from two mice were panned separately against ACT coated in 8-wells of a 96-well plate. For the first round, plates were washed 5 times with PBST. After elution of the bound phage with 0.1 N HCl and neutralization with 2M Tris

base (output1), half was used to infect log-phase *E. coli* XL-Blue. The amplified phage libraries (input2) were used for the more stringent second round panning, in which the plates were washed 10 times before elution (output2). To monitor the enrichment of ACT-specific antibodies during the panning process, the input phage libraries of each round were tested for binding to ACT by ELISA. The input1 phage from both libraries showed barely detectable binding with ACT. After only one round of panning, the input2 showed significant specific binding to ACT (Figure 2.2). In order to maintain maximal diversity, a third round of panning was not conducted.

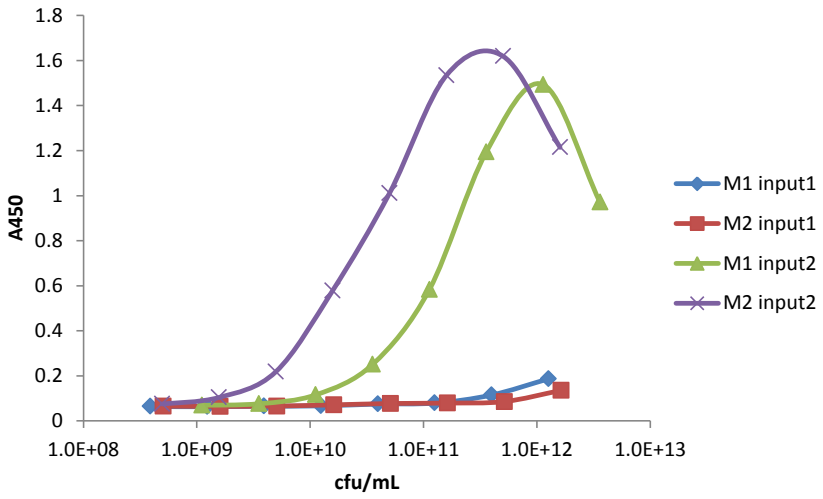

Figure 2.2: Monitor panning enrichment by Phage ELISA.

Input1 and input2 phage libraries from mouse #1 and #2 were titrated on ELISA plate coated with 1 µg/mL ACT. The concentrations of phage (colony forming unit/mL, cfu/mL) were determined by infecting *E. coli* cells with serially diluted phage and enumeration of the resulting colony on agar plate with ampicillin.

To minimize the dominance by clones with faster growth rates, two methods were used for the propagation of eluted phage (output1): *E. coli* XL-blue cells were infected by the eluted phage, rescued by helper phage, and then either plated on agar plates or grown in liquid culture. It was thought that plating would allow the clones with slower growth

rates to form colonies. Ninety individual clones from the output2 of each library were grown in 96-well plates and assessed for ACT binding by phage ELISA. Of these, 57 and 60 clones from the two libraries yielded signals two-fold above background, respectively (Table 2.1).

Table 2.1: Monoclonal phage screening by ELISA

M1

	1	2	3	4	5	6	7	8	9	10	11	12
A	0.074	0.074	0.54	0.069	0.859	0.07	0.073	0.073	0.615	1.372	0.071	0.067
B	0.066	0.064	0.064	0.069	0.072	0.072	0.073	1.302	0.072	1.226	0.07	1.258
C	0.062	0.066	0.068	0.067	0.3	0.071	0.07	0.067	0.066	0.083	0.548	1.142
D	0.063	0.066	1.287	1.096	0.069	0.069	0.068	0.113	1.328	1.199	1.476	1.543
E	0.514	1.041	0.373	1.632	1.156	0.065	0.573	1.112	0.906	0.999	1.103	1.291
F	0.574	1.398	0.445	0.619	1.493	0.669	1.196	0.228	0.911	1.481	0.455	1.496
G	0.54	1.137	0.605	1.18	1.235	1.294	0.822	0.468	0.823	0.687	1.48	1.443
H	0.68	1.264	1.615	1.079	0.739	1.338	0.262	0.392	0.836	0.25	0.148	0.065

M2

	1	2	3	4	5	6	7	8	9	10	11	12
A	1.381	0.076	0.067	0.803	0.069	0.474	0.069	0.071	1.099	0.069	0.883	0.069
B	0.068	0.072	0.07	0.071	1.154	0.067	0.068	1.077	0.068	1.051	0.067	0.067
C	1.068	1.417	1.171	0.075	0.072	1.104	0.069	1.09	0.113	0.067	1.344	0.068
D	1.242	1.296	0.077	0.981	1.495	0.075	0.072	1.163	1.049	0.071	1.28	1.3
E	0.335	1.52	0.915	1.176	1.251	1.117	1.176	0.654	1.226	0.559	1.277	1.326
F	1.452	0.069	0.187	0.066	1.344	0.065	1.11	1.239	1.137	1.366	1.208	0.224
G	1.3	1.292	1.444	1.491	0.21	1.372	1.129	1.208	1.351	1.245	0.066	0.395
H	1.281	1.304	0.548	1.406	1.328	1.3	0.203	0.497	0.093	0.114	0.065	0.064

Individual *E. coli* colonies infected by output2 phage from M1 and M2 were inoculated into 96-well plates and grown for monoclonal phage production. Colonies on row A-D were from phage amplified through the plating method. Colonies on row E-H were from phage amplified in the liquid medium. The supernatants containing secreted phage were diluted 2.5 fold with M-PBST in ELISA plates coated with 1 µg/mL ACT. After incubation and washing, bound phage was detected with 1:2000 HRP-conjugated anti-M13 antibody. Wells with absorbance two-fold above background were highlighted and defined as positive. Wells H7-H11 were positive controls—phage clones known to bind ACT; H12 was negative control—no *E. coli* inoculated.

In order to determine the unique positive clones, colony PCR was performed to amplify the VL-VH region, with the resulting PCR products digested with *BstN*I and analyzed on agarose gels (Figure 2.3). Phagemid plasmids were extracted from clones with unique digestion patterns and sent for DNA sequencing. 29 and 21 unique sequences were determined from library M1 and M2 respectively.

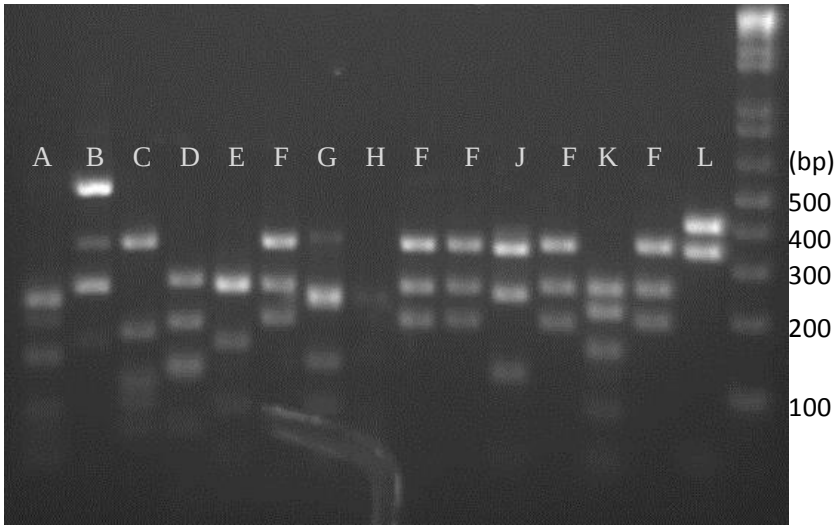

Figure 2.3: Fingerprint by colony PCR and *BstN*I digestion.

Representative fingerprinting. Positive clones identified by phage ELISA were chosen for colony PCR followed by digestion with *BstN*I. The letters above each lane represent unique digestion patterns.

2.3.2 Most binders bind the RTX domain

To determine the domain specificities of unique antibodies, monoclonal phage was assessed for binding to individual domains by ELISA (Table 2.2). Few antibodies bound the catalytic domain; none bound the hydrophobic domain, while the rest (27 of 29 and 20 of 21, respectively) bound the RTX_{985} domain. This observed high frequency of RTX_{985}–specific antibodies concurs with previous report by Lee *et al.* that the majority of

antibodies discovered by hybridoma technology recognized the RTX domain and report by Betsou *et al.* that this domain may be immunodominant [147, 154].

Table 2.2: Single dilution phage ELISA for epitope grouping.

	ACT	1-400	399-1060	985-1706
M1-A3	1.9652	0.1014	0.0982	1.6337
M1-A5	1.9638	0.0796	0.0794	1.441
M1-A9	1.8463	0.0786	0.0929	1.516
M1-B12	1.8217	0.0728	0.0823	1.6892
M1-C11	1.8666	0.075	0.0772	1.8213
M1-C12	1.8264	0.0705	0.0826	1.8347
M1-D3	1.7286	0.0758	0.0897	1.8421
M1-D9	1.7636	0.0722	0.0874	1.6915
M1-E10	1.1071	0.0757	0.0815	0.5097
M1-E11	1.2157	0.0732	0.0877	1.1108
M1-E12	1.1633	0.0716	0.087	1.1541
M1-E2	1.0106	0.0682	0.0987	0.9874
M1-E3	1.162	0.0701	0.0924	0.9449
M1-E4	0.9522	0.0819	0.1027	0.9792
M1-E8	1.4392	0.0671	0.0773	1.2082
M1-E9	1.1212	0.0797	0.095	1.1664
M1-F10	1.2058	0.0686	0.0852	1.1693
M1-F11	1.3675	1.4022	0.0728	0.1147
M1-F3	0.9466	0.0728	0.0968	0.2269
M1-F5	1.0568	0.0707	0.0761	1.1192
M1-F7	1.3175	0.0661	0.0773	0.9668
M1-F8	0.908	0.0647	0.069	0.9826
M1-G11	1.3277	0.0768	0.0887	1.162
M1-G4	1.3453	0.0823	0.0681	1.2439
M1-H1	1.8285	0.0737	0.0953	1.8631
M1-H2	1.6972	0.0743	0.0963	1.7145
M1-H4	1.7476	0.0694	0.075	0.5275
M1-H5	1.614	0.0724	0.085	1.3939

	ACT	1-400	399-1060	985-1706
M2-A6	1.8884	0.0756	0.0975	0.402
M2-B10	1.8739	0.0698	0.0822	1.9024
M2-B5	1.858	0.0746	0.0784	1.2708
M2-B8	1.8034	0.0676	0.0743	0.989
M2-C11	1.8338	0.0815	0.0953	1.3191
M2-C2	1.805	0.0828	0.0882	1.2902
M2-D8	1.8378	0.0804	0.0897	1.2218
M2-E1	0.9076	0.0734	0.0849	0.3537
M2-E10	1.1518	0.0702	0.0784	1.2366
M2-E3	1.1022	0.071	0.0797	0.6464
M2-E4	1.2694	0.0782	0.0846	1.1732
M2-E5	1.2655	0.0862	0.0737	1.1883
M2-E6	1.2053	0.0895	0.0745	1.0815
M2-E7	1.1924	0.0842	0.0782	1.2028
M2-F1	1.8828	0.0791	0.0986	1.9251
M2-F3	1.7444	0.0714	0.0892	1.8767
M2-F5*	1.2457	0.0675	0.0681	1.4011
M2-F9	1.2476	0.065	0.0729	1.139
M2-G5	1.4581	1.4718	0.0655	0.0638
M2-G9	1.3462	0.0975	0.1193	0.9175
M2-H3	1.2171	0.0727	0.095	1.4757
Neg ck	0.143	0.07	0.119	0.066

Unique phage clones confirmed by sequencing were grown, purified, diluted 6-fold with M-PBST, and tested for binding to ACT and domains (CAT_{400}, $HP_{399\text{-}1060}$, and RTX_{985}) coated on ELISA plates. The numbers were absorbance at 450nm. Positive wells were highlighted. The table was compiled from assays performed on different days.

2.3.3 Identification of neutralizing antibodies using *in vitro* cell-based assay

Next, we screened unique antibodies identified from phage libraries for the ability to neutralize ACT activities using an *in vitro* cell-based assay. There are several steps

during ACT intoxication of cells that are susceptible to antibody-mediated neutralization including receptor binding, membrane insertion, and translocation. Interference with any of these will be reflected in decreased intracellular cAMP accumulation in or reduced lysis of target cells. For this assay, we employed the murine macrophage cell line J774A.1 bearing the $\alpha_M\beta_2$ integrin.

For the neutralization assay, antibodies were expressed as recombinant single-chain antibody fragments (scAb), comprised of the variable light chain (V_L) joined to a flexible $(Gly_4Ser)_2$ linker and the variable heavy chain (V_H), followed by a C-terminal human kappa chain constant region to increase solubility and serve as a detection handle [17]. Based on multiple sequence alignment, 31 antibodies with unique CDR sequences were selected for scAb expression (Figure 2.4 A and B). Ten scAbs either expressed poorly (<200 μg/L culture) or bound ACT weakly (concentration >238 nM required for saturation) and were not tested further.

To identify antibodies neutralizing ACT function, ACT and individual scAbs were incubated at a 1:160 molar ratio before addition to adherent J774A.1 cells and determination of intracellular cAMP levels by competition ELISA. Of the 21 scAbs tested, nine reduced the cAMP level by more than 90%, as compared to cells treated with ACT alone, which we considered highly neutralizing in this assay (Figure 2.4C). We also determined the ability of these scAbs to rescue J774A.1 cells from lysis using a lactate dehydrogenase release assay, observing a strong correlation with cAMP neutralization (Figure 2.4D). This is in agreement with findings by Basler *et al*. that intracellular ATP depletion is sufficient to promote cell lysis [155]. Notably, all neutralizing antibodies identified recognize the RTX domain.

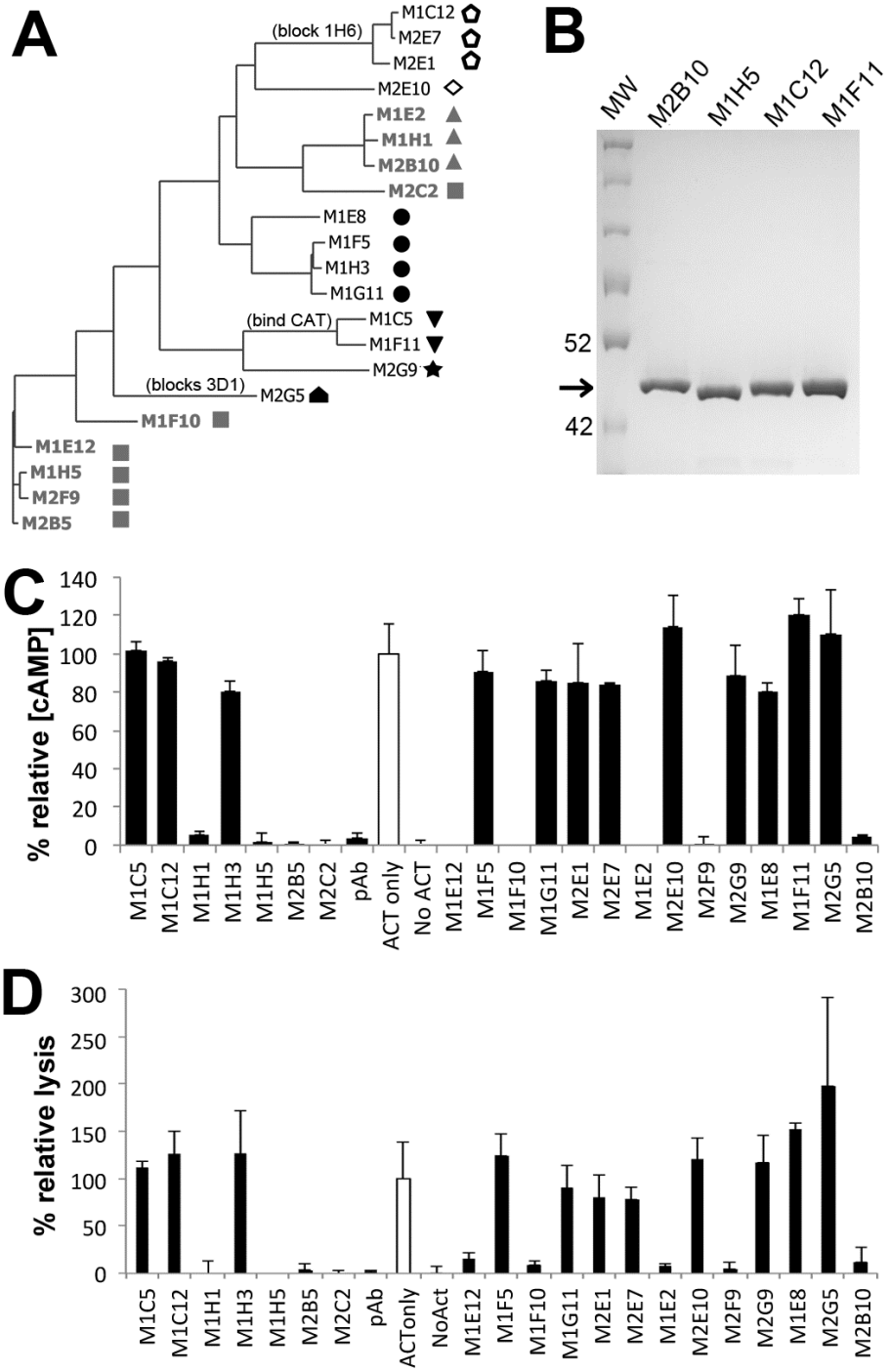
A
(block 1H6)
M1C12
M2E7
M2E1
M2E10
M1E2
M1H1
M2B10
M2C2
M1E8
M1F5
M1H3
M1G11
(bind CAT)
M1C5
M1F11
M2G9
(blocks 3D1)
M2G5
M1F10
M1E12
M1H5
M2F9
M2B5
B
MW
M2B10
M1H5
M1C12
M1F11
52
42
C
% relative [cAMP]
0
20
40
60
80
100
120
140
M1C5
M1C12
M1H1
M1H3
M1H5
M2B5
M2C2
pAb
ACT only
No ACT
M1E12
M1F5
M1F10
M1G11
M2E1
M2E7
M1E2
M2E10
M2F9
M2G9
M1E8
M1F11
M2G5
M2B10
D
% relative lysis
0
50
100
150
200
250
300
M1C5
M1C12
M1H1
M1H3
M1H5
M2B5
M2C2
pAb
ACTonly
NoAct
M1E12
M1F5
M1F10
M1G11
M2E1
M2E7
M1E2
M2E10
M2F9
M2G9
M1E8
M2G5
M2B10

Figure 2.4

Figure 2.4: ACT immunization induces a diverse antibody response.

(A) A phylogenetic tree depicting antibody sequence relatedness was generated using the light and heavy variable region amino acid sequences. Neutralizing scAbs are colored gray, with unique shapes denoting recognition of distinct epitopes among this antibody group as determined by competition ELISA. Hollow shapes denote antibodies whose binding does not depend on the presence of calcium. Antibodies competing with previously characterized monoclonal antibodies are indicated; all antibodies bind RTX except M1C5, M1F11 and M2G5 which bind CAT_{400}. **(B)** Representative SDS-PAGE of scAbs after purification by IMAC and Superdex S200. Arrow indicates expected size of ~40 kDa, 2 μg each of M1F11, M1C12, M1H5, and M2B10 scAbs were loaded. **(C)** Twenty-one unique scAbs identified from the immune phage libraries were tested for the ability to neutralize ACT-mediated increases in intracellular cAMP concentration. ACT was incubated with a 160-fold molar excess of scAb protein before adding to J774A.1 cells. Data is reported as the percent relative cAMP, calculated from the total cAMP concentration in the cellular lysate as determined by cAMP ELISA, divided by the protein concentration of the lysate, and normalized to control cells treated only with ACT (empty bar). Error bars indicate range of duplicate assays. **(D)** The 21 scAbs were evaluated for their ability to rescue J774A.1 macrophages from ACT-induced lysis, using a similar protocol as for cAMP neutralization. Cell lysis was measured via lactate dehydrogenase release using the Cytotox 96 kit (Promega), normalized to control cells treated only with ACT (empty bar) and reported as the percent relative lysis. Error bars indicate standard deviation of triplicate assays.

We next sought to classify neutralizing antibodies based on their recognition of unique or overlapping epitopes. Here, we used a competitive binding ELISA, in which a single phage-displayed antibody was mixed with buffer or a second antibody in the scAb format, added to an ELISA well coated with ACT, followed by detection of bound phage remaining in the well. Reduced signal in the presence of a second antibody compared to phage antibody alone indicates competition between the two antibodies for the same or overlapping epitopes. Using this approach, the nine neutralizing antibodies were divided into two groups binding non-overlapping epitopes, while non-neutralizing antibodies recognized four unique epitopes, for a total of six epitopes represented in this study (Figure 2.4A, Figure 2.5, and data not shown).

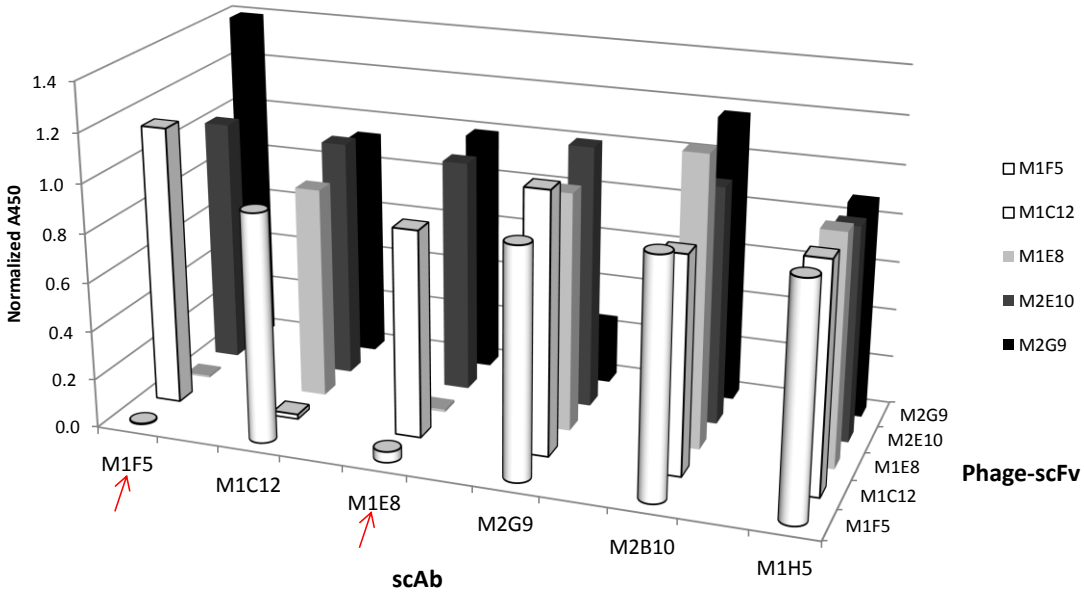

Figure 2.5: Competition ELISA.

ELSIA plates were coated with 1 µg/mL ACT. Sub-saturating concentration of five phage-displayed non-neutralizing scFv and excessive amount of competing scAb (200 nM) were combined and added to ACT coated wells. After incubation, bound phage was detected by HRP-conjugated anti-M13 antibody. M1F5 and M1E8 competed with each other as scAb and phage displayed formats.

One representative antibody binding each neutralizing epitope was selected based on sequence uniqueness, expression level, and binding affinity for conversion into a full-length chimeric immunoglobulin, with human IgG1 and kappa constant domains (Figure 2.6A). ELISA assays with the two RTX constructs helped to further define the epitopes recognized by these two antibodies, named M1H5 and M2B10. Both antibodies bound RTX_{751}* with almost identical affinity as full-length ACT (Figure 2.6B), while M1H5 bound the shorter RTX_{985} domain weakly (Figure 2.6C), suggesting that its epitope is not fully contained or properly presented in this construct.

To determine whether the antibodies identified here bind epitopes overlapping with those of previously defined murine monoclonal antibodies [147], we performed a

second set of competition ELISAs (Figure 2.6D and data not shown). None of the murine antibodies competed with M2B10 or M1H5 for ACT binding, demonstrating that these antibodies recognize previously undescribed neutralizing epitopes in the RTX region.

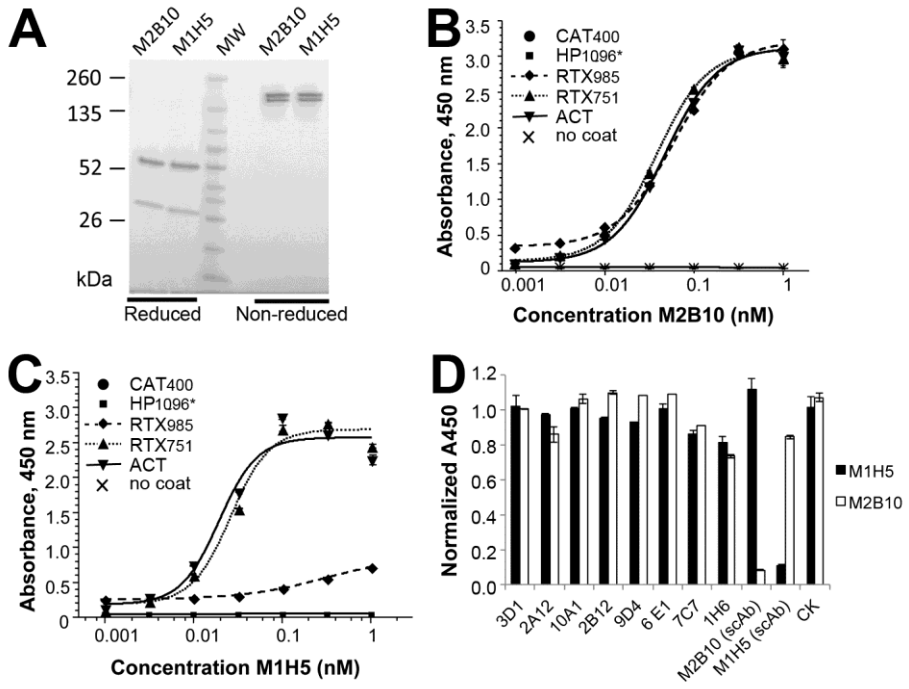

Figure 2.6

Figure 2.6: Two novel neutralizing epitopes are present in the RTX domain.

(A) Two representative neutralizing scAbs were converted to chimeric IgG1/κ antibodies, in which the murine variable regions are appended by human constant domains. These were transiently expressed in CHO-K1 cells and purified by $(NH_4)_2SO_4$ precipitation and protein A affinity chromatography. SDS-PAGE (4-20% gradient gel, 2 μg loaded) shows high purity and expected size of the recombinant IgG: 25 kDa (light chain) and 50 kDa (heavy chain) when reduced, 150 kDa under non-reducing condition. ELISA demonstrates the ACT domain specificity of the **(B)** M2B10 and **(C)** M1H5 IgG antibodies. Microtiter plates were coated with ACT or ACT domains at equimolar concentrations, followed by serial dilution of antibody from 1 nM followed by detection with anti-human Fc antibody-HRP conjugate. **(D)** Competition ELISA determined that the M2B10 and M1H5 antibodies bind novel, non-overlapping epitopes. A 200-fold molar excess (20nM) of previously described murine mAbs (3D1, 2A12, 10A1, 2B12, 9D4, 6E1, 7C7, 1H6) [147] or scAb versions of M1H5 and M2B10 were mixed with M2B10 and M1H5 IgG (0.1nM) and incubated on ACT-coated ELISA plate, with bound M2B10 or M1H5 detected as above. The absorbance was normalized to that of M2B10 or M1H5 with no competitor; absorbance significantly <1.0 indicates competition between the antibody pair.

Together, we observed antibodies binding six non-overlapping epitopes on RTX, two neutralizing and four non-neutralizing and all but two requiring the presence of calcium (Figure 2.4A). An representative antibody binding one epitope, M1C12, competes with antibody 1H6, one of the four non-neutralizing RTX binding antibodies described by Lee *et al*. [147]. Their remaining three anti-RTX antibodies bind unique epitopes, suggesting a total of at least nine distinct epitopes in the RTX domain. Identification of new epitopes is not unexpected, since neither hybridoma nor phage-display technology is exhaustive, and each has trade-offs: the former is low-throughput and labor-intensive; whereas the latter does not preserve the pairing between the light and heavy chains and preferentially selects for antibodies with high bacterial expression levels. Even recently described repertoire mining approaches based on high-throughput sequencing of antibodies from individual B cells does not identify the same sequences as phage-display [156].

2.3.4 Effect of calcium on antibody binding

To determine the effect of calcium on antibody binding to ACT, ELISAs were performed using the following diluent: HBST-5% dried non-fat milk, or HBST-1%BSA supplemented with 0.2 mM $CaCl_2$, 2 mM $CaCl_2$, 20 mM $CaCl_2$, or 5 mM EDTA. Washing buffer was HBST for all samples. The diluents for the HRP-conjugated secondary antibodies were kept the same as the diluent used for the primary antibody in respective wells. There was no detectable binding when HBST-1%BSA + 0.2 mM $CaCl_2$ or 5 mM EDTA was used as diluent. Only when calcium concentration was above 2 mM did the antibody binding recover to the same level as in 5% milk, which naturally contains > 10mM free Ca^{2+} (Figure 2.7A).

The RTX domain contains 40~45 Asp-Gly rich motifs depending on the consensus criteria. Each repeat binds one Ca^{2+} ion, most of which have low affinities (K_d=0.5~0.8mM); while 3~5 repeats bind Ca^{2+} ions so tight that they could not be removed by EGTA or EDTA without denaturing the protein first. Calcium loading in the high affinity sites was shown to be important for membrane binding and hemolytic activity, while calcium loading in the low affinity sites induced large conformational change that was important for the cAMP intoxication process [157]. Considering the fact that we used PBST-5% milk as diluent and blocking buffer during phage panning, it is not surprising that most of the binders recovered are recognizing calcium-dependent epitopes.

To determine whether calcium is only required for the initial folding of ACT, or need to be present constantly, we coated RTX_{751} or ACT on ELISA plates in the absence or presence of 2 mM $CaCl_2$. The wells were blocked with HBST-1%BSA +/- 2 mM $CaCl_2$. Then, M2B10 and M1H5, diluted to 10 nM in HBST-1%BSA +/- 2 mM $CaCl_2$, were added to the wells. Washing buffer was HBST for all samples. The diluent for the

HRP-conjugated secondary antibodies were kept the same as the diluent used for the primary antibody in respective wells. For both ACT and RTX_{751}, coating in the presence of 2 mM $CaCl_2$ but incubating with antibodies in the absence of calcium yielded no detectable signal. The presence of 2 mM calcium during antibody incubation yielded similar signal intensities, regardless of the calcium concentration in the coating solution. The result suggests that the calcium-dependent folding is a reversible process, and the epitopes of M2B10, M1H5 and other antibodies might require an RTX conformation with full calcium loading.

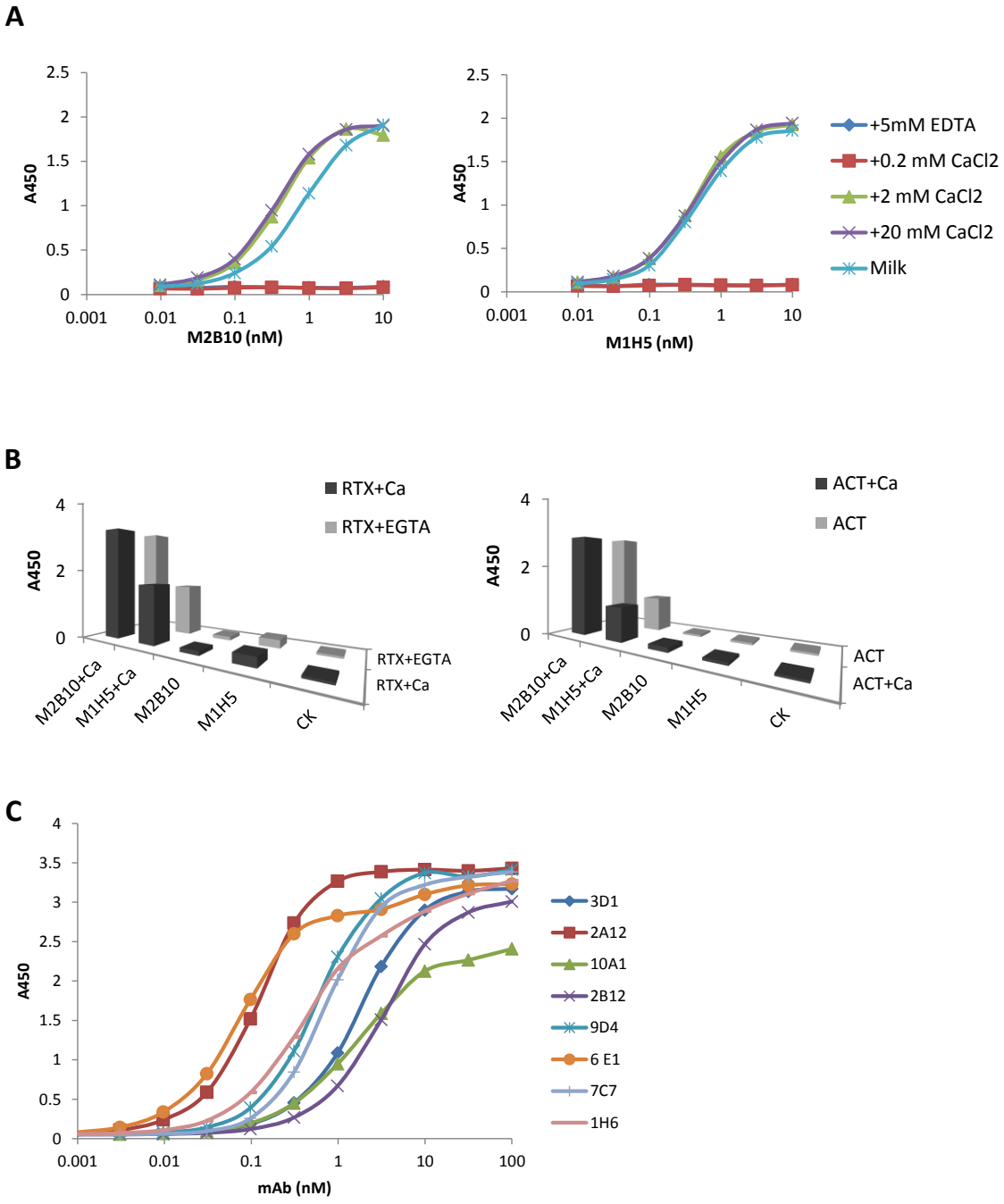
A
A450
M2B10 (nM)
M1H5 (nM)
+5mM EDTA
+0.2 mM CaCl2
+2 mM CaCl2
+20 mM CaCl2
Milk
B
RTX+Ca
RTX+EGTA
ACT+Ca
ACT
M2B10+Ca
M1H5+Ca
M2B10
M1H5
CK
C
mAb (nM)
3D1
2A12
10A1
2B12
9D4
6 E1
7C7
1H6

Figure 2.7

Figure 2.7: Effect of calcium on antibody binding.

(A) ELISA plates were coated with 0.2 µg/mL of ACT diluted in PBS. After washing with HBST, different columns were blocked with HBST-1%BSA supplemented with 0.2 mM $CaCl_2$, 2 mM $CaCl_2$, 20 mM $CaCl_2$, or 5 mM EDTA; or HBST-5% non-fat milk. Then, M2B10 or M1H5 were serially diluted in respective blocking solution. For detection, anti-human Fc HRP antibody was diluted in respective blocking solution for each column. (B) RTX_{751} was coated in HBS + 5mM EGTA or HBS + 2 mM $CaCl_2$; ACT was coated in HBS or HBS + 2 mM $CaCl_2$. The wells were blocked with HBST-1% BSA +/- 2mM $CaCl_2$. Then, M2B10 and M1H5 diluted to 10 nM in HBST-1%BSA +/- 2mM $CaCl_2$ were added to the wells. Washing buffer was HBST for all samples. The diluents for the HRP-conjugated secondary antibodies were kept the same as the diluent used for the primary antibody in respective wells. (C) ELSIA plate was coated with 1 µg/mL ACT in PBS and blocked with HBST-1% BSA. Monoclonal antibodies were serially diluted in blocking buffer. After incubation and washing, bound antibodies were detected with 1:4000 HRP-conjugated anti-mouse Ig(H+L) antibody.

In contrast to our findings, only one of the 12 mAbs reported by Lee *et al.*, 1H6, was calcium dependent as determined by immunoblotting [147, 158]. However, in our ELISA assay, it bound ACT in the absence of calcium (Figure 2.7C).

2.3.5 Mechanism-of-action of the neutralizing antibodies

ACT primarily targets cells bearing the $\alpha_M\beta_2$ receptor under conditions in which the RTX domain assumes a receptor-binding competent conformation mediated by the presence of calcium ions and post-translational acylation [32]. Combining this with our observation that the M2B10 and M1H5 antibodies showed a much weaker neutralizing effect at the same 160-fold molar excess when CHO-K1 cells lacking this receptor were used than when J774A.1 cells expressing the receptor were used (Figure 2.8A), we hypothesized that these two antibodies act by blocking the interaction between ACT and the $\alpha_M\beta_2$ integrin.

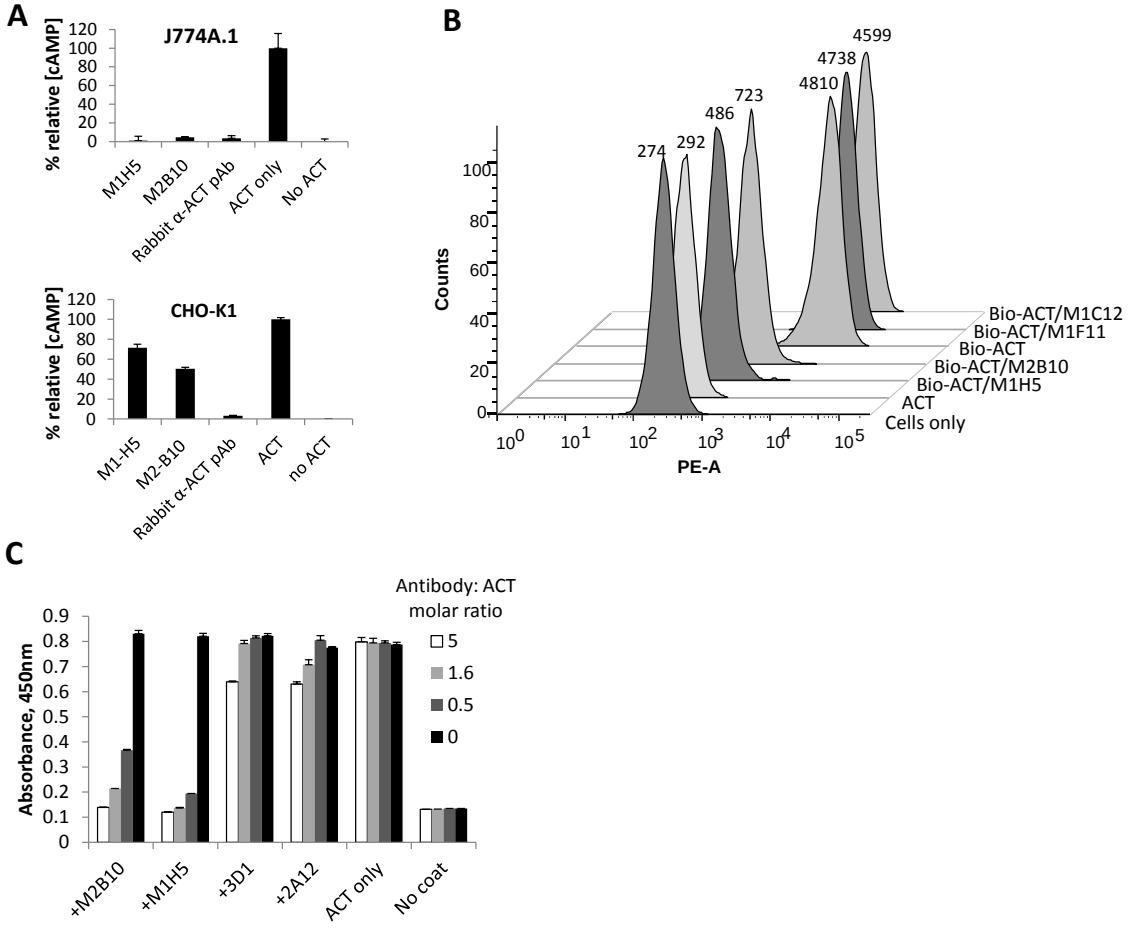

Figure 2.8: M2B10 and M1H5 antibodies block the ACT - $\alpha_M\beta_2$ integrin interaction.

(A) Antibody neutralization of cAMP intoxication using J774A.1 presenting the $\alpha_M\beta_2$ receptor and CHO-K1 cells lacking the receptor. Both assays were performed with a 160-fold molar excess of scAb over ACT. **(B)** Antibody blockade of ACT binding to J774A.1 cells assessed by FACS. Biotinylated ACT was incubated with a 300-fold molar excess of scAb and added to 4×10^5 J774A.1 suspension cells on ice. After washing, bound biotinylated ACT (B-ACT) was detected with streptavidin-PE and analyzed by FACS (mean fluorescence noted next to each peak). Controls include untreated cells ("Cells only") and cells treated with non-biotinylated ACT followed by streptavidin-PE ("ACT"). **(C)** Antibody blockade of ACT binding to soluble $\alpha_M\beta_2$ integrin by ELISA. ACT (0.5 μg/mL) was incubated with serial dilutions of M2B10, M1H5, 3D1 and 2A12 antibodies at 5-, 1.6- and 0.5-fold molar excess, before transfer to an ELISA plate coated with murine $\alpha_M\beta_2$ integrin. Bound ACT was detected with rabbit anti-ACT polyclonal antibody followed by HRP-conjugated goat anti-rabbit IgG antibody.

To test this hypothesis, we used flow cytometry to monitor ACT bound to J774A.1 cells in the presence or absence of the M2B10 or M1H5 scAb. Biotinylated ACT (toxicity reduced but still active, data not shown) was incubated with a 300-fold molar excess of neutralizing or non-neutralizing scAbs, added to J774A.1 cells and detected with phycoerythrin-conjugated streptavidin by FACS. The M2B10 and M1H5 antibodies significantly reduced binding of ACT-biotin to J774A.1 cells, while two non-neutralizing control scAbs (M1F11 and M1C12) had no significant effect (Figure 2.8B). This difference was not due to affinity, as all four scAbs have similar affinities (EC_{50}=0.3-0.7 nM; data not shown).

To further confirm that the diminished binding of ACT to J774A.1 cells was due to interference with a specific receptor, a competition ELISA with soluble $\alpha_M\beta_2$ integrin was performed. ACT (0.5 μg/mL) was incubated with the M2B10, M1H5, M1F11 or 3D1 antibodies (IgG) in molar ratios ranging from 5 to 0.5 and transferred to an $\alpha_M\beta_2$ integrin-coated plate. The result was consistent with the flow cytometry assay: M2B10 and M1H5 reduced ACT binding to immobilized $\alpha_M\beta_2$ integrin in a dose-dependent manner, >90% at a two-fold molar excess (Figure 2.8C). In contrast, 3D1, a neutralizing IgG which blocks translocation of the catalytic domain [159] and 2A12, a neutralizing antibody with unclear mode-of-action, had no effect. Minimal non-specific binding was observed under these assay conditions.

2.3.6 Affinity measurement by KinExA

The equilibrium dissociation constants, K_d, of M2B10 and M1H5 were measured by kinetic exclusion assay (KinExA). KinExA is a label-free method based on a principle similar to competition ELISA. The K_d analysis requires immobilization of one binding partner (A) on solid phase. Fixed concentration of the other binding partner (B) is pre-

incubated with a series of concentrations of A until equilibrium is reached. Then mixtures are passed through the packed beads. Free B will be captured by immobilized A on the beads, and quantified by a fluorescent antibody. The pre-formed AB complex in the solution is not affected due to the short contact time, thus it is "kinetically excluded" from competition with immobilized A.

Here, RTX_{751} antigen was coated on PMMA beads, and M2B10 and M1H5 pre-incubated with RTX_{751} concentration series were passed through the packed beads. Bound antibodies were detected by Alexa647 anti-human Fc antibody. The signal intensity was negatively correlated with antigen concentration. The K_d values for M2B10 and M1H5 were estimated to be 0.8 and 1.5 nM respectively (Figure 2.9).

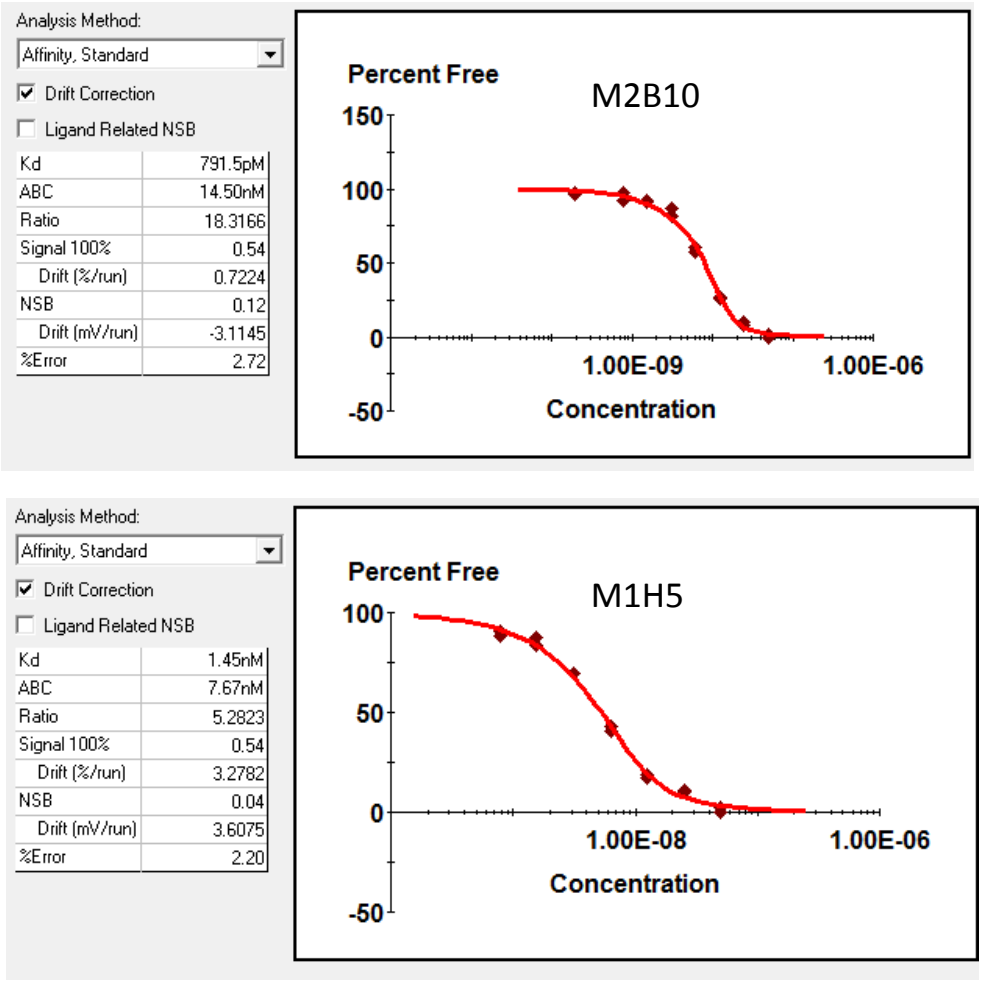

Figure 2.9: Affinity measurement by KinExA.

RTX_{751} was coated on 200 mg PMMA beads. Fixed concentration of M2B10 (3nM) or M1H5 (2nM) was pre-incubated with RTX_{751} ranging from 50 to 0.2 nM for 1hr at room temperature, before being passed through packed RTX_{751}-coated beads. The bound antibodies were detected by Alexa647 anti-human Fc antibody. Each antigen concentration was performed in duplicates. Data was analyzed with KinExA Pro software.

2.3.7 Antibody interaction with live *Bordetella* bacteria

To determine whether ACT neutralization occurs in the context of the whole bacterium, we repeated this assay with live *B. pertussis* instead of purified ACT.

According to Gray *et al.*, newly synthesized ACT is responsible for intoxication [36]. Therefore, *B. pertussis* was washed in PBS to remove any secreted ACT. Bacteria (OD_{600} = 0.2) added to J774A.1 cells resulted in cAMP levels similar to that induced by 125 ng/mL purified ACT. When the M2B10 and M1H5, but not the non-neutralizing M1F11 or 7C7 [103] antibodies, were added with the bacteria, they resulted in dose-dependent reduction of cAMP levels (Figure 2.10). This suggests these antibodies should be able to neutralize ACT in the context of active infection.

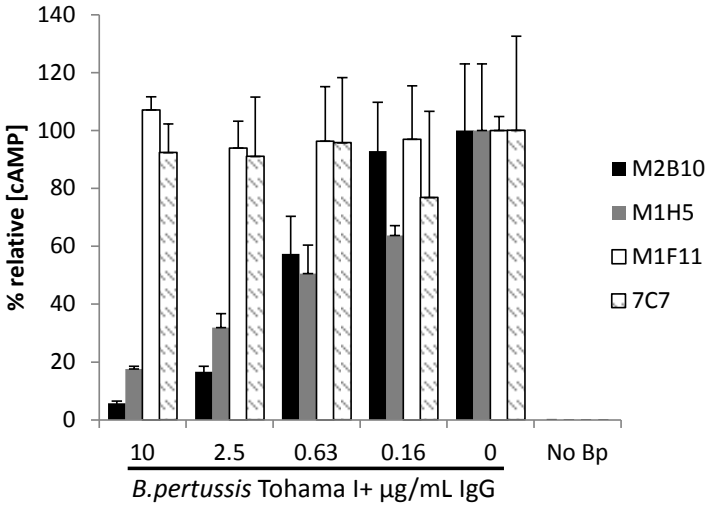

Figure 2.10: Antibody neutralization of ACT secreted by live *B. pertussis*.

Antibodies at 10, 2.5, 0.63, and 0.16 µg/mL were incubated with live *B. pertussis* (OD_{600} = 0.2) before adding to adherent J774A.1 cells. The resulting intracellular cAMP concentrations were measured, normalized to total protein concentration, and expressed as % relative cAMP.

Besides preventing the association of ACT with its cellular receptor, neutralizing antibody could also exert protection *in vivo* by other mechanisms, such as complement dependent cytotoxicity (CDC, or complement mediated killing) or antibody-dependent cell-mediated cytotoxicity (ADCC) toward the whole bacteria. It is known that the

majority of secreted ACT is aggregated on the bacterial surface [143]. Therefore, we tested whether the neutralizing antibodies could bind the whole bacteria via surface ACT. An antibody specific for *B. pertussis* lipopolysaccharide A (LOS-A) was used as positive control, and showed 89.6% positive. *B. parapertussis* has a different lipopolysaccharide (LPS) structure from *B. pertussis* [160], and was used as a negative control. No binding was observed by D26E, suggesting it is specific to the LOS-A structure of *B. pertussis* (data not shown). M2B10 and M1H5 showed 48.5% and 59% positive, respectively. Rabbit polyclonal anti-ACT antibody showed 52.3% positive (Figure 2.11). Although used at 10-fold higher concentration than the anti-LOS antibody (100 µg/mL versus 10 µg/mL), anti-ACT monoclonal or polyclonal antibodies showed much lower binding to *B. pertussis* cells. It is possible that the epitopes on cell-surface associated ACT are no longer intact or fully accessible. Unlike LOS, which is anchored in the bacterial membrane, ACT is only loosely associated with other surface antigens and might come off during the washing or incubation steps. Whether this weak interaction is sufficient to promote CDC or ADCC effect remains to be tested in future experiments.

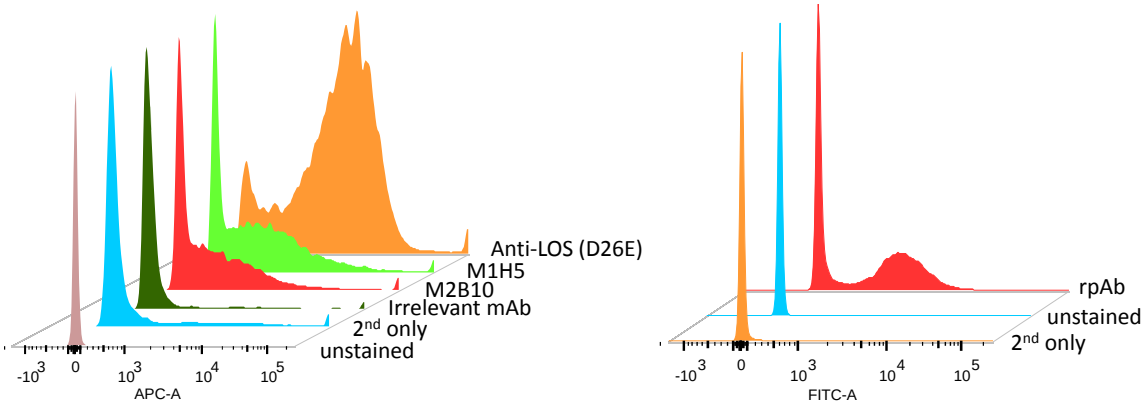

Figure 2.11

Figure 2.11: Antibody binding to *B. pertussis* cells.

B. pertussis and *B. parapertussis* colonies on Bordet Gengou agar plates were scraped off using disposable inoculation loops, dislodged into FACS buffer (HBSC-1%BSA, filtered through 0.22 μm filter) in microfuge tubes and washed 3 times (6,000g, 4min). The OD_{600} was measured and adjusted to 1.0. Then 10 μL each of the bacteria were added into 100 μL of antibodies (10 μg/mL for anti-LOS antibody (D26E, Life Technologies); 100 μg/mL for M2B10, M1H5, irrelevant mAb, and anti-ACT rabbit polyclonal antibody). After 30 min incubation on ice, the samples were washed twice before detection with 1:50 fluorescent antibodies (Alexa647 anti-human Fc for M2B10, M1H5, and irrelevant mAb; Alexa647 anti-mouse Fc for D26E; FTIC anti-rabbit IgG for rabbit polyclonal antibody). After 30min incubation on ice, the samples were washed twice before resuspension in 700 μL FACS buffer and analyzed on an LSR Fortessa II.

2.4 DISCUSSION

Despite its importance in pathogenesis and induction of protective immunity *in vivo*, ACT is not included in current acellular vaccines. Few ACT neutralizing antibodies have been discovered and characterized. Here, we analyzed the immune mouse antibody libraries by phage display, and discovered two novel neutralizing antibodies. Most of the binders recovered from the phage display library bound the RTX region, while the 12 monoclonal antibodies previously identified by Lee *et al.* bound across the different regions of ACT [147]. Furthermore, out of the 6 unique epitopes we identified on RTX domain based on competition ELISA, only one overlaps with one of the four RTX epitopes identified in their study. Several factors might explain this discrepancy. For example, the 12 mAbs discovered by hybridoma technology was a cumulative collection from several different immunizations using different ACT preparations, adjuvants, immunization schedule, and administration routes, which all might affect the outcome of immune response [147]. The selection condition, such as the presence of calcium in binding assays, might also affect the type of antibodies being recovered. Besides, neither hybridoma nor phage-display technology is exhaustive; each has trade-offs: the former is

low-throughput and labor-intensive; whereas the latter does not preserve the pairing between the light and heavy chains and preferentially selects for antibodies with high bacterial expression levels. Even recently described repertoire mining approaches based on high-throughput sequencing of antibodies from individual B cells does not identify the same sequences as phage-display [156]. Selection of the antibodies using yeast display might yield a more diverse population of binders than phage display [161].

A previously discovered potent neutralizing antibody, 3D1, binds a conformational epitope between residues 373-399, adjacent to the catalytic domain, trapping a translocation intermediate and preventing complete delivery of the catalytic domain to the host cytosol [162, 163]. Although rare, we did recover an antibody, M2G5, which bound overlapping epitope with 3D1 but was not neutralizing. Two other antibodies binding the catalytic domain, M1C5 and M1F11, do not compete with 3D1 and are non-neutralizing. Based on the mode-of-action of 3D1, it is possible that its conformational epitope is only transiently present to the immune system during the toxin insertion process and therefore difficult to elicit 3D1-like neutralizing antibodies.

For all the neutralizing and most of non-neutralizing antibodies recovered from our phage libraries, the binding with ACT is dependent on the constant presence of > 2 mM calcium, suggesting we selected against conformational epitopes on folded proteins during phage panning. Interestingly, most, if not all, of the antibodies reported by Lee *et al.* [147] are not calcium dependent. The difference in calcium dependence between our antibodies and theirs is likely due to the different conditions used during antibody selection processes, which might also explain why we observed quite different epitopes.

Our data suggests the mode of action of the two representative neutralizing antibodies is to disrupt the interaction between ACT and its cellular receptor $\alpha_M\beta_2$ integrin. Similar mode-of-action has been observed with other anti-toxin mAbs [164-

166], but it is the first time to be reported in RTX family toxins. The choice of cell line for the *in vitro* cell-based assay was essential for the discovery of these antibodies, as J774A.1 expressing the $\alpha_M\beta_2$ integrin was efficiently protected by the neutralizing antibodies; while CHO-K1 cells not expressing the $\alpha_M\beta_2$ was intoxicated by ACT through a receptor independent mechanism (or through unknown receptors) and was not efficiently protected by M2B10 or M1H5.

Besides directly blocking toxin binding and entry into host cells, neutralizing antibodies might also exert bactericidal activity by binding to the toxin on bacterial surface and inducing complement mediated killing or antibody-dependent cell-mediated cytotoxicity. M2B10 and M1H5 and rabbit polyclonal antibodies all showed significant binding to *B. pertussis* cells, but not as efficiently as anti-LOS antibody as determined by flow cytometry. Possible reasons include the misfolding or loose attachment of ACT on bacterial surface. Whether this weak binding can elicit bactericidal activity remains to be determined in future experiments.

Chapter3: Immunogenicity and protective activity of ACT and individual domains

3.1 INTRODUCTION

The switch from whole-cell pertussis vaccine to acellular vaccines coincides with the recent resurgence of pertussis cases in many developed countries. Accumulating evidence has implicated the current acellular pertussis (aP) vaccine as a major cause. Several factors likely contribute: mismatch between vaccine antigens and circulating strains, induction of a Th1/ Th2 immune response instead of the more effective Th1 response, and a shorter duration of protection [8, 167-169]. Recently, acellular vaccines were shown to only protect against disease symptoms but not subclinical infection and transmission in nonhuman primate model [10, 170].

An improved vaccine better able to prevent disease transmission is an urgent need. However, returning to the original whole cell vaccine is unlikely due to higher rate of adverse reactions and highly variable lot-to-lot efficacy. Alternative strategies include the use of new adjuvants to elicit preferred responses and inclusion of additional highly conserved protective antigens.

ACT has been frequently suggested as a candidate to be included in the next generation acellular vaccine, based on several lines of evidence. First, ACT-deficient *Bordetella* strains have shown significantly compromised colonization and persistence in various mouse models [18-20], while some hypervirulent strains express higher ACT levels [21]. Moreover, active or passive immunization with polyclonal anti-ACT antibodies protected mice against lethal respiratory challenges by *B. pertussis* and *B. parapertussis* [21] and shortened the period of bacterial colonization in the respiratory tract [22]. Finally, natural infection or immunization with whole cell vaccine resulted in strong anti-ACT antibody responses in humans [23], and ACT was present in the more

Chapter 3 is based on previous publication: **Wang, X**, Gray MC, Hewlett EL, and J.A. Maynard, *The Bordetella Adenylate Cyclase Repeat-in-Toxin (RTX) Domain Is Immunodominant and Elicits Neutralizing Antibodies.* **J Biol Chem**, 2015. **290**(6): p. 3576-91. XW and JAM conceived the study. XW performed and analyzed the experiments. MG and EH provided critical reagents. EH provided suggestions. XW and JAM wrote the manuscript.

protective whole cell vaccine and is highly conserved across strains and clinical isolates [3, 4].

However, early reports present inconsistent data regarding the extent of protection conferred by ACT and which part of ACT is most important. Active or passive immunization with ACT was shown to limit bacterial colonization and formation of lung lesions in mice with an efficacy similar to whole cell (wP) or acellular (aP) pertussis vaccines [171-173]. ACT preparations in these early studies were likely contaminated with high levels of *Bordetella* lipooligosaccharide (LOS) or *E. coli* LPS [174]. *B. pertussis* LOS is highly immunogenic and anti-LOS antibodies exhibit complement-dependent bactericidal activities [175, 176]. *E. coli* LPS might also affect the type of response elicited by ACT. More recent studies stringently removed LPS during ACT purification after recombinant expression in *E. coli*, observing a modest synergy when co-administered with aP, but surprisingly, no protection with ACT immunization alone [177].

Regarding the essential domain for the protective activity of ACT, early studies using catalytic domain purified from *B. pertussis* culture supernatant showed protective activity in mouse models [21, 22]. However, the same group later reported opposite result using recombinant fragments of ACT purified from *E. coli*, and suggested that the earlier findings were probably due to cross-contamination with fragments from the C-terminal RTX domain [178].

Given our discovery of the neutralizing antibodies binding the RTX domain and disrupting receptor binding, we are especially interested to see if RTX is able to induce similar neutralizing antibodies *in vivo*. By examining the neutralizing antibody responses induced by individual domains of ACT, our analysis will not be complicated by the effect of anti-LOS antibodies as in animal challenge studies.

First, we expressed, purified, and conducted biophysical and biochemical characterizations of the individual domains of ACT. The catalytic and RTX domains were predominantly monomeric, and retained much of the expected structural behavior; while the hydrophobic domain formed high molecular weight aggregates even in the presence of MBP fusion partner. Similar to previous reports on ACT behavior, the presence of calcium and acylation appears to stabilize the RTX monomers. Acylated RTX_{751} domain showed specific binding to immobilized $\alpha_M\beta_2$ integrin. All domains were recognized by the panel of previously characterized mAbs.

Next, mice were immunized with individual domains or full-length ACT. In ACT immunized mice, serum responses were predominantly directed toward the RTX domain. In mice immunized with domains, those immunized with RTX had much higher anti-ACT titers than those immunized with catalytic domain. Mice immunized with MBP fusion of the hydrophobic domain developed antibodies mostly targeting MBP.

Mice immunized with RTX domain had similar levels of neutralizing activity in sera to those immunized with full length ACT. In both groups, the sera contained antibodies binding overlapping epitopes with M2B10 and M1H5. Our results support the notion that RTX domain is both immunodominant and elicits neutralizing antibodies *in vivo*.

We also measured the reactivity of 9 random serum samples of humans who recovered from *B. pertussis* infection, toward the catalytic domain, RTX domain, and full length ACT. Again, the antibody responses were predominantly targeting the RTX domain with only one outlier. The low immunogenicity of the catalytic domain could be due to its intrinsic property or immunological tolerance as a result of its structural similarity with mammalian adenylate cyclases [179, 180].

In summary, ACT is prone to aggregation and proteolysis, and its purification and integrity require the presence of 8M urea which is not suitable for vaccine formulation. Here, we have determined that the RTX domain of ACT is immunodominant and elicits neutralizing antibodies in mice. As a promising substitute of full-length ACT to be included in next-generation acellular vaccines, it remains to be determined whether immunization with RTX domain could protect animals from bacterial challenge, and how it synergizes with other antigens in the current acellular vaccines.

3.2 MATERIAL AND METHODS

3.2.1 Molecular cloning

Individual ACT domains were expressed in the bacterial cytoplasm of E. coli with His6-tags. To generate plasmids expressing only the catalytic domain (residues 1-373, 1-385 or 1-400), the corresponding coding regions were amplified from pT7CACT3 [154] by PCR, with common forward primer 5'-aggaaacaCATATGcagcaatcgcatcaggctgg-3' and reverse primers 5'-actaGAATTCttacgaacgtccgctcggcacg-3', 5'-cacaGAATTCttacgccggcaccgtttccagtacatc-3', and 5'-cataGAATTCttactggcgttccactgcgcc-3' respectively (restriction sites in uppercase and underlined). The amplified fragments were gel purified and double digested with *Nde*I and *EcoR*I and ligated into similarly digested pET28a vector. To generate plasmids expressing the RTX domains (residues 751-1706 or 985-1706), DNA fragments encoding these regions were amplified using forward primers 5'-tcacgaaCATATGgccaattcggacg-3' and 5'-ctacggcCATATGacggagaatgtcca-3', and common reverse primer 5'-ataGGATCCtcagcgccagttgacag-3'. The resulting PCR products were gel purified, double digested with *Nde*I and *Bam*HI, and ligated into similarly digested pET28a vector.

To enhance folding and solubility, the hydrophobic domain, encompassing the region between the catalytic and RTX domains (residues 399-1096) was cloned into pMalc-5x vector (NEB) between *Nde*I and *BamH*I sites, downstream of the maltose binding protein (MBP). The primers for PCR were 5'-gggcgcaCATATGcgccaggattccggct-3' and 5'-atcggcGGATCCtta**atggtgatgatggtgatgggcgctggc**ctcggaaggctggtgcac-3'; with the bold nucleotides encoding a C-terminal His_6-tag. The *cya*C gene was inserted downstream of the hydrophobic domain between the *Bam*HI and *Hind*III sites, with an upstream ribosome binding site to allow for co-expression.

3.2.2 Protein expression and purification

Full-length ACT was expressed from the plasmid pT7CACT3 with co-expression of the palmitoylating enzyme CyaC in *Escherichia coli* strain XL-1 Blue [154]. The holo-toxin was purified using a single-step calmodulin agarose affinity chromatography as described by Sebo *et al*.[7]. Purified ACT was stored in 50mM Tris, 8M urea, 2mM EDTA, pH 8.0 at 4˚C for short term or -80˚C for long term storage. The protein concentration was determined by absorbance at 280 nm using a molecular extinction coefficient of 143590 $M^{-1}cm^{-1}$ as calculated from its amino acid sequence [151]. ACT from BEI Resources was used as a reference for purity and toxicity.

The catalytic and RTX domains of ACT were expressed in *E. coli* strain BL21(DE3). Briefly, 250mL of TB media were inoculated from starter cultures to an optical density at 600 nm (OD_{600}) of 0.05, grown at 37˚C until OD_{600} = 0.3-0.6, at which time 0.4mM IPTG (isopropyl-β-D-thiogalactopyranoside) was added to induce expression. After 4 h of room temperature growth, the cells were harvested, resuspended in Buffer A (50mM Hepes, 250mM NaCl, 2mM $CaCl_2$, 40mM imidazole,

pH 8.0), and lysed with a French Press (Thermo Scientific). After a 20 min centrifugation step at 20,000 rpm (JA-20 rotor), the supernatant was applied to a HisTrap column on an ÅKTA FPLC (GE healthcare), followed by elution with a linear gradient of Buffer B (Buffer A + 500mM imidazole). The hydrophobic domain was expressed in *E. coli* strain BL21 as above, although purification included immobilized metal affinity chromatography (IMAC) resin followed by an MBPTrap affinity column (GE healthcare) and elution with 10mM maltose.

3.2.3 Murine immunization

To assess the immunogenicity of individual ACT domains, 4-6 BALB/c mice per group were immunized subcutaneously with equal moles of ACT and individual domains (10 μg for ACT, 2.6 μg for CAT_{400}, 6.7 μg for HP_{1096}*, and 4.4 μg for RTX_{985}) in complete Freund's adjuvant. Four weeks later, the mice were boosted subcutaneously with the same amount of antigen in incomplete Freud's adjuvant, a process which was repeated at 6 and 8 weeks. Blood was collected before immunization, four weeks after the first injection, and two weeks after each boost.

3.2.4 Serum titer measurement by ELISA

Anti-ACT antibody titers in mouse sera were determined by ELISA as previously described, with titers defined as the 50% effective concentration (EC_{50}) from a 4-parameter logistic fit.

To assess the reactivity of sera from humans exposed to *B. pertussis*, purified ACT (1 μg/mL) or domains (equimolar concentrations as ACT) were coated on ELISA plates. Plates were blocked as above, human sera serially diluted in M-PBST, and bound antibodies detected with goat anti-human IgG (Fc-specific) HRP-conjugated antibody. Nine randomly selected samples were tested in duplicate. The absorbance value for

each sample binding to a domain was normalized to that sample's signal on an ACT-coated well at a 100-fold dilution (in the linear dose-response range) as follows: [$A_{450\ (domain\ coated\ well)}$–$A_{450\ (uncoated\ well)}$]/[$A_{450\ (ACT\ coated\ well)}$- $A_{450\ (uncoated\ well)}$]. Human sera were obtained from Vanderbilt University Medical Center under a protocol approved by the local institutional review board (IRB 061262, 070258 and 090806). Use of those samples was approved by the University of Texas at Austin (2009-05-0096). The study was conducted in accordance with the Declaration of Helsinki, with written informed consent obtained from each participant prior to study entry. The original consent forms allowed for sample use in subsequent studies. $CaCl_2$ levels in all ELISA assays were maintained at >2 mM unless indicated and each assay was performed at least twice.

3.2.5 J774 intoxication assay

Neutralizing activity in the mouse sera were measured at a 400-fold dilution with J774A.1 cells, as described previously.

3.3 RESULTS

3.3.1 Expression, purification, and characterization of ACT and individual domains

To identify which, if any, ACT domains are predominantly recognized by polyclonal antibody responses, we expressed individual domains in *E. coli* with affinity tags to facilitate purification (Table 3.1). Based on prior reports [24, 154, 181-183], the N-terminal catalytic domains (residues 1-373 [CAT_{373}], 1-385 [CAT_{385}] and 1-400 [CAT_{400}]) and C-terminal RTX domains (residues 751-1706 [RTX_{751}] and 985-1706 [RTX_{985}]) were cloned into the pET28a vector for cytoplasmic expression with N-terminal His_6 tags to facilitate purification (Figure 3.1A). In our hands, $RTX_{482-1706}$ was poorly soluble and purified inefficiently; instead we selected RTX_{985} as the largest

fragment to exclude both acylation sites but retaining the N-terminus before the first Gly-Asp rich repeat. To enhance solubility, the hydrophobic domain (residues 399-1096 [HP_{1096}], encompassing the region between the catalytic and RTX domains) was fused downstream of maltose binding protein (MBP), with a C-terminal His_6 tag and di-cistronic expression of the specific acylating enzyme *CyaC* (indicated by *). After cytoplasmic expression of each construct and cell lysis, a one-step affinity chromatography with a HisTrap column yielded ~5-80 mg protein per liter culture with >90% purity as determined by SDS-PAGE (Figure 3.1C). For HP-MBP-fusion proteins, a second chromatographic step with an MBPTrap column was required to reach a similar level of purity, although purity, proteolysis and solubility issues persisted.

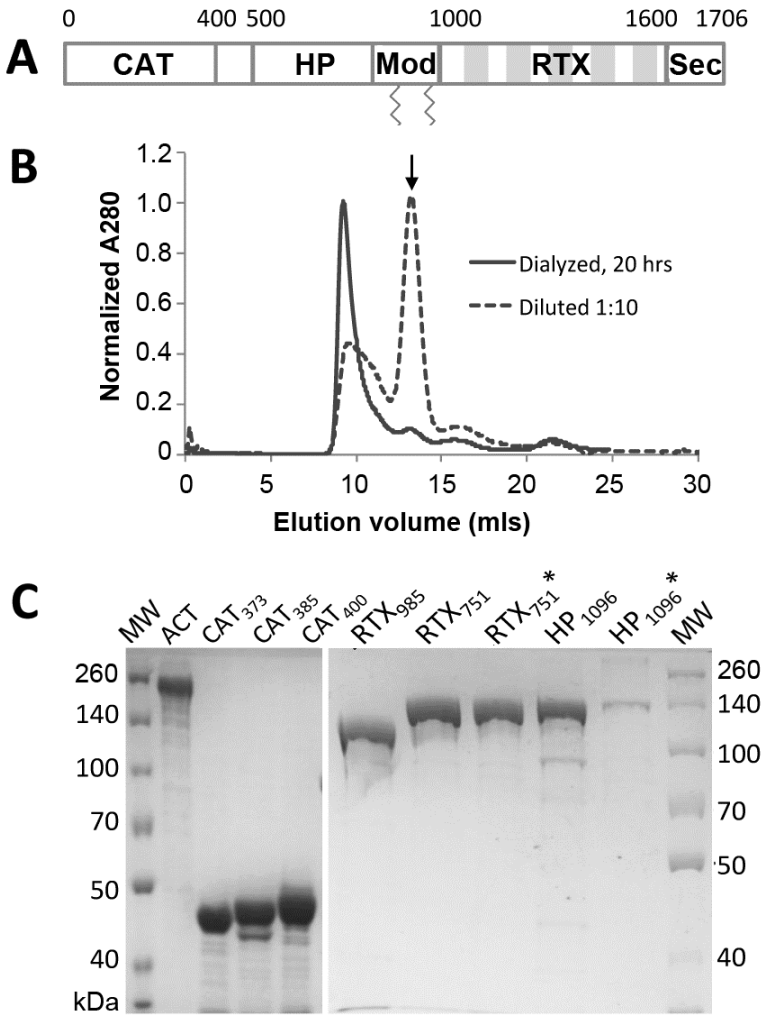
A
0
400
500
1000
1600
1706
CAT
HP
Mod
RTX
Sec
B
Normalized A280
1.2
1.0
0.8
0.6
0.4
0.2
0
0
5
10
15
20
25
30
Elution volume (mls)
Dialyzed, 20 hrs
Diluted 1:10
C
MW
ACT
CAT373
CAT385
CAT400
RTX985
RTX751
RTX751*
HP1096
HP1096*
MW
260
140
100
70
50
40
kDa

Figure 3.1

Figure 3.1: Expression and purification of intact ACT and domains.

(A) Adenylate cyclase toxin domain architecture. ACT is a 177kDa protein toxin, consisting of five sequential domains: the catalytically active N-terminal adenylate cyclase (CAT) domain, the central hydrophobic (HP) domain, modification (Mod) region carrying two acylation sites K860 and K983, the C-terminal repeat-in-toxin (RTX) domain and finally a C-terminal secretion signal (Sec). The five shaded blocks in the RTX region represent tandem Gly-Asp rich repeats. **(B)** ACT forms high molecular weight species (>600 kDa) when urea is removed by dialysis or dilution. Size exclusion chromatograms of ~120 µg ACT using a Superdex 200 column were collected directly after a 1:10 dilution (final urea concentration 0.8 M) or overnight dialysis into HBSC with 1 M urea. Arrow indicates the size expected for monomer, 177 kDa. **(C)** SDS-PAGE gel comparing full-length ACT with different domain constructs after purification from *E. coli*. Three versions of the CAT domain (residues 1-373 [CAT_{373}], 1-385 [CAT_{385}] and 1-400 [CAT_{400}]) and three versions of the RTX domain (residues 985-1706 [RTX_{985}], 751-1706 [RTX_{751}] and acylated 751-1706 [RTX_{751}*]) were expressed from plasmid pET28a with an N-terminal His_6-tag. The HP domains (residues 399-1096 [HP_{1096}] and acylated 399-1096 [HP_{1096}*]) were expressed from plasmid pMalc-5x with an N-terminal maltose binding protein (MBP) fusion for enhanced solubility and C-terminal His_6-tag.

Table 3.1: Biophysical analysis of ACT constructs.

		SEC calc. MW (kDa)		
Domain	**Theoretical MW** (kDa)	**+Ca**	**+EGTA**	**Melting temp**. (°C)
ACT	177	>600	ND	ND
CAT_{400}	45	40	40	43.3
HP_{1096}	118	>600	>600	ND
HP_{1096}*	118	>600	>600	ND
RTX_{985}	77	78	380	40.7
RTX_{751}	102	108	115	57.7
RTX_{751}*	102	91	>600	56.8

ACT and various derivatives were purified and subjected to size exclusion chromatography in the presence of 2 mM calcium or an excess of EGTA to chelate free calcium ions. The expected molecular weight for each construct is noted, as is the observed size and thermal melting temperature of the major peak. Constructs noted with * were co-expressed with *CyaC* to acylate residues K860 and K983.

To determine whether the purified domains exhibited native-like structure and expected calcium-dependent structural changes, size exclusion chromatography (SEC) was used to assess the oligomeric state while circular dichroism (CD) spectroscopy was

used to assess the secondary structure content. The catalytic domains eluted as a single peak of expected size (40 kDa) with the estimated composition of secondary structures (56% helix, 14% strands, 13% turns and 17% unordered) by circular dichroism, similar to that determined by X-ray crystallography (Figure 3.2A) [24]. While the catalytic domain formally encompasses residues 1-373, the construct encompassing residues 1-400 was selected for further use to include the neutralizing epitope recognized by antibody 3D1 [147].

The hydrophobic fusion proteins eluted as broad aggregate peaks when acylated or non-acylated. In the absence of acylation, multiple smaller peaks were observed, suggesting that acylation may stabilize folding of this domain and protect against proteolysis. In both cases, the CD spectra were not characteristic of unfolded or aggregated proteins (Figure 3.2B). The solubility and CD spectra of these constructs may be dominated by the MBP fusion partner, but we did not attempt to remove it, as a shorter hydrophobic domain was reported to further aggregate under these circumstances [163].

The RTX domain comprises ~40 calcium binding Gly-Asp repeats, grouped into five blocks, separated by non-RTX flanking regions (Figure 3.1A). Structural data for RTX-containing proteins suggest the repeats fold into parallel beta-helix structures. In the presence of calcium ions, the protein converts from an intrinsically disordered domain into a compact β-roll structure with altered CD spectrum and reduced hydrodynamic radius which appears to be further stabilized by acylation [37, 184, 185]. RTX_{985} exhibited a shift from largely monomer in the presence of calcium (78 kDa) to a mixture of oligomers (~380 kDa) upon the addition of EGTA to chelate calcium ions. These structural changes are captured by CD, which shows a more ordered state in the presence of calcium ions (Figure 3.2C), consistent with that observed with a similar construct also

lacking the acylation sites (residues 1006-1706) [186]. SDS-PAGE indicates the two peaks observed with calcium have the same molecular weight suggesting that RTX_{985} forms two stable states with different hydrodynamic radii (Figure 3.2C).

Theorizing that these two forms are a consequence of the missing acylation sites, we generated a larger construct to include both sites. RTX_{751} expressed without CyaC eluted as a single peak of expected size (~110 kDa) in the presence or absence of calcium. When co-expressed with CyaC, presumably resulting in acylation at residues K860 and K983, RTX_{751}* exhibited a calcium-dependent conversion from a compact monomer (~90 kDa) to a soluble higher-molecular weight aggregate (~600 kDa) after depeletion of calcium (Figure 3.2D).

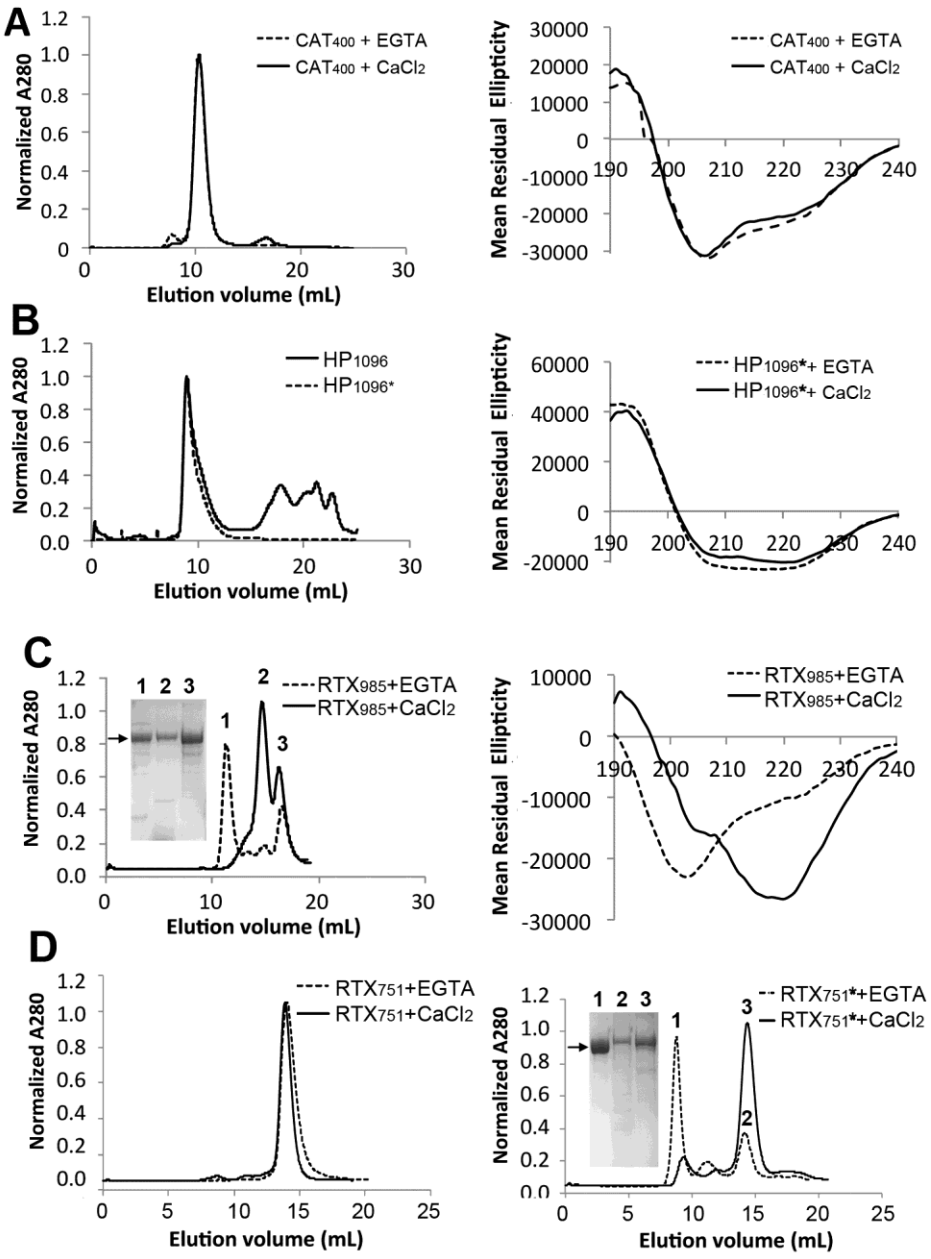
A
Normalized A280
Elution volume (mL)
CAT400 + EGTA
CAT400 + CaCl2
Mean Residual Ellipticity
B
HP1096
HP1096*
HP1096*+ EGTA
HP1096*+ CaCl2
C
1 2 3
RTX985+EGTA
RTX985+CaCl2
D
RTX751+EGTA
RTX751+CaCl2
RTX751*+EGTA
RTX751*+CaCl2

Figure 3.2

Figure 3.2: ACT domain oligomeric state and secondary structure.

Purified domains were separated by size exclusion chromatography (Superdex200 column, except Superdex75 for CAT_{400}), with far UV circular dichroism spectra (Jasco J-815) used to assess secondary structure in the presence of 2 mM $CaCl_2$ or absence of calcium ions. **(A)** The catalytic domain, spanning residues 1-400 (CAT_{400}) eluted as a single peak of expected size. The secondary structure is similar to that observed in the CAT_{373} crystal structure (56% helix, 14% strands, 13% turns and 17% unordered). **(B)** The HP domain, spanning residues 399-1096, with an N-terminal MBP fusion protein eluted off SEC as high molecular weight aggregates whether acylated (*) or non-acylated. **(C)** The RTX_{985} formed high molecular weight aggregates in the absence of calcium ions, but eluted as two peaks, one corresponding to the expected molecular weight, 78 kDa in the presence of calcium. Circular dichroism revealed significant conformational change upon addition of 2mM $CaCl_2$ corresponding to an increase in beta-strand content. **(D)** The RTX_{751} domain exhibits a similar calcium-dependent delay in elution volume, which is more pronounced when the protein is acylated (*) and under these conditions yields a single monomer peak. Inset SDS-PAGE gels show proteins present in indicted peaks, with arrows indicating the expected monomer size.

The catalytic and RTX domains retain much of the expected structural behavior, with RTX_{751}* appearing to better stabilize the monomeric form than RTX_{985}. Similar to previous reports on ACT behavior [32, 33, 186-188], the presence of calcium and acylation appears to stabilize the RTX monomers. Anecdotally, the RTX domains were stable for at least six months at 4 ˚C with minimal aggregation or degradation (RTX_{751} and RTX_{751}* were slightly more stable than RTX_{985}), as measured by SDS-PAGE and SEC to assess the monomeric fraction. While the CAT_{400} domain also remains monomeric, it starts to degrade after three months under the same conditions, as measured by SDS-PAGE. The compact β-roll structure RTX domains adopt in the presence of calcium may contribute to their overall higher melting temperature and resistance to proteolysis than CAT_{400} (Table 3.1).

To determine if our domain constructs retain structural elements present in ACT, we screened a panel of nine previously characterized monoclonal antibodies for binding

to ACT and individual domains by ELISA [147]. All nine antibodies tested recognized only the expected domain and did not distinguish between acylated and non-acylated domains (Table 3.2), supporting the notion that they are properly folded. One exception is 2B12, whose epitope includes residues 888-1006, did not recognize HP_{1096}. This may be due to incomplete folding of HP_{1096} or the binding site may require additional residues distal to residue 1006 not present in this construct.

Table 3.2: Biochemical analysis of ACT constructs.

ACT domain	Epitope	3D1 373-399	2A12 399-828	10A1 624-780	2B12 888-1006	6E1 1320-1489	9D4 1156-1489	7C7 1320-1627	1H6 1590-1706	10A8 1590-1706
CAT_{400}		+++								
HP_{1096}			+++	+						
HP_{1096}*			+++	+						
RTX_{985}						++	++	++	+++	+++
RTX_{751}					+	++	++	+	+++	+++
RTX_{751}*					+	++	++	+	+++	+++
ACT		+++	+++	++	++	+++	+++	+	++	+++

Binding of previously characterized anti-ACT murine antibodies [147] to ACT and various derivatives described in this work in ELISA assays. ACT constructs were coated on ELISA plates, the antibodies titrated and detected with anti-mouse IgG-HRP.

As the RTX domain harbors the receptor binding site between residues 1166-1281 [32], we assessed the ability of our RTX constructs to bind purified murine extracellular $\alpha_M\beta_2$ receptor, a known ACT cell-surface receptor [31]. While ACT and RTX_{751}* both bound the murine receptor when acylated and in the presence of calcium (apparent EC_{50} ~20 nM; Figure 3.3), ACT exhibited considerable non-specific binding to wells without the receptor. This is similar to the sticky behavior observed when ACT without urea was

applied to and retained by the SEC column and likely reflects solvent exposed hydrophobic patches in misfolded ACT molecules. The monomeric RTX_{985} peak did not bind the $\alpha_M\beta_2$ receptor, consistent with prior studies showing post-translational acylation is essential for receptor binding [154, 189]. In summary, the individual domains were readily purified, with yields of CAT_{400} at ~ 80 mg/L culture, non-acylated RTX and HP domains at ~5mg/L culture, and the acylated domains at < 2mg/L culture. The CAT and RTX domains share many structural features with ACT, while the HP domain is mostly aggregated.

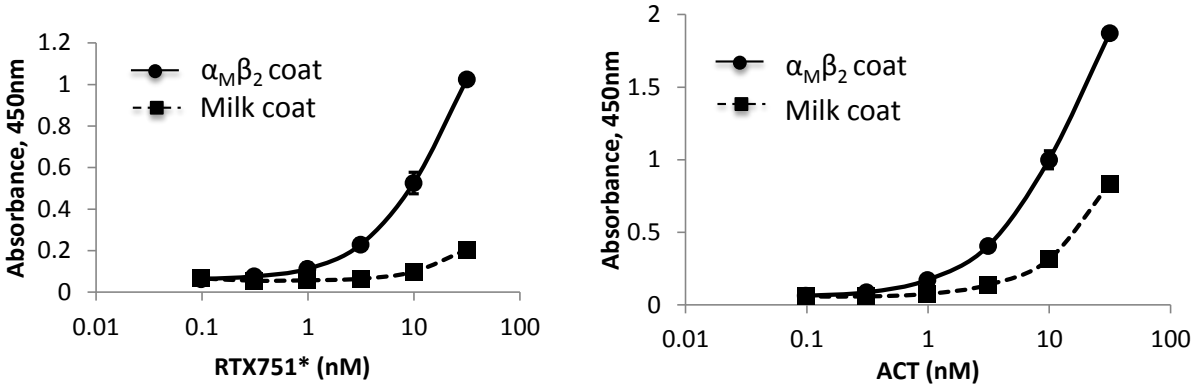

Figure 3.3: ACT and RTX domains bind purified $\alpha_M\beta_2$ receptor.

Soluble murine $\alpha_M\beta_2$ receptor was coated onto ELISA plates and blocked. ACT or individual domains were serially diluted in M-PBST. Bound protein was detected with polyclonal rabbit anti-ACT antibody followed by goat-anti-rabbit-HRP. To assess non-specific binding, control wells were not coated with $\alpha_M\beta_2$ receptor but blocked with M-PBST only. **(A)** RTX_{751}* and **(B)** acylated ACT showed receptor-dependent binding, although ACT also exhibited significant non-specific binding. All other domains showed no specific or non-specific binding.

3.3.2 Mouse immunization with ACT and individual domains

To determine if any ACT domain dominates the immune response, we immunized mice with ACT and tested the resulting sera four weeks after primary immunization for binding to individual ACT domains. Interestingly, strong responses were observed for

ACT, RTX_{985} and RTX_{751}, but no responses were observed for the CAT_{400} or HP_{1096}* domains (Figure 3.4A).

To determine whether this was the result of RTX immunodominance or a lack of immunogenicity by the CAT and HP domains, we immunized additional groups of mice with CAT_{400}, HP_{1096}* or RTX_{985}. Here, RTX_{985} was selected since it shares many features with RTX_{751}*, including recognition by at least one neutralizing antibody, yet lacks the acylation sites rendering it simpler to produce and less likely to engage the native receptor. The calcium concentration in extracellular fluid in the body is 2.2~2.7 mM [190], which is sufficient to support bacterial secretion and folding of ACT during an infection and expected to support proper folding during immunization.

Mice immunized with ACT or RTX_{985} showed high anti-ACT titers four weeks after the first injection, which increased after boosting (weeks 6 and 8, Figure 3.4B). On the contrary, the catalytic domain was much less immunogenic, reaching a detectable anti-ACT titer of ~1500 only after two boosts (week 8; Figure 3.4B). This weak response may reflect structural similarities between CAT and eukaryotic adenylate cyclases, resulting in immunological tolerance or an evolutionary mechanism to protect key toxin components from neutralizing antibodies [179, 180]. Only one of the four mice immunized with the hydrophobic domain reacted with ACT, supporting the SEC data that this construct is poorly folded (Figure 3.4B). Antibody responses in the three remaining mice were directed toward the MBP fusion, as determined by ELISA (data not shown).

Next, we wanted to determine which domains induced sera best able to neutralize ACT cAMP intoxication activities *in vitro* with J774A.1 cells. Here, only immunization with RTX_{985} elicited sera able to protect cells to a similar extent as sera elicited by full-length ACT (Figure 3.4C).

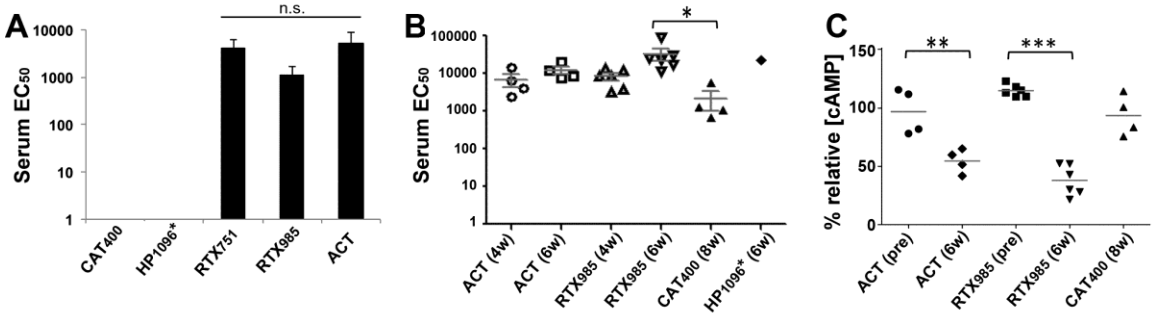

Figure 3.4: The RTX domain is immunodominant and elicits neutralizing antibodies.

(A) Immunization with ACT yields sera preferentially recognizing the RTX domain. Purified domains were coated at equal moles on microtiter plates, with sera serially diluted starting at 1:200. The average EC_{50} for individual domains is shown. Error bars are the standard deviations of the EC_{50} among four mice. **(B)** Immunogenicity of purified domains. Mice were immunized with intact ACT or individual domains, with the serum EC_{50} for ACT measured by ELISA after the first boost (6 weeks) or second boost (8 weeks). **(C)** Sera from mice immunized with ACT and RTX_{985} domain neutralize cAMP intoxication similarly. Sera from each immunization group at a 1: 400 dilution were incubated with 125ng/mL ACT in DMEM before adding to J774A.1 cells. Intracellular cAMP levels were measured by cAMP ELISA, divided by the total protein concentrations, and normalized to cells treated with ACT alone. "Pre" indicates baseline sera collected prior to immunization. Statistical significance was determined by one-way ANOVA with Tukey's test; ** indicates $p \leq 0.01$, *** $p \leq 0.001$. For all panels, an * indicates an acylated domain.

Although mechanisms other than receptor blockade may contribute to neutralization, the presence of M2B10- and M1H5-like antibodies in the sera of ACT- or RTX-immunized animals were confirmed by competition ELISA (Figure 3.5). Since RTX_{985} binds antibody M1H5 weakly, it is possible that this domain harbors critical residues and sufficient conformational similarities to induce overlapping but non-identical M1H5-like antibodies.

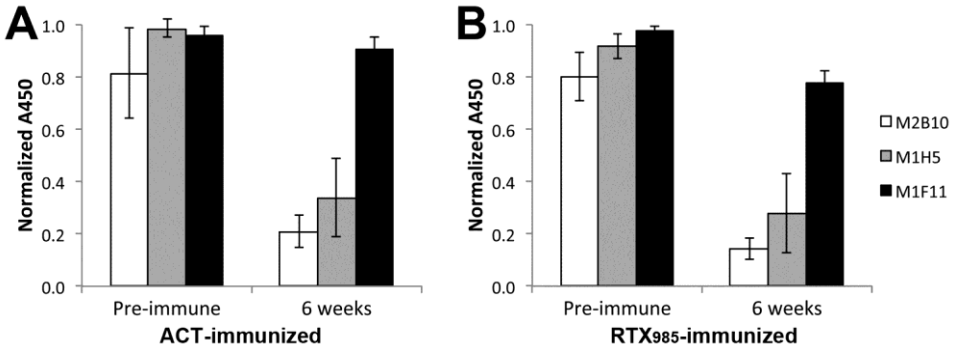

Figure 3.5: Mice produce antibodies binding the M1H5 and M2B10 neutralizing epitopes whether immunized with ACT or RTX985.

Mice were immunized with (A) ACT or (B) RTX_{985}. Sera at a 1:200 dilutions were incubated on ELISA plates coated with ACT, before addition of 0.1nM of M2B10, M1H5, or M1F11 as a competitor. After incubation, immobilized monoclonal antibody was detected with anti-human Fc-HRP, with absorbance normalized to wells without sera. Lower absorbance indicates a higher concentration of epitope-specific murine antibodies.

3.3.3 Human serum response to individual ACT domains upon infection

Finally, to determine whether humans show a similar bias towards RTX recognition, we tested nine serum samples from humans exposed to *B. pertussis,* selected randomly from a larger collection [191]. All nine sera recognized RTX_{751} at a similar level as full-length ACT, while sera from only one individual bound CAT_{400} (Figure 3.6). Taken together, these data provide proof of-concept that RTX dominates the anti-ACT immune response and that the RTX domain can recapitulate the humoral immune responses induced by ACT.

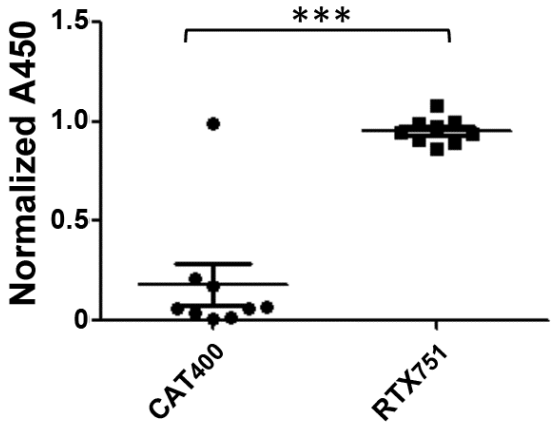

Figure 3.6: RTX dominates the human immune response to ACT.

Nine serum samples from humans exposed to *B. pertussis* were tested for reactivity to the catalytic domain, RTX_{751}, or intact ACT by ELISA. Absorbance values at a 100-fold dilution of the sera were normalized to that of ACT at the same dilution. A paired t-test was used to determine the statistical significance between signals for CAT and RTX domains binding.

3.4 DISCUSSION

The recent surge in pertussis cases, coupled with increasing recognition of the current acellular vaccine's shortcomings has motivated design of third generation vaccines to prevent pertussis. In humans, even a single dose of whole cell vaccine significantly reduces the risk of illness [192], while in baboons, acellular immunization prevented the severe symptoms of disease, but allowed bacterial persistence and transmission to naïve animals [10]. In order to design future vaccines which minimize sub-clinical disease and reduce transmission to susceptible infants, it is crucial to understand the roles played by various protective antigens. ACT has been shown to be protective in animal models and is immunogenic in humans [21, 22, 173, 193, 194]. Since ACT activities hinder local anti-bacterial immune responses [195-197], anti-ACT antibodies may protect these cells, indirectly facilitating bacterial elimination. Here, we

demonstrated that the RTX domain is able to largely recapitulate the protective humoral immune response induced by ACT in mice and is better expressed and more stable than the intact ACT.

ACT was first discovered based on its ability to increase cAMP levels in neutrophils, inhibiting their anti-bacterial functions, including phagocytosis and respiratory burst and promoting the early stages of disease establishment [195]. At physiologically relevant concentrations (<50 ng/ml) [145], ACT results in cytotoxicity to the murine macrophage cell line J774A.1 after two hours exposure; IL-2 secretion and proliferation of T cells and chlorine efflux from polarized epithelial cells [198]. More recently, ACT has been shown to suppress development of an IL-17 mediated immune response which appears key for bacterial clearance [27]. As a result, passively administered antibodies blocking ACT function may be able to enhance neutrophil-mediated phagocytosis of opsonized bacteria [196]. Murine studies have shown that immunization with ACT alone or as a supplement to the acellular vaccine reduces bacterial colonization, an effect which correlated with increased immunoglobulin levels and a Th1/ Th2 cytokine phenotype [22, 189]. Finally, ACT is a highly conserved antigen, able to induce protective immunity in mouse models against the three dominant *Bordetella* species (*B. pertussis*, *B. parapertussis*, and *B. bronchiseptica)* [146, 199, 200]. While ACT is unlikely to be highly protective as an isolated antigen, it may be a valuable addition to vaccines.

The complex mechanism by which ACT directly translocates its catalytic domain into the host cell cytosol remains incompletely understood. The current working model consists of three steps [50, 162, 163]. ***First,*** in the presence of millimolar levels of calcium and acylation, the RTX domain forms a beta barrel which binds the $\alpha_M\beta_2$ receptor on neutrophils or the β_2-containing integrin LFA receptor on T cells through N-

linked oligosaccharides. ***Second,*** this is followed by insertion of two loops (four predicted transmembrane alpha helices between residues 502-522 and 565-591) into the host cell membrane, resulting in a translocation intermediate which permeabilizes the membrane to allow an influx of extracellular calcium ions, activating calpain-mediated cleavage of the integrin's talin tether. ***Third,*** the ACT-receptor complex is then free to diffuse to cholesterol-rich lipid rafts, which triggers complete translocation of the catalytic domain dependent on residues 375-485 [163]. Interestingly, the catalytic domain allows insertion of peptides up to 206 amino acids long for intracellular delivery [53].

This structure-function information provides insight into epitopes required for cellular intoxication and those likely to induce protective responses. For instance, antibodies could block translocation steps, yet only one such antibody has been characterized. Immunization with ACT, followed by analysis of the resulting polyclonal serum suggested that antibodies recognizing the RTX domain dominate the response, as 6 of 12 monoclonal antibodies recognized this domain [146, 147]. The 3D1 antibody binds a conformational epitope between residues 373-399, adjacent to the catalytic domain, trapping a translocation intermediate and preventing complete delivery of the catalytic domain to the host cytosol [162, 163], while the anti-hydrophobic region antibody 2A12 inhibits intoxication and to a lesser extent, hemolysis, and the anti-RTX antibody 6E1 inhibits only hemolysis [147]. Consistent with these prior reports, we observed that the majority of antibodies recovered from phage libraries bind the RTX domain, while sera from four mice immunized with the holo-toxin bind RTX only. To the best of our knowledge, no antibodies blocking ACT-receptor binding, such as M1H5 or M2B10, have been previously described.

A barrier to development of additional technologies based on ACT has been the challenges of recovering monomeric protein from *in vitro* refolding processes. Standard

protocols, including dilution and dialysis from denaturing buffers containing 8 M urea recover high molecular weight species with variable activity levels. Recently, refolding on a size exclusion column was performed to prevent aggregation of partially folded species and resulted in purification of monomers with very high activity, dependent on the presence of calcium, acylation and molecular confinement [185]. While promising, the yields and scalability of this process are currently unclear. As shown here, the RTX domain presents an alternative to ACT that retains many structural features, is more readily expressed and exhibits greater stability. Furthermore, since RTX lacks the catalytic domain, it has no homology to endogenous proteins and thus poses no potential autoimmunity concerns for human use. We evaluated two different RTX constructs, initially RTX_{985} lacking the acylation sites and thus simpler to express and then the larger RTX_{751}* retaining the acylation sites. While both exhibited expected calcium dependent structural shifts and binding to previously described monoclonal antibodies, RTX_{751}* appears superior to RTX_{985} in terms of monomericity, stability and recognition of soluble $\alpha_M\beta_2$ receptor *in vitro*.

Since RTX_{985} is well behaved and binds at least one neutralizing antibody (M2B10), we used this construct for immunization before discovering that RTX_{751} and RTX_{751}* are better behaved and retain the ability to bind both neutralizing antibodies. Regardless, sera from mice immunized with RTX_{985} neutralized cAMP intoxication *in vitro* as efficiently as sera from ACT-immunized mice. This may be because these non-overlapping epitopes induce antibodies neutralizing toxin via similar receptor blocking mechanisms. Supporting this idea, no synergy was observed when the M2B10 and M1H5 antibodies were combined *in vitro* (data not shown). Thus, it may be possible to induce a strong neutralizing response when only one of the epitopes is structurally intact. We do

not have data on RTX_{751}* immunization, but based on the biochemical and biophysical data presented here, we expect it to perform as well as or better than RTX_{985}.

We have demonstrated proof-of-concept that constructs based on the RTX domain are better behaved than ACT, while retaining key epitopes and inducing neutralizing antibodies. Using the structures of homologous RTX toxins [201, 202], RTX variants with optimized stability, expression level and reduced immunogenicity of non-neutralizing epitopes could be engineered to evaluate a possible role for RTX as a vaccine antigen in murine challenge models.

Chapter 4: Epitope mapping of neutralizing antibodies

4.1 INTRODUCTION

After discovery of new antibodies or engineering of existing antibodies with desired properties, it is important to define their epitopes — the residues on the antigen that form the binding surfaces with the antibodies. Determination of the epitope helps to ensure the specificity of antibodies, to understand the mechanism of action, and to show the uniqueness of the antibody if it is to be patented. Epitope mapping is also the starting point for designing epitope-based immunogens.

There are linear (continuous) and non-linear (also described as conformational or non-continuous) epitopes. Linear epitopes are not affected by the folding state of the protein; while conformational epitopes in their denatured states are no longer recognized by the antibody. The distinction between these two types is not absolute. Most conformational epitopes have some linear components (e.g. a continuous stretch of residues). A common method to determine if an epitope is highly conformational is to subject the antigen to SDS-PAGE and test for binding with the antibody in a western blot. Although SDS-PAGE usually breaks disulfide bonds and unfolds the proteins, a small portion of the proteins might remain or fold into their native forms. Therefore, a conformational epitope might still be recognized in western blots [203].

The gold standard of epitope mapping is X-ray crystallography of the antibody-antigen complex, which unambiguously identify the residues in direct contact between the antibody and antigen pair. However, this requires huge amount of efforts and is not always achievable. Similarly, NMR spectroscopy can determine the interacting residues in solution, but is only suitable for small proteins due to the limitation of resolution [204]. Hydrogen-deuterium exchange mass spectrometry (HDX-MS) measures the differences between the exchange rate of protein amides hydrogen with deuterium in the solvent, in

the absence and presence of the interacting partner. HDX-MS provides peptide level epitope mapping without the need to crystalize proteins and not limited by the molecular weight of the antigen. It is becoming more and more popular with the advancement of mass spectrometry instruments and software [205].

For a large antigen with multiple domains, the first step of epitope mapping is to narrow down the domain that contains the epitope, by testing antibody binding to individual domains or series of truncations on either N- or C-terminal end of the antigen. More detailed information can be gained through peptide scanning or mutation of individual residues systematically or randomly.

For the peptide scanning method, synthetic overlapping peptide libraries or phage-displayed random or antigen-derived peptides are screened for antibody binding. Though high-throughput, peptide scanning mainly identifies linear epitopes or linear components of conformational epitopes [206, 207]. A shotgun scanning strategy combines alanine-scanning mutagenesis and phage display technologies. A phage-displayed antigen can be divided into 20-residue stretches with each of the side chains being mutated to alanine. Then the library is selected against the antibody for functional clones, which are sequenced to determine the ratio of alanine: wild-type residue at each position. Enrichment of wild-type residue at one position indicates its contribution to the binding energy. As the antigen size increases, the number of libraries required for full coverage of the antigen sequence increases proportionally [208].

Due to the stringent endoplasmic quality control of protein folding and secretion in yeast cells and the ability to be sorted by fluorescence-activated cell sorting (FACS), yeast display has been the choice of method for domain- and residue-level mapping of conformational epitopes. Cochran *et al.* displayed domains of the epidermal growth factor receptor (EGFR) on yeast surface and mapped the binding domain of several

mAbs. Conformational and linear epitopes were distinguished by heat-denaturing the yeast displayed domains. Overlapping epitopes were determined by cross-blocking assays between the mAb pairs [209]. For residue level epitope mapping, the antigen is randomly mutated by error prone PCR, followed by FACS to sort the population of cells that have reduced or loss of binding to the antibody. Individual clones are then grown, induced and analyzed to confirm the reduced or loss of binding before being sequenced to reveal the residues that has been mutated. Then these residues are mapped onto the structure of the antigen to identify the ones that cluster together on the antigen surface, which potentially form the epitopes [210]. More recently, instead of sequencing individual clones, the sorted clones can be sequenced *en masse* by high-throughput sequencing. By comparing the starting library and sorted populations, the enrichment ratios at each residue position can be calculated, and the contribution of potential epitope residues can be confirmed experimentally by site-directed mutagenesis [211, 212].

The epitopes of the 12 anti-ACT monoclonal antibodies previously discovered were mapped using a series of truncations and in-frame deletions of the full-length ACT molecule [147]. In our study, we had already determined that the neutralizing antibodies M2B10 and M1H5 both bound the RTX_{751} domain, while M2B10 also bound the shorter RTX_{985} domain. Further truncations on the N- or C-termini of RTX_{751} were conducted to identify the smallest domain that could be recognized by the two neutralizing antibodies. Western blot and ELISA of the purified RTX truncations indicate that the epitopes of M2B10 and M1H5 might be conformational, involving residues that are not continuous in the primary sequence.

Currently, only the N-terminal adenylate cyclase domain of ACT has been crystallized [24]. Crystal structure of another RTX family protein with low sequence similarity shows that the Gly-Asp rich repeats folds into calcium binding β-roll motifs

[186, 201]. The RTX domain is intrinsically disordered in the absence of calcium. The calcium induced folding is reversible and requires the flanking region at the C-terminus of block V through a mechanism of entropic stabilization [184].

The ACTs from three major species of *Bordetella* are highly homologous, 97.7 % identity at the amino acid level with most of the variations in the RTX domain. The *B. bronchiseptica* and *B. parapertussis* RTX domains are only different by three residues. ELISA with purified RTX domains from the three species showed that M2B10 bound all three versions with identical affinity; while M1H5 bound RTX_{751} of *B. pertussis* ~100-fold tighter than those of *B. parapertussis* and *B. bronchiseptica*, indicating different residues among the three species might be involved in the epitope of M1H5. To confirm this hypothesis, we chose three stretches of residues with multiple differences to be swapped from *B. parapertussis* to *B. pertussis* RTX_{751} domain. As expected, swapping any of the three stretches of residues did not affect M2B10 binding; while swapping of region 1237-1256 (at the beginning of block III, 9 substitutions) completely abolished binding with M1H5, suggesting these residues are involved in M1H5 epitope together with residues outside this region.

Next, we displayed the RTX_{751} domain on the surface of yeast cells. Monoclonal antibody 1H6 recognizing the RTX C-terminus was used to control the surface display level. We generate a library containing random mutations between residues 751-1358, which was stained with M2B10 (or M1H5) + 1H6 and sorted by FACS. Populations with normal and reduced binding affinities were both collected. The mutated regions were amplified from the plasmids extracted from the starting library and sorted populations for high-throughput sequencing. By comparing the frequencies of mutations at each position between original library and sorted populations, the enrichment ratios at each position

were calculated. In the population with reduced binding, positively enriched positions are likely involved in the epitopes or structurally important.

4.2 MATERIAL AND METHODS

4.2.1 Molecular cloning

To generate plasmids expressing the soluble RTX N-terminal truncations (residues 1132-1706, 1244-1706, 1381-1706, and 1530-1706), DNA fragments encoding these regions were amplified with forward primers RTX-1132aa-For, RTX-1244aa-For, RTX-1381aa-For, and RTX-1530aa-For, and common reverse primer RTX-Rev-1706 (Table 4.1). The amplified fragments were gel purified and double digested with *Nhe*I and *Bam*HI and ligated into similarly digested pET28a plasmid. To generate plasmids expressing the c-terminal truncation, the DNA fragments were subcloned from respective yeast display vectors using *Nhe*I and *Bam*HI sites.

To generate plasmids for yeast display of RTX_{751} domain and its C-terminal truncations (residues 751-1131, 751-1242, 751-1376, and 751-1529), DNA fragments encoding these regions were amplified with common forward primer RTX-751-for and reverse primers RTX-REV-1131, RTX-REV-1242, RTX-REV-1376, and RTX-REV-1529 respectively (Table 4.1). The amplified fragments were gel purified and double digested with *Nhe*I and *Bam*HI and ligated into similarly digested pCTCON plasmid.

To add linker between RTX domain and c-myc tag, the DNA fragment encoding residues 751-1680 was amplified with forward primer 5'-actattGCTAGCgccaattcggacggcctacgg-3' and reverse primer 5'-ttgttcGGATCC**gcccccc**gtccggatactgcgccattgc-3' (bold nucleotides encode Gly-Gly) or 5'-ttgttcGGATCC**gccacctccagatccgcctccacc**gtccggatactgcgccattgc-3' (bold nucleotides encode Gly-Gly-Gly-Gly-Ser-Gly-Gly-Gly).

To generate plasmids expressing the RTX_{751} domains of *Bordetella parapertussis* and *Bordetella bronchiseptica*, DNA fragments encoding these regions were amplified from respective colonies using primers 5'-actattGCTAGCgccaattcggacggcctacgg-3' and 5'-ataGGATCCtcagcgccagttgacagccag-3' (restriction sites in uppercase and underlined) with Q5 polymerase (NEB). The PCR condition was 98˚C for 30 s, followed by 35 cycles of 98˚C for 10s, 72˚C for 1 min, and a final extension at 72˚C for 2min. The resulting PCR products were gel purified, double digested with *Nhe*I and *Bam*HI, and ligated into similarly digested pET28a vector.

Q5 Site-Directed Mutagenesis Kit (NEB) was used to swap the stretches of residues that are likely involved in the selectivity of M1H5 antibody. To swap residues 1140-1164 of *B. bronchiseptica* RTX into *B. pertussis* RTX (within Block II, total of 5 residue changes), 1 ng of pET28a-RTX751 plasmid was amplified using primers Q5SDM-Block2-swap-F and Q5SDM-Block2-swap-R with Q5 polymerase. The PCR condition was: 98˚C for 30 s, followed by 25 cycles of 98˚C for 10s, 72˚C for 4 min 40 s, and a final extension at 72˚C for 2min. Then, 1 µL of the PCR product was incubated with 5 µL of 2X KLD Reaction Buffer, 1 µL of 10X KLD Enzyme Mix, and 3 µL H_2O at room temperature for 5min, before transformation into chemically-competent *E. coli* cells. The desired mutations were confirmed by DNA sequencing. Similarly, to swap residues 1237-1256 (at the beginning of Block III, a total of 9 residue changes), primers Q5SDM-BlockIII-swap-F and Q5SDM-BlockIII-swap-R were used; to swap residues 1357-1365 (between Block III and IV, a total of 3 residue changes), primers Q5SDM-aa1357-1365-F and Q5SDM-aa1357-1365-R were used (Table 4.1).

Table 4.1: Primer list for RTX domain truncation and site-directed mutagensis.

RTX-1132aa-For	actattGCTAGCaatatcgagaatctgcacggctcccg
RTX-1244aa-For	actattGCTAGCtccgcgctgggcgtggactattac
RTX-1381aa-For	actattGCTAGCgtcgacaagctgggcgaggc
RTX-1530aa-For	actattGCTAGCagcgcgcgtgatgacgtgc
RTX-Rev-1706	actattGGATCCgcgccagttgacagccaggga
RTX-751-for	actattGCTAGCgccaattcggacggcctacgg
RTX-REV-1131	actattGGATCCcttgacatggtcgacgctgaacagg
RTX-REV-1242	actattGGATCCcttgcgcacccattccctggac
RTX-REV-1376	actattGGATCCcaggtcagccaggatgcccag
RTX-REV-1529	actattGGATCCgcccacggcgttctcgatattgc
Q5SDM-Block2-swap-F	cgagctctggggcgacgatggcaacgacacgatacacGGCCGGGGCGGCGACGAC
Q5SDM-Block2-swap-R	ttgtcccggtcgtcgccggcgatgctgtcgttcaggctGGAGCCGTGCAGATTCTCGATATTCTTGACATGGTC
Q5SDM-BlockIII-swap-F	ggcatgggctactacgacagtgtccgcagtGTCGAAAACGTCATCGGTACG
Q5SDM-BlockIII-swap-R	gcgccgggccgccttgcgcacccacccttcGGACAGGTCCGCCTCGAT
Q5SDM-aa1357-1365-F	cggcgttgccacgGGTCGCATCGGGCTGGGC
Q5SDM-aa1357-1365-R	gcatgcgcgcccgcCTGGCTGTAATCGACGGTATCCAC

Restriction sites are in uppercase and underlined. Primers for site-directed mutagenesis were designed using NEBaseChanger, in which uppercase nucleotides are identical or complementary to wild-type sequence and lowercase nucleotides contain the desired mutations.

4.2.2 Protein expression and purification

The different versions RTX domains or truncations were expressed in *E. coli* strain BL21(DE3) and purified as described previously in section 3.2.2.

4.2.3 Western blot of whole cell lysates

To roughly determine the epitope locations of M2B10 and M1H5, 900 µL each of *E. coli* cultures expressing different truncations were pelleted, resuspended in 50 µL 2X SDS-PAGE loading dye, and boiled for 10min before loading 5 µL to each lane. Purified RTX_{751} (30 ng) was loaded as a positive control. Three identical gels were run and transferred to PVDF membranes, which were probed by 5nM M2B10, 5nM M1H5, or 1:2500 anti His-tag HRP antibodies respectively. M2B10 and M1H5 were detected by anti-human Fc HRP (1:4000).

4.2.4 Yeast culture and transformation

Saccharomyces cerevisiae EBY100 strain was used for yeast display. EBY100 cells were streaked on YPD agar plate supplemented with 1 X penicillin/streptomycin (Life Technologies), and incubated at 28-30 ˚C for 2-3 days until colonies showed up.

Heat shock competent cells were prepared using Frozen-EZ Yeast Transformation II kit (Zymo Research). Briefly, an EBY100 colony was inoculated from a fresh plate into 10mL YPD broth with 1X penicillin/streptomycin, and grown at 30°C until mid-log phase (OD_{600} = 0.8-1.0). Then, the cells were pelleted at 500 x g for 4 min, washed with 10 ml EZ 1 solution, pelleted again, and resuspended with 1 ml EZ 2 solution. The competent cells were divided into 50 µL aliquots and used immediately or frozen slowly to -80°C and stored. To transform, the frozen competent cells were thawed at room temperature. Each 50 µL of aliquot was mixed with 0.2-1 µg of DNA in less than 5 µl volume, followed by addition of 500 µl EZ 3 solution. The mixture was incubate at 30°C for 45 min, and mixed vigorously by flicking with finger or vortexing 2-3 times at the beginning and during this incubation. Next, 100 µL of undiluted and 100-fold diluted mixture were spread with glass beads on selection plates and incubated at 28-30 ˚C for 2~3 days.

Electrocompetent cells were prepared as described by Benatuil *et al.* [213]. Briefly, EBY100 culture grown at 30˚C overnight is diluted into 100mL YPD broth to a final OD_{600} of ~0.3, and continued to grow at 30°C until OD_{600} ~1.6 (about 5 hrs). All following steps were performed at 4˚C: the cells were pelleted at 1000 g for 5 min, and washed twice by 50 mL ice-cold water, once by 50 mL of ice-cold electroporation buffer (1 M sorbitol), resuspended in 20 mL conditioning buffer (0.1 M LiAc/10 mM DTT), and shaken at 225 rpm in a flask for 30 min at 30 °C. Then, the cells were pelleted, washed once by 50 mL ice-cold electroporation buffer, and resuspended in electroporation buffer to reach a final volume of 1 mL. The cells were kept on ice until electroporation. 200~400 µl electrocompetent cells were gently mixed with 2 µg linearized plasmid backbone and 3~6 µg purified and desalted PCR product, and transfer to a pre-chilled BioRad GenePulser cuvette (0.2 cm gap). The mixture was kept on ice for 5 min before electroporation at 2.5 kV and 25 µF. The electroporated cells were transferred into 8 mL of 1:1 mixure of 1 M sorbitol/YPD media, shaken at 225 rpm and 30°C for 1 hour, pelleted and resuspended in selection media.

Yeast transformants were selected on YNB-CAA-glucose agar plates or liquid medium (0.67% yeast nitrogen base, 0.5% casamino acid, 2% glucose). For surface display, yeast colonies harboring the pCTCON plasmids were inoculate into YNB-CAA-glucose medium, grown at 30°C overnight until OD_{600} of 2.0~5.0, pelleted, resuspended in YNB-CAA-2% galactose medium at an OD_{600} of 0.75~1.0, and grown at room temperature for 20~50 hrs.

4.2.5 Random mutagenesis library construction

To randomly mutate the 1968bp (not including the primers) region, 480 ng of plasmid pCTCON-RTX751 (equivalent of ~ 100 ng target DNA) was amplified with

primers 5'-ccatacgacgttccagactacgctctgcag-3' and 5'-ggcagcagcgcctacgatac-3', using Mutazyme II (Agilent). The PCR condition was: 95˚C for 2 min, followed by 30 cycles of 95˚C for 30s, 57˚C for 30 s, 72˚C for 2 min 10 s; and a final extension at 72˚C for 5min. Yield of PCR product was estimated based on densitometry. After gel purification, the product was re-amplified with nested primers 5'-tggtggttctggtggtggtgg-3' and 5'-caggtcagccaggatgccc-3', using Q5 Polymerase (NEB). The PCR condition was: 98˚C for 30 s, followed by 30 cycles of 98˚C for 10s, 72˚C for 40 s; and a final extension at 72˚C for 2min. A total of 800 µL PCR was performed in 50 µL aliquots. After gel purification, the DNA was precipitated with isopropanol, resuspended in water, and quantified with NanoDrop.

To prepare the linearized vector, 60 µg of pCTCON plasmid were digested with *Nhe*I and *Sph*I and resolved on agarose gel to remove the ~1.8kb wild-type fragment. After gel purification with GeneJET gel extraction kit (Thermo Scientific), the linearized vector backbone was precipitated with isopropanol, resuspended in water, and quantified with NanoDrop.

To construct the library, 5 µg of insert DNA and 3 µg of DNA backbone were added into 300 µL freshly prepared yeast electrocompetent cells and electroporated as described above. Three separate electroporations were performed and pooled. A control electroporation with linearized vector only was performed. Aliquots of the library and control electroporations were serially diluted and plated on selection plates to determine the total number of yeast transformants. The pooled transformants were grown in selection medium at 30˚C and passaged twice to resolve multiplicity.

To sequence the mutagenized region, plasmids were first extracted from yeast, transformed into *E. coli* XL-Blue, extracted again from *E. coli*, and sequenced with 3

primers to cover the full region: 5'-CGATTGAAGGTAGATACCCATAC-3', 5'-CAAGGTGGTGTCGCAACTGGTC-3', and 5'-GCACGGCTCCCGCCTGAA-3'.

4.2.6 Yeast staining and flow cytometry

To stain the yeast cells for flow cytometric analysis, 0.1OD of cells were pelleted at 1000 g for 2min, and resuspended in 100 μL of 10 μg/mL M2B10 (or M1H5) + 10 μg/mL 1H6 in HBSC-1% BSA. The presence of 2mM $CaCl_2$ in HBSC is essential for the folding of the displayed RTX domain and its recognition by the antibodies. For sorting, 5 OD of cells were stained with 5mL of 2 μg/mL M2B10 (or M1H5) + 2 μg/mL 1H6; 0.1OD of positive and negative control were stained with 100 μL of antibodies at the same concentrations. After incubating at 4˚C with rotation for 30min, the cells were washed twice with HBSC-1% BSA, and resuspended in the same volumes of 1:200 secondary antibodies (Alexa647 anti-human Fc and Alexa488 anti-mouse Fc). After another 30min incubation and final washing, the cells were resuspended in 5mL (library) and 1mL (controls) HBSC-1% BSA, and kept on ice until sorting. Controls were first run and cells were gated by front and side scatters to exclude diploid cells. Gates were drawn around populations with diminished binding (P4) and normal binding (P7) to respective antibodies. Another gate (P5) in between was drawn to circumvent the population with reduced binding. Sorted cells were collected in tubes containing YNB-CAA-glucose medium, which were then pelleted to remove the carryover shealth fluid, resuspended in fresh medium, and grown at 30˚C until $OD_{600} > 2.0$.

4.2.7 Yeast miniprep and PCR

The yeast plasmid DNA was extracted from 0.1~0.2OD of cells using the Zymoprep Yeast Plasmid MiniPrep II kit (Zymo Research), according to the manufacturer's instruction. Due to the low quantity and purity of DNA directly extracted

from yeast cells, the plasmid was transformed into *E. coli* XL1-Blue competent cells, and plasmids were extracted from individual colonies for sequencing.

To perform deep sequencing of the sorted clones, the randomly mutated region was amplified using Q5 polymerase and primers 5'-tggtggttctggtggtggtgg-3' and 5'-caggtcagccaggatgccc-3', from the yeast plasmid DNA extracted from the sorted and propagated cells.

4.2.8 High throughput sequencing

Purified PCR products were fragmented to an average size of 250bp by sonication, and processed for sequencing by Genomic Sequencing and Analysis Facility at UT-Austin according to the protocol [214]. The sequencing instrument was Illumina Hiseq 2500. Minimal number of reads for P5 and P7 were set to $4X10^6$; and $3.6X10^7$ for the starting library. PCR fragment using the wild-type sequence as template was also included as a control for the sequencing error rate, with a minimal reads of 10^6.

4.3 RESULTS

4.3.1 Cross reactivity of the neutralizing antibodies

ACT is highly conserved among the three major species of *Bordetella*, with an amino acid sequence identity of ~97.7 %, and most of variations are within the C-terminal RTX region. The *B. bronchiseptica* and *B. parapertussis* ACTs are only different by three residues, two in the RTX domain and one in the hydrophobic domain (Figure 4.1).

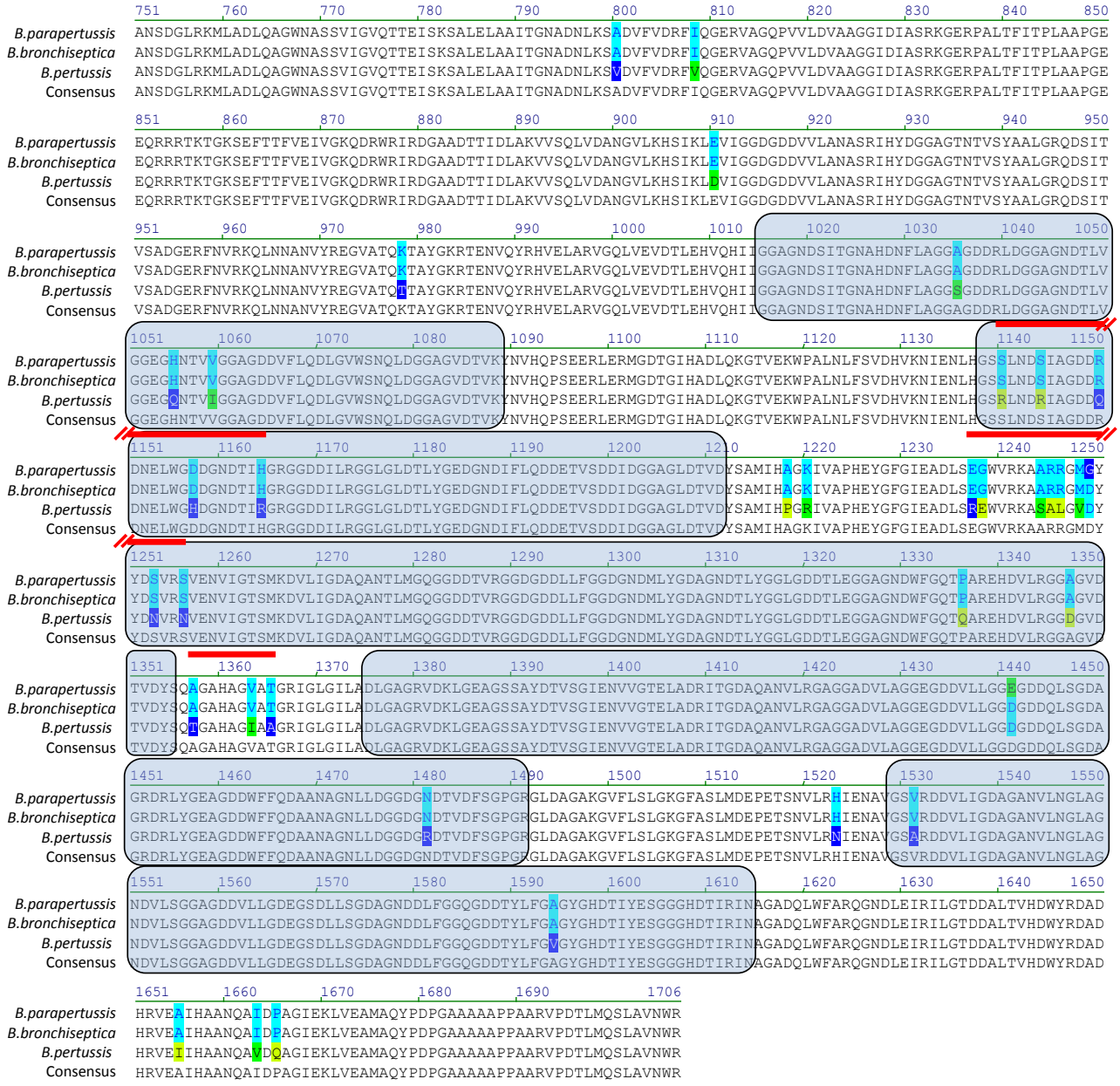

Figure 4.1

Figure 4.1: Sequence alignment of RTX domains of *B. pertussis, B. parapertussis*, and *B. bronchiseptica*.

The amino acid sequences of RTX (residues 751-1706 of adenylate cyclase toxin) from *B. pertussis, B. parapertussis, and B. bronchiseptica* were aligned. Residues with variations in any of the 3 species were highlighted. The numbers above the alignment represent the residue numbering of the full-length ACT. The shaded boxes represent the 5 blocks of repeats of the GGXG(N/D)DX(L/I/F)X (X represent any amino acid) motif. The red bars above the numbers represent the 3 regions being swapped from *B. bronchiseptica* to *B. pertussis* RTX domain. Residues 1166-1287 was suggested to be involved in interaction with $\alpha_M\beta_2$ integrin [32].

In order to determine the species specificity of the neutralizing antibodies, the RTX_{751} domains from *B. parapertussis* and *B. bronchiseptica* were similarly cloned into pET28a vector, expressed as soluble proteins with N-terminal His-tag in *E. coli* BL21(DE3), and purified with immobilized metal affinity chromatography (IMAC) and Superdex200 size-exclusion chromatography. Similar to RTX_{751} of *B. pertussis*, the RTX_{751} domains of *B. parapertussis* and *B. bronchiseptica* were predominantly in monomeric form (Figure 4.2A). The purified RTX domains were coated on ELISA plates and tested for binding with M1H5 and M2B10 IgGs. M2B10 bound all three RTX_{751} versions with almost identical affinity; while M1H5 bound RTX_{751} of *B. parapertussis* and *B. bronchiseptica* with ~100-fold lower affinity comparing to RTX_{751} of *B. pertussis* (Figure 4.2B). The result suggests that the epitope of M1H5 might involve residues that are different among the three species.

To determine if the selectivity of the antibodies correlates with the neutralization ability, M2B10 and M1H5 were tested for the ability to protect J774A.1 cells from challenges by live *B. pertussis* and *B. bronchiseptica*. First, the bacteria were grown in liquid medium, and a pilot experiment measured the cAMP levels generated in J774A.1 cells by serially diluted *B. pertussis* and *B. bronchiseptica* cells. Then, the optical densities that generated moderate levels of cAMP in J774A.1 cells were chosen for the neutralization assay. M2B10 neutralized cAMP intoxication of J774A.1 cells by both

bacteria to a similar extent; while M1H5 neutralized intoxication by *B. bronchiseptica* much less efficiently, suggesting affinity of the antibody affects its neutralization ability (Figure 4.2C).

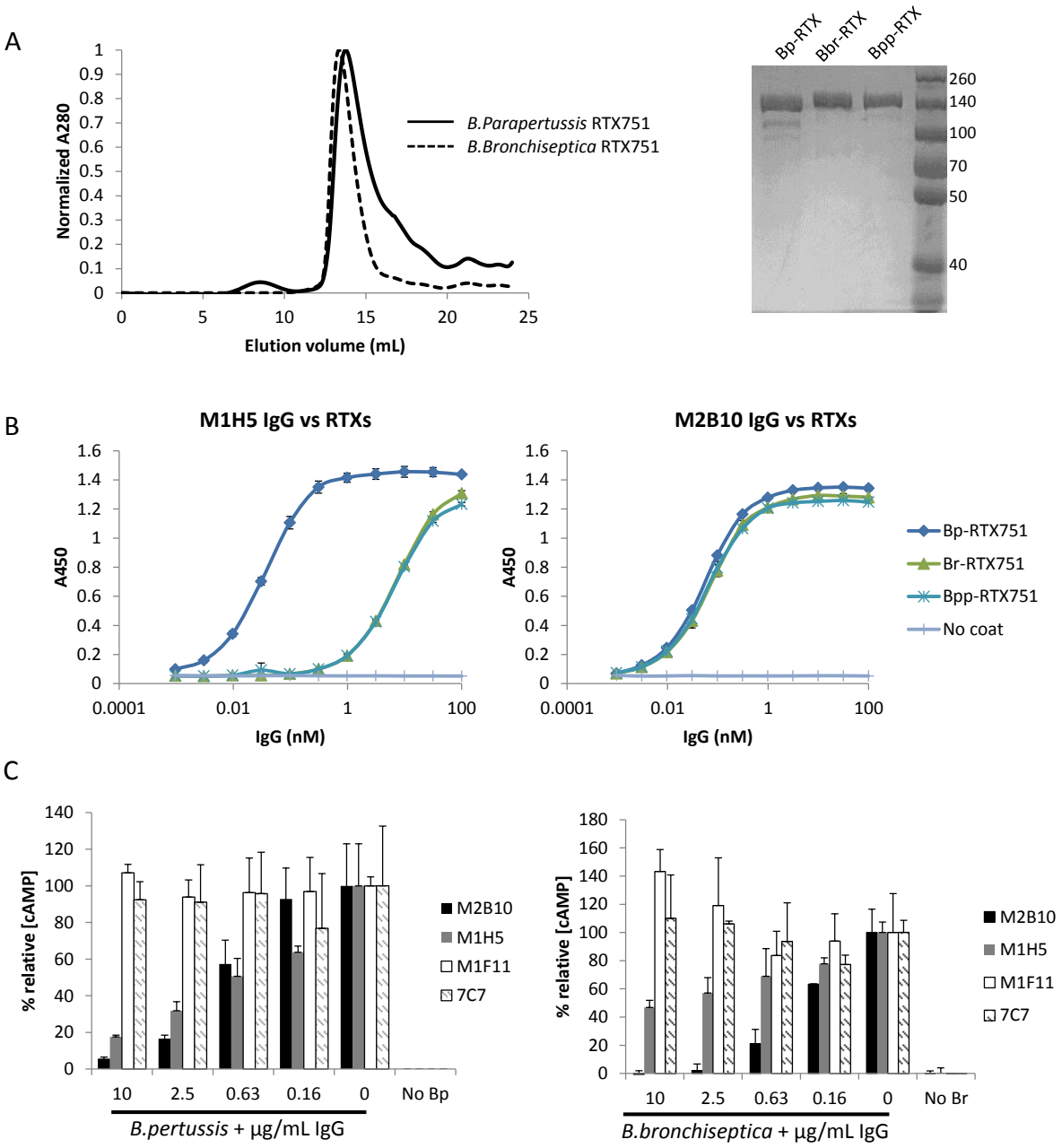
A
Normalized A280
Elution volume (mL)
B.Parapertussis RTX751
B.Bronchiseptica RTX751
Bp-RTX
Bbr-RTX
Bpp-RTX
260
140
100
70
50
40
B
M1H5 IgG vs RTXs
M2B10 IgG vs RTXs
A450
IgG (nM)
Bp-RTX751
Br-RTX751
Bpp-RTX751
No coat
C
% relative [cAMP]
M2B10
M1H5
M1F11
7C7
10
2.5
0.63
0.16
0
No Bp
No Br
B.pertussis + µg/mL IgG
B.bronchiseptica + µg/mL IgG

Figure 4.2

Figure 4.2: Species specificity of the neutralizing antibodies.

(A) The RTX_{751} domains of *B. bronchiseptica* and *B. parapertussis* were cloned, expressed, and purified by IMAC and size exclusion chromatography (left). Purity was assessed by SDS-PAGE (right). **(B)** Purified RTX_{751} of the 3 species were coated on ELISA plates and compared for binding affinity with M2B10 and M1H5 by ELISA. **(C)** M2B10 and M1H5 IgGs were tested for protection of J774 cells from cAMP intoxication by live *B. pertussis* (left, same as Figure 2.10) and *B. bronchiseptica* (right).

By examining the sequence alignment of the RTX region of the 3 species, three stretches of residues (1140-1164, 1237-1256, and 1357-1365) containing multiple residues with large differences (e.g. charged vs non-charged, bulky vs small side chains) were suspected to affect the specificity for M1H5. To determine the effect of each stretch, *B. pertussis* RTX was mutated to the respective residues of *B. parapertussis* RTX by site-directed mutagenesis. The resulting "swapped" domains were expressed and purified as the wild-type RTX domain. Then, the swapped domains were compared with the wild-type *B. pertussis* RTX for binding to M1H5 and M2B10 by ELISA. As expected, M2B10 bound all versions with almost identical affinity, suggesting the swapped domains all fold properly. For M1H5, "Block3 swap" (residues 1237-1256) completely abolished binding, while other two swapped domains had identical binding affinities to wild-type RTX. The swapped region 1237-1256 contained 9 substitutions, 7 of which changed the charges of the side chains. M1H5 bound *B. parapertussis* RTX but had no detectable binding when the 1237-1256 region of *B. parapertussis* RTX was grafted onto the *B. pertussis* RTX. One possible explanation is that these residues might coordinate with other residues present in the *B. parapertussis* RTX to form the intact epitope for M1H5.

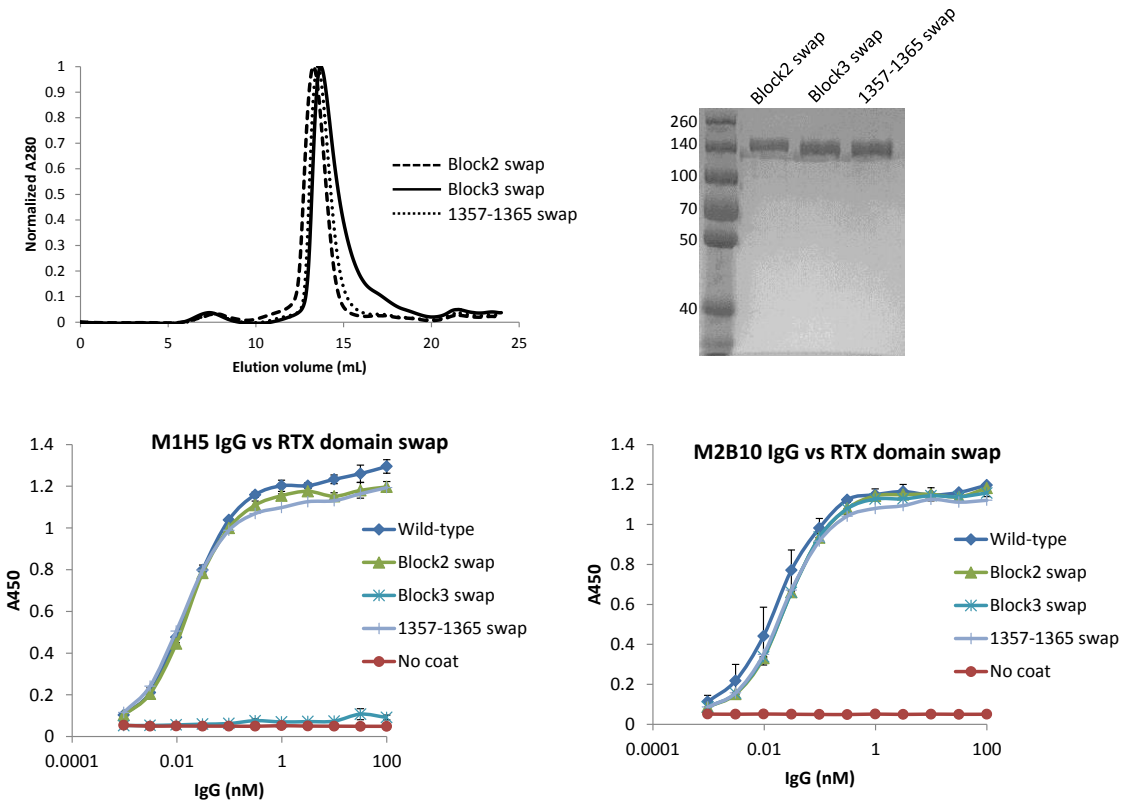

Figure 4.3: Sequence shuffling of the RTX domains.

(A) Three stretches of residues on *B. pertussis* RTX were each changed to those of *B. parapertussis* RTX sequences by site directed mutagenesis. The three variants were purified in monomeric (left) and highly pure form as indicated by SDS-PAGE (right). **(B)** Purified RTX domain variants were coated on ELISA plates. M1H5 and M2B10 antibodies were serially diluted from 100 nM.

4.3.2 Yeast display of RTX domain

So far, various proteins have been displayed on yeast surface, most of which have molecular weights below 60kDa [215]. Therefore, whether the RTX_{751} (~100kDa) could be displayed was a question. As a proof of concept, the entire RTX_{751} gene was cloned into the pCTCON vector downstream of Aga2p for yeast surface display. Staining of the induced yeast cells by M2B10 (or M1H5) + anti c-myc antibodies followed by flow

cytometric analysis showed that the RTX_{751} domain was successfully displayed on yeast surface and could be specifically recognized by M2B10 or M1H5. However, the c-myc tag immediately downstream of the RTX domain was barely detectable (Figure 4.4A).

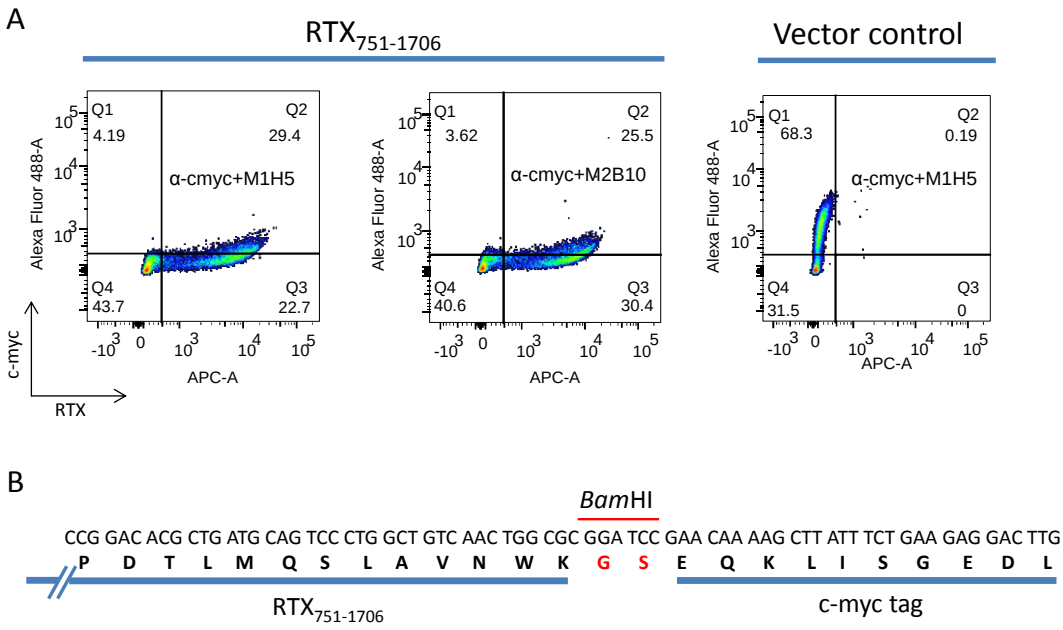

Figure 4.4: Yeast display of RTX751 domain.

(A) RTX_{751} was cloned between *Nhe*I and *Bam*HI on pCTCON vector, downstream of Aga2, and upstream of c-myc tag. After induction with 2% galactose for 20hr at 25˚C, the yeast cells were stained with M1H5 (or M2B10) + anti-c-myc antibodies, followed by co-staining of Alexa647 anti-human Fc and Alexa488 anti-mouse Fc antibodies. Vector with an unknown protein instead of RTX_{751}, was used as a control. The numbers in each quarter represent the percentage of cells. **(B)** The schematic diagram shows the junction between RTX and c-myc tag.

It is suspected that the absence of a long flexible linker between RTX C-terminus and c-myc tag caused steric hindrance between M2B10 (or M1H5) and the anti c-myc antibody or interaction between the c-myc tag and RTX domain (Figure 4.4B). Previously, it was shown that residues 1681-1706, the secretion signal, were not required for the correct folding of RTX domain [184]. Therefore, $RTX_{751\text{-}1680}$ was cloned similarly

into pCTCON vector, inserting a Gly-Gly-Gly-Gly-Ser or $(Gly\text{-}Gly\text{-}Gly\text{-}Gly\text{-}Ser)_2$ linker between RTX and c-myc tag. The removal of C-terminal signal peptide did not affect RTX recognition by M2B10 or M1H5. However, the insertion of GS linker did not improve the c-myc tag detection either (Figure 4.5).

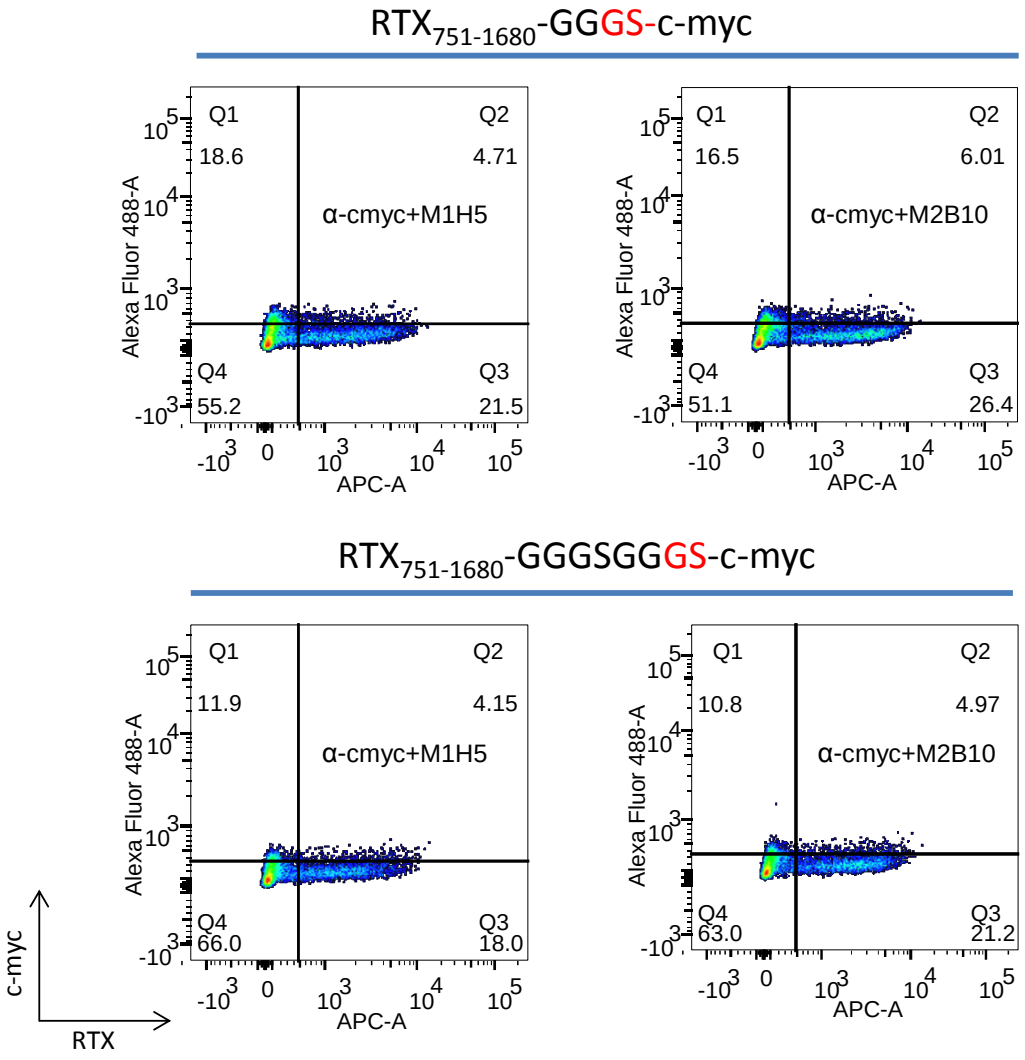

Figure 4.5

Figure 4.5: Addition of flexible linker did not improve c-myc tag detection.

The shorter $RTX_{751-1680}$ domain without C-terminal signal peptide was cloned into pCTCON vector, adding a G_4S or $(G_4S)_2$ linker between RTX and c-myc tag. The resulting yeast clones were induced and stained similarly as above to detect surface RTX and c-myc tag. The numbers in each quarter represent the percentage of cells.

In order to identify an alternative antibody to control for the RTX display level, mouse monoclonal antibodies 6E1, 7C7, and 1H6 [147] were tested. Although all of them bound immobilized RTX_{751} in ELISA format, only 1H6 was able to bind the yeast-displayed RTX_{751} (data not shown). It is possible that the conformation of RTX_{751} on yeast surface is different from the soluble protein, or the epitopes of 6E1 and 7C7 were shielded by glycosylation on the RTX. The reason was not further explored. When the yeast cells displaying RTX_{751} was co-stained with 1H6 + M1H5 (or M2B10), a tight population along the diagonal of the Q2 quarter indicates a good correlation between RTX display level and M1H5/M2B10 epitopes (Figure 4.6).

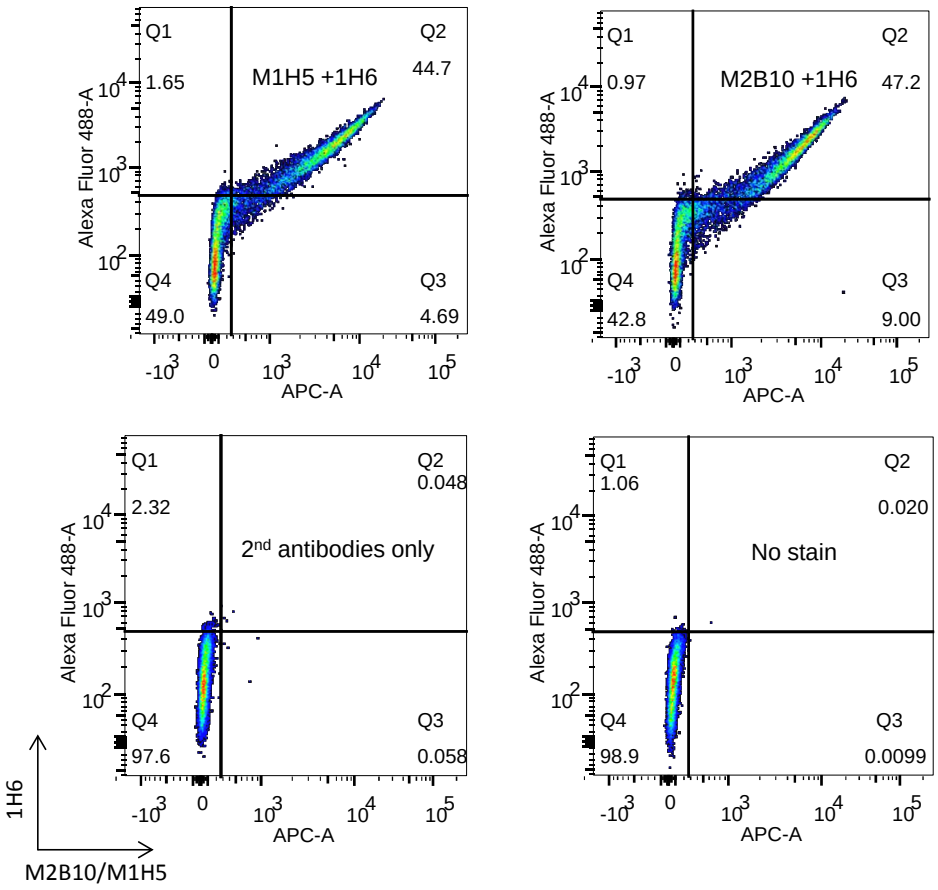

Figure 4.6: Two color staining of yeast displaying RTX_{751} domain.

Yeast cells displaying RTX_{751} were stained with M1H5 or M2B10 together with 1H6, followed by Alexa647 anti-human Fc and Alexa488 anti-mouse Fc. The numbers in each quarter represent the percentage of cells.

The yeast-displayed RTX domain can be analyzed for binding to antibodies without the need to purify individual variants. In order to narrow down the epitopes of the neutralizing antibodies, a series of C-terminal truncations, each missing one block, were constructed (Figure 4.7A). The induced yeast cells were stained with M2B10 or M1H5. Only $RTX_{751\text{-}1706}$ was recognized by M2B10 or M1H5, while the truncations were not (Figure 4.7B). Since the anti c-myc and 1H6 antibodies could not be used to check the

display level of RTX C-terminal truncations, a rabbit polyclonal anti-ACT antibody was used to stain all the variants. All truncations were displayed on the yeast surface, with RTX751-1242 at a lower level comparing to others (Figure 4.7C). This confirmed that the RTX C-terminal truncations were secreted and displayed on yeast surface; but still, it is possible that they were not properly folded, since polyclonal antibody recognized both linear and conformational epitopes.

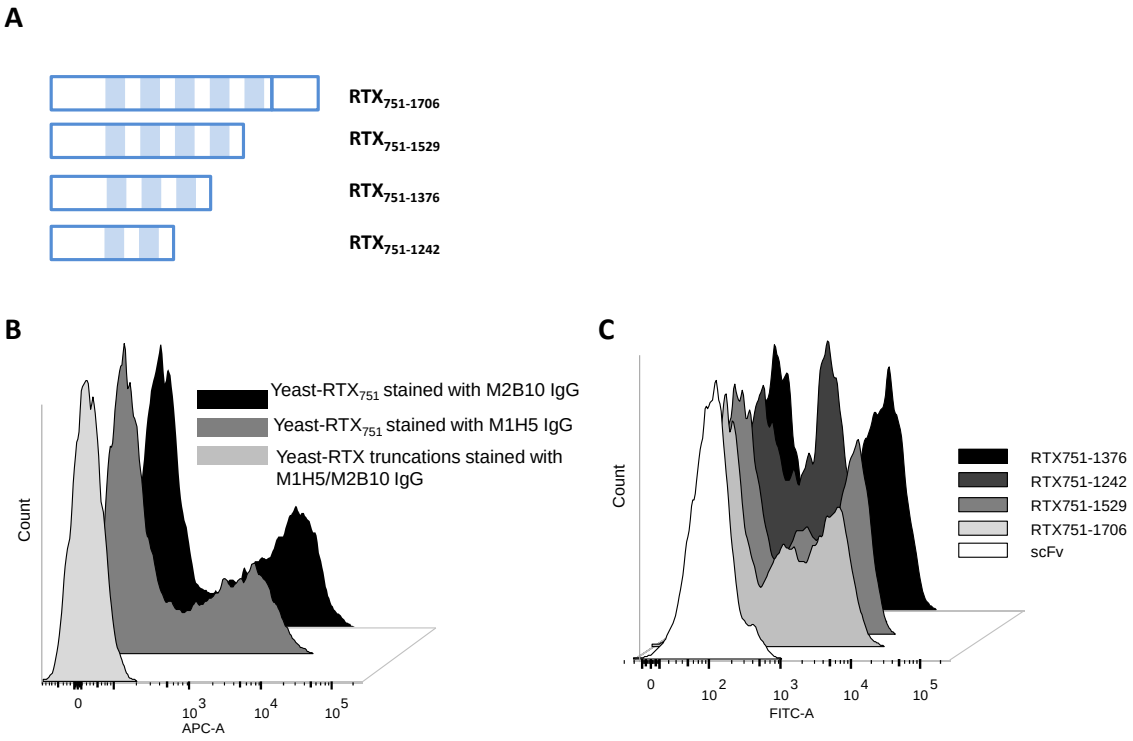

Figure 4.7: Yeast display of RTX C-terminal truncations.

(A) Diagram showing the boundaries of the C-terminal truncations of RTX domain. **(B)** Yeast cells displaying RTX_{751} and C-terminal truncations were each stained with M2B10 or M1H5, followed by Alexa647 anti-human Fc antibody. **(C)** All the variants were stained with rabbit anti-ACT polyclonal antibody, followed by FITC anti-rabbit IgG antibody. A strain displaying a scFv was included as negative control.

4.3.3 Domain truncations

To confirm the truncation results from yeast display, constructs expressing serial truncations from both the C- and N-termini of RTX_{751} domain were constructed in pET28a vector (Figure 4.8A), and expressed similarly to RTX_{751}. Small aliquots of *E. coli* cells were first lysed by boiling in SDS-PAGE sample buffer and analyzed by western blots for recognition by neutralizing antibodies M2B10 and M1H5. Purified RTX_{751} (30ng) was included as a positive control. The recognition pattern of M2B10 and M1H5 were identical (Figure 4.8B). Of the four N-terminal truncations, only RTX1244-1706 was recognized; all three C-terminal truncations were recognized. Since both 751-1242 and 1244-1706 were recognized, it suggests that the epitopes of both antibodies were discontinuous, involving residues both upstream of residue 1242 and downstream of residue 1244. The M1H5 seemed to cross-react with an endogenous *E. coli* protein at ~50kD.

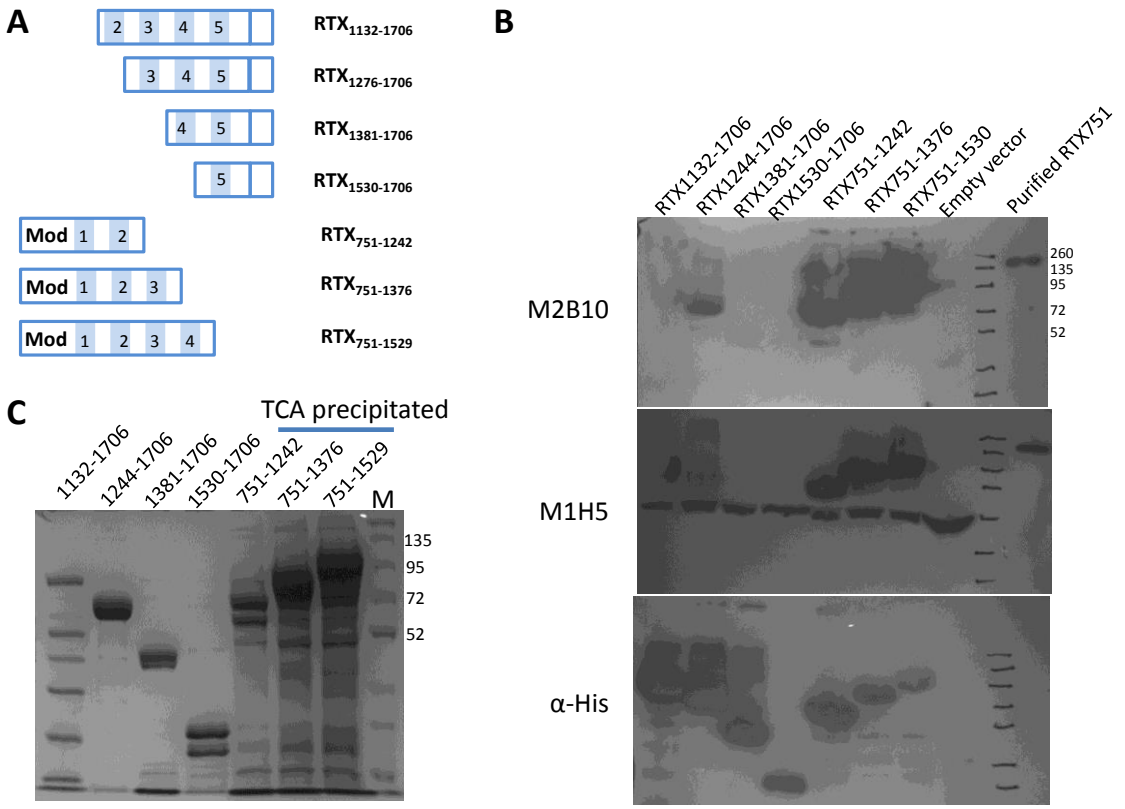

Figure 4.8: Expression of N- and C-terminal RTX truncations as soluble proteins.

N- and C-terminal truncations of RTX domain were cloned into pET28a vector for soluble expression in *E. coli*. (A) Diagram showing the boundaries of serial truncations. Shaded blocks with numbers indicate the five blocks of repeats. (B) Western blot of whole cell lysates of the truncations, probed with M2B10, M1H5, and anti-His tag antibodies. (C) SDS-PAGE of Histrap fractions of the domain truncations.

The anti His-tag antibody recognized proteins at the expected sizes for each domain truncation, confirming that all constructs were successfully expressed (Figure 4.8B). The absence of a band for the purified RTX_{751} positive control is likely due to the loss of His-tag by proteolysis. Similar phenomena were observed before with other his-tagged proteins after a few weeks of storage at 4˚C.

Then, the domains were purified as previously described from *E. coli* cell lysates using a Histrap column. For the N-terminal truncations, the areas of the elution peaks

decreased as the molecular weights got smaller. All the C-terminal truncations had very low yield. About 200 µL of the fractions were TCA-precipitated before loading onto the SDS-PAGE gel (Figure 4.8C). It has been reported that Block V (residues 1529 to 1612) including its C-terminal flanking residues (up to residue 1681) are important for the proper folding of RTX and toxicities of ACT [186]. Since the C-terminal truncations without Block V were easily detected in western blot using whole cell lysates, it is likely that they formed inclusion bodies and therefore not purified from the soluble lysates.

Then, Histrap fractions of the N-terminal truncations were analyzed on size exclusion chromatography for monomericity. All truncations were predominantly in monomeric form, except RTX1132-1706 (Figure 4.9). Consistent with the SDS-PAGE showing severe degradation of RTX1132-1706, the chromatography showed a large peak corresponding to molecular weight smaller than the full-length protein. The molecular weights calculated from amino acid sequences and estimated based on a standard curve matched very well (Figure 4.9, insert).

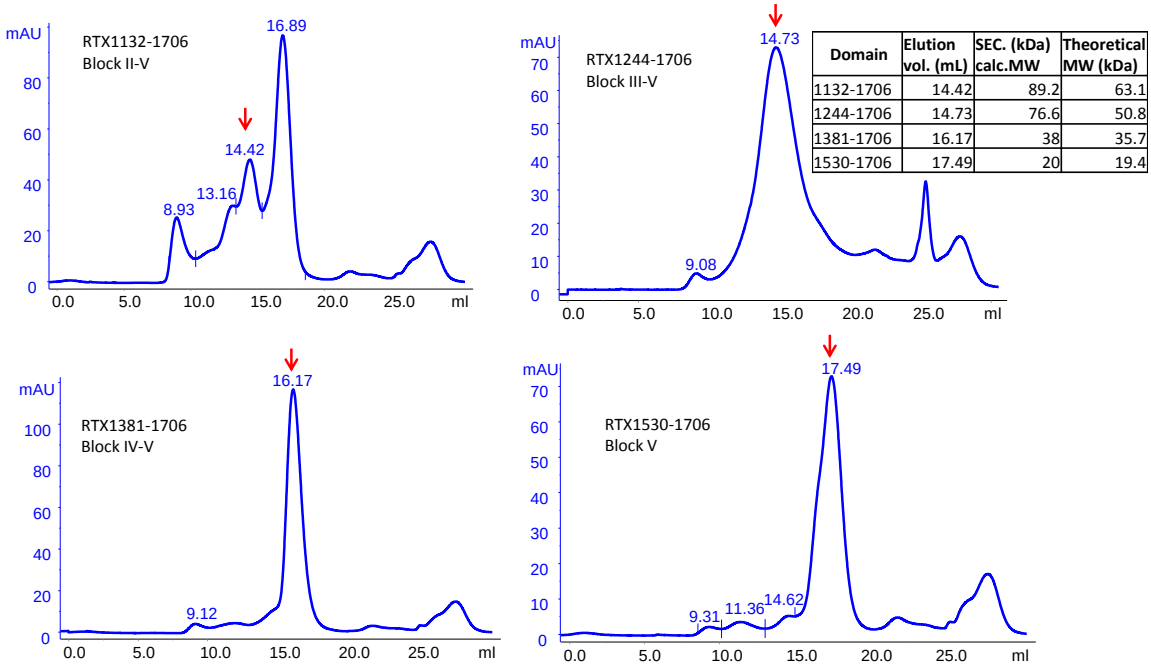

Domain	Elution vol. (mL)	SEC. (kDa) calc.MW	Theoretical MW (kDa)
1132-1706	14.42	89.2	63.1
1244-1706	14.73	76.6	50.8
1381-1706	16.17	38	35.7
1530-1706	17.49	20	19.4

Figure 4.9: Size exclusion chromatography of RTX N-terminal truncations.

Fractions from the Histrap column were loaded onto a Superdex 200 column with HBSC as running buffer. The arrows indicate monomeric fractions. The numbers above each peak indicate the elution volume. The table insert includes the theoretical molecular weights calculated from amino acid sequences and estimated molecular weights based on a standard curve generated with protein standards.

The purified N-terminal truncations were assessed for binding to M2B10 and M1H5 by ELISA. Only RTX1132-1706 showed detectable yet weak binding to both antibodies. All other truncations had no detectable binding. All truncations bound rabbit polyclonal antibody strongly (Figure 4.10). Since M1H5 also bound RTX985 weakly, it is likely that residues between 985 and 1132 do not contribute to its epitope. In contrast, this region might contribute to M2B10 epitope, since M2B10 bound RTX_{985} as strongly as RTX_{751}, yet bound $RTX_{1132\text{-}1706}$ much weaker. For $RTX_{1132\text{-}1706}$ and $RTX_{1244\text{-}1706}$, the discrepancy between western blot and ELISA results is likely due to different conformations the proteins adopt or different assay sensitivity (Figure 4.8B and 4.10).

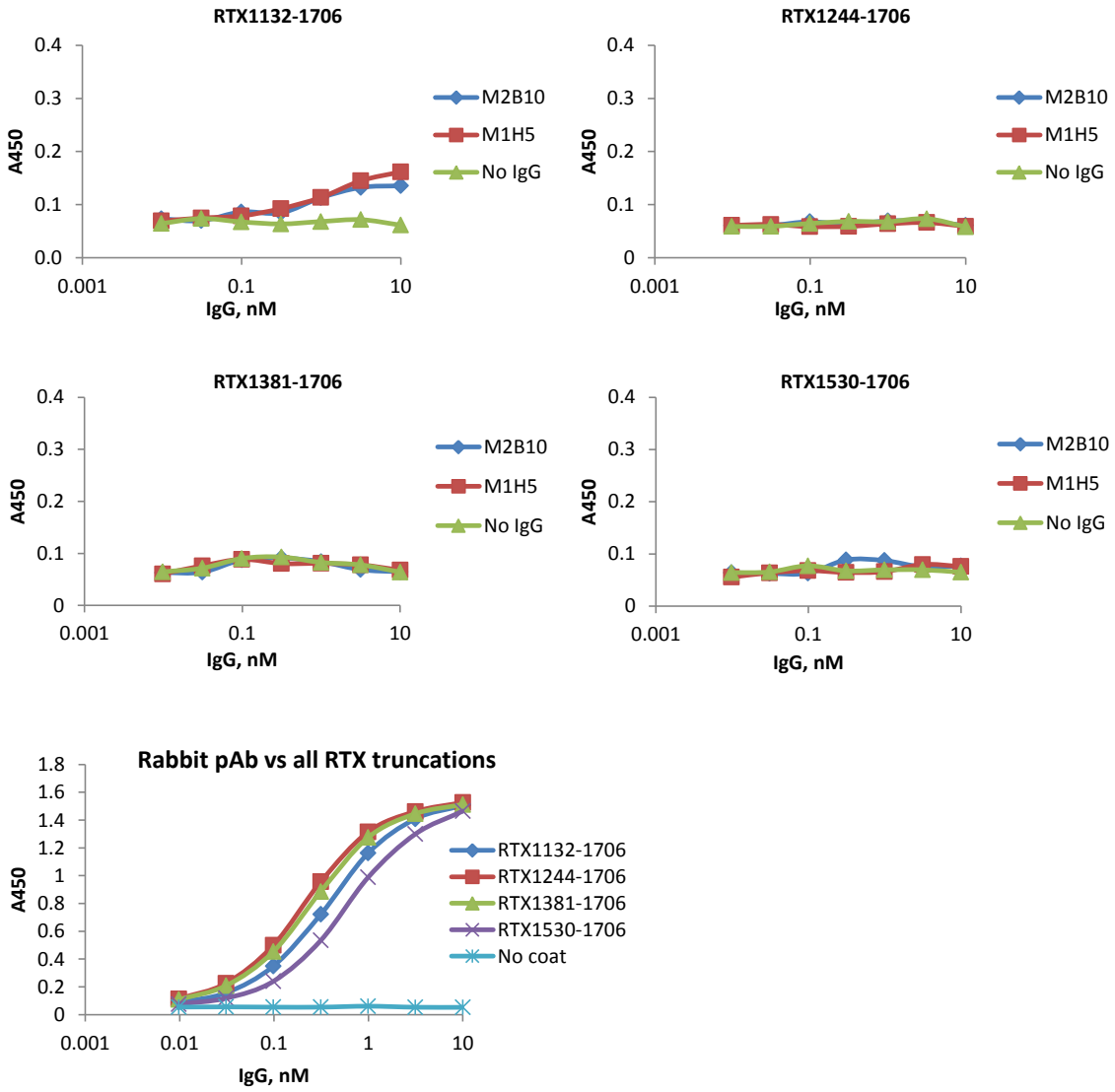

Figure 4.10: Recognition of N-terminal truncated RTX domains by M1H5, M2B10 and rabbit polyclonal antibody.

Purified N-terminal truncations of RTX domain were coated on ELISA plates. M1H5, M2B10, and rabbit polyclonal anti-ACT antibodies were serially diluted from 10nM, and detected by anti-human Fc or anti-rabbit IgG antibody-HRP conjugates.

4.3.4 Yeast display random mutagenesis library construction, sorting, and characterization

Truncations of the RTX domain from both the N- and C-termini severely affected the binding with M2B10 and M1H5, suggesting their epitopes were discontinuous and conformational. Therefore, we decided to randomly mutate residues on yeast-displayed RTX_{751} and sort the resulting library for clones that showed defects in binding to the target antibodies, a general strategy for epitope mapping using yeast display [210, 212, 216]. Unlike the preparation of phage display libraries where scFv fragments were ligated into linearized phagemid plasmids followed by transformation of the ligation product, yeast cells allow co-transformation of linearized vector backbone and insert DNA with 30~50 bp overlap on both ends. Gap repair via homologous recombination in yeast eliminates the need for ligation, provides higher efficiency, and results in larger libraries than transformation of circular plasmids into yeast.

Our initial plan was to perform random mutagenesis on stretches of ~200 residues, with block II-III being the first target. Due to the lack of unique restriction sites to generate linearized vector backbone, we tried to amplify the backbone by PCR. However, several pairs of primers and different polymerases all failed to specifically amplify the full-length backbone, likely due to the highly repetitive sequence within the RTX coding region. A unique *Sph*I restriction site lies within the RTX gene, spanning residues 1359-1361. Since the receptor binding region is suggested to be between residues 1166-1287 [32] and the region 1359-1706 contains few drastic differences among three *Bordetella* species, we decided to randomize the region between *Nhe*I and *Sph*I (corresponding to residues 751-1358), and double-digest pCTCON-RTX_{751} plasmid with *Nhe*I/*Sph*I to prepare the linearized vector (Figure 4.11A). A second library mutating the residues 1361-1706 can be constructed later, if necessary.

Error-prone PCR was performed with primers upstream of *Nhe*I and downstream of *Sph*I using 480 ng of pCTCON-RTX_{751} plasmid (equivalent of ~ 100 ng target DNA) as template. The yield was estimated to be 1.68 μg by densitometry, resulting in an amplification fold of 16. The estimated average mutation frequency is ~6 nucleotides per kb, according to the manufacture's instruction. The purified PCR product was re-amplified with a pair of nested primers. Then, purified and desalted PCR product and linearized vector was electroporated into yeast competent cells. The resulting yeast library contained a total of $2.1X10^7$ transformants as determined by serial dilution and plating on selection plates. Yeast electroporated with linearized vector without PCR product (vector-only control) had ~1000 fold less transformants. Sequencing of 12 random clones from the library showed that each one contained unique 5~9 random nucleotide mutations.

The library, vector-only control, wild-type RTX_{751}, and empty-vector yeast cultures were grown, induced, and stained by M2B10 (or M1H5) + 1H6 (Figure 4.11B). The yeast displaying wild-type RTX_{751} showed a single double positive population. The random mutagenesis library showed 3 populations: a double positive population similar to that of wild-type RTX751, a population with lower Alexa647 fluorescence indicating reduced binding with M2B10, and a population with abolished binding to M2B10 (Figure 4.11C). Interestingly, the vector-only control also showed three populations: no binding, regular binding, and one that is parallel with the regular binding population but with higher Alexa488 fluorescence. These populations are likely from *in vivo* ligation of double- or single-cut vectors or abnormal recombination events.

The random mutagenesis library stained with M2B10 + 1H6 was sorted on cell sorter. P4 and P5, cells displaying RTX_{751} with severely or moderately reduced binding affinity with M2B10, were collected. Sequencing of 12 random clones each from P4 and

P5 populations indicates that most of the P5 clones contained full length RTX_{751} domain with multiple random mutations, while the P4 clones contained truncated RTX domain with multiple mutations, deletions and insertions, many of which caused frame shift. The truncation is probably due to incorrect recombination events as a result of the highly repetitive sequence in the RTX region (Figure 4.11C).

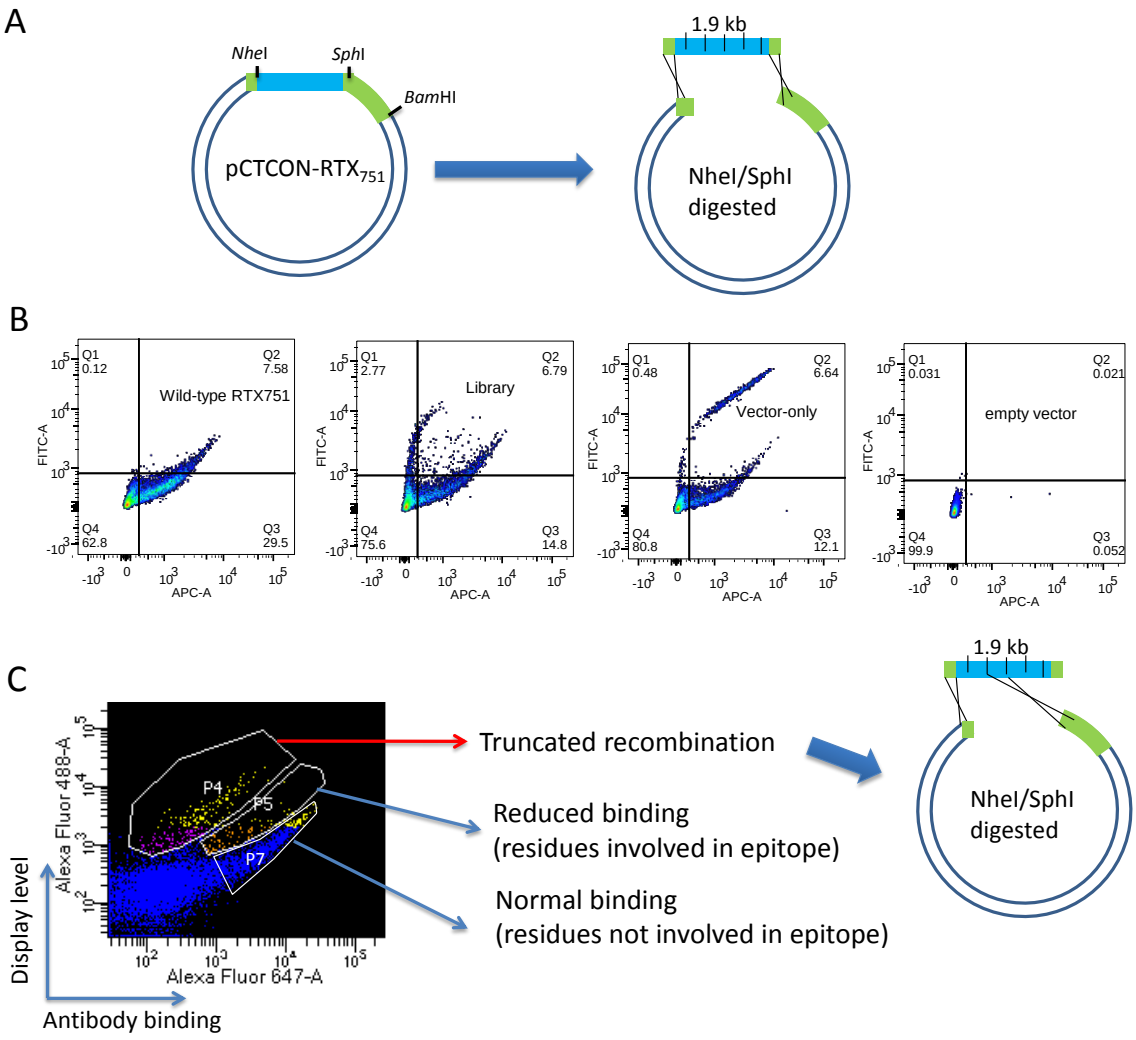

Figure 4.11

Figure 4.11: Yeast library construction and sorting.

(A) Schematic diagram demonstrating the generation of random mutagenesis library. The pCTCON-RTX_{751} plasmid was linearized with *Nhe*I and *Sph*I. The 1.9kb region with ~40bp overlap on both ends was randomized using Mutazyme II and re-amplified with Q5 polymerase. Then the linearized vector and PCR product were co-transformed into yeast by electroporation. The vertical lines within the insert DNA represent random mutations. **(B)** Yeast displaying wild-type RTX_{751}, random mutagenesis library, vector-only control, and empty-vector were grown, induced, and stained by M2B10+1H6, followed by Alexa488 anti-mouse Fc and Alexa647 anti-human Fc and analysis on an LSR Fortessa II. **(C)** Induced yeast library were stained with M2B10 and 1H6 and sorted on a FACS Aria cell sorter. DNA sequencing revealed that the P4 population with severely reduced binding to M2B10 contained truncated RTX domain, while the P5 population with moderately reduced binding to M2B10 contained full length RTX_{751} with multiple random mutations.

To assess the precision of the sorting, the sorted P4 and P5 populations were grown, induced, stained with M2B10 and 1H6, and analyzed by flow cytometry again. Most of the cells fall within the original sorting gate with minor bleed-through (Figure 4.12).

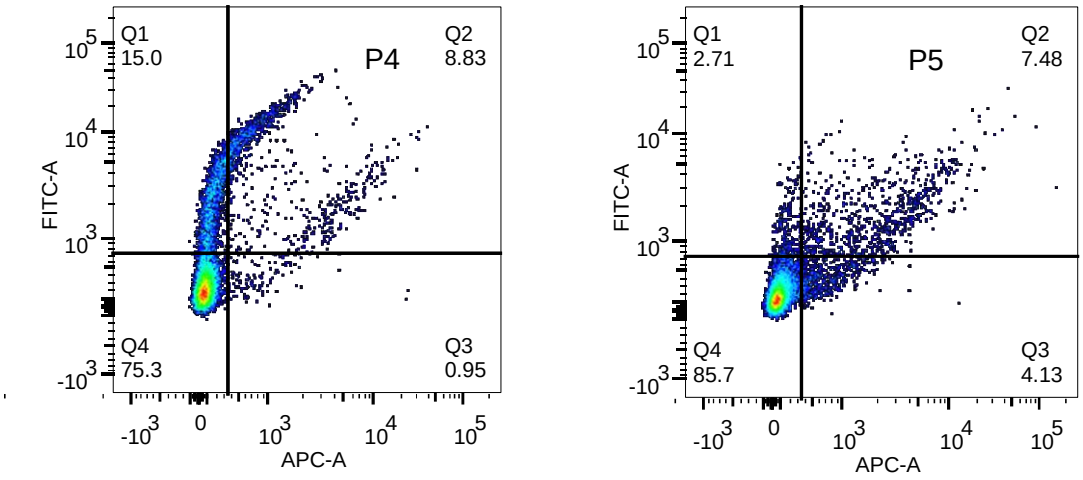

Figure 4.12: Validation of sorted populations.

P4 and P5 cells collected by the cell sorter were grown, induced, and stained with 10 µg/mL M2B10 + 1H6, followed by Alexa488 anti-mouse Fc and Alexa647 anti-human Fc and analysis on an LSR Fortessa II.

To further characterize the sorted clones, 4 plasmids each from the sequenced P4 and P5 clones were re-transformed into EBY100 yeast cells, and the displayed RTX variants were stained with M2B10 and 1H6 (Figure 4.12). Yeast displaying wild-type RTX_{751} was included as a positive control, and a gate was drawn around the double positive population. All four clones from P4 showed severely reduced binding with M2B10, consistent with the sorting gate; while 3 out of 4 clones from P5 showed moderately reduced binding with M2B10. For P5 clones, clone #2 contained 5 substitutions (T865I, E1153D, D1200V, A1214V, K1242N); clone #5 contained 4 substitutions (H1009L, K1008R, L1124M, I1231F); clone #9 contained 8 substitutions (G774R, V902M, H905Y, K983R, G1072E, P1120S, R1164C, A1214V); Clone #12 contained 9 amino acid substitutions (G825C, A924T, G999R, S1075T, G1177D, D1179N, H1225L, N1302K, E1339G) and was completely abolished for M2B10 binding.

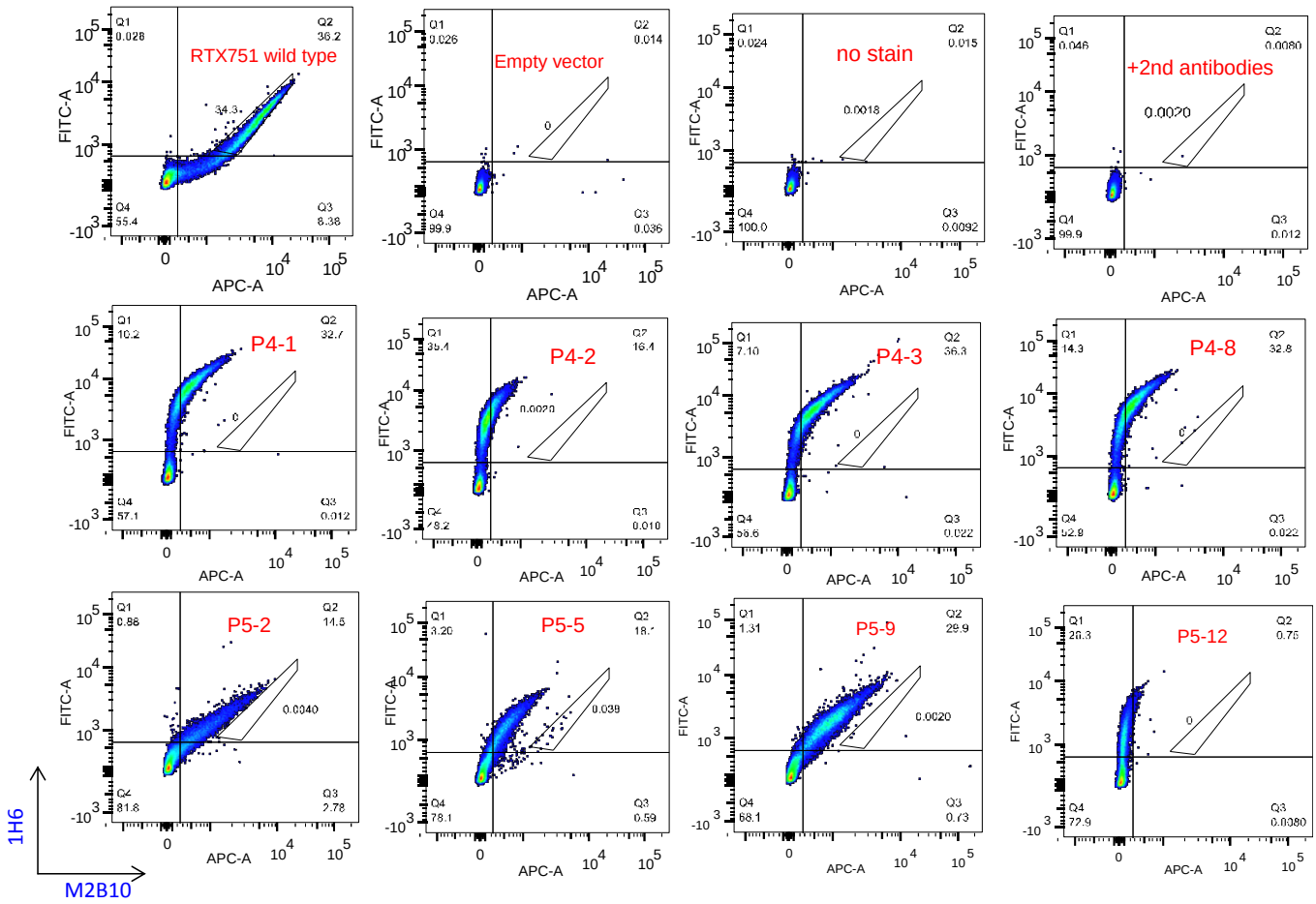

Figure 4.13: Flow cytometric analysis of sorted clones.

Four plasmids each from the P4 and P5 populations were transformed into EBY100 cells, grown, induced, and stained with M2B10 and 1H6, to determine whether the sorted clones fall within the respective gates.

One round of sorting separated the different populations very well. Therefore, no successive sorting was performed on the sorted population. Considering that mutations not affecting antibody binding would be orthogonal to those affecting binding, sortings were performed on the starting library stained with M2B10 (or M1H5) + 1H6, collecting ~50,000 cells of the P5 and P7 populations.

4.3.5 Next-generation sequencing of sorted libraries

After FACS, the collected cell populations were grown in selection medium until OD600 > 2.0. Equivalent of 0.2OD cells (P5, P7, and starting library) were pelleted and used for plasmid extraction. Then the region that had been mutagenized was amplified from the plasmids. For P5 and P7, a major band at the expected size, 1.9 kb, was amplified; while for the starting library, an extra band at ~ 850 bp was amplified. This lower band might come from nonspecific amplification or from the P4 population with truncated RTX domain (Figure 4.14). Only the 1.9kb fragment was excised and gel purified.

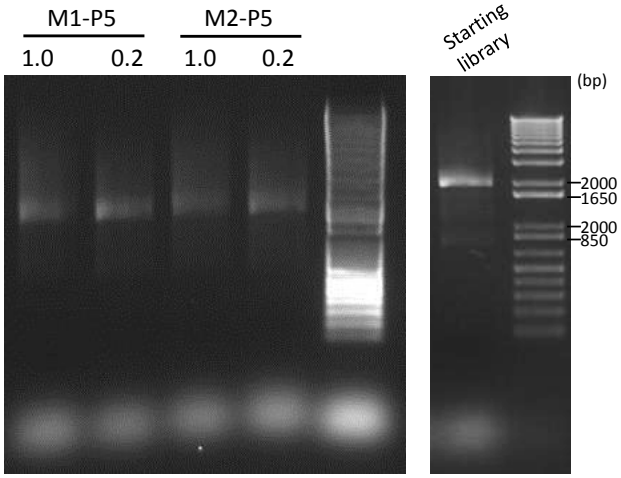

Figure 4.14: PCR amplification of mutagenized region for high-throughput sequencing. Yeast cultures were pelleted and plasmids were extracted from 0.2 or 1.0 OD. The mutagenized region was amplified by Q5 polymerase using 1 µL each of the plasmids per 25 µL reaction.

The resulting gel-purified PCR fragments were fragmented to an average size of 250bp and sequenced on an Illumina Hiseq2500 in 2X125bp mode. The data analysis is in progress.

4.4 DISCUSSION

Structure-function analyses of antibody-antigen interactions can identify residues forming protective epitopes, key information to guide design of immunogens able to elicit neutralizing antibodies. This approach has been employed for complex antigens with high sequence variability and metastable protective epitopes, such as fHBP from *Neisseria meningitidis* [217], and the F-protein from respiratory syncytial virus [218].

The expression of highly conserved ACT by all three major species of *Bordetella* makes it an attractive target for neutralizing antibodies treating pertussis caused by different species, and also provide insight into the residues involved in the epitopes of neutralizing antibodies. The majority of the variations are within the RTX domain of ACT. M2B10 binds all three RTXs, while M1H5 preferentially recognizes RTX of *B. pertussis*. Changing 9 residues in the beginning of *B. pertussis* RTX block III into corresponding residues of *B. parapertussis* RTX abolished binding by M1H5 but not by M2B10, suggesting these residues are involved in M1H5 epitope. The antibody specificity is also correlated with the protection of J774A.1 cells from ACT produced by the different species.

Truncation of the RTX domain at N- and C-termini was performed, aiming to determine the minimal domain that retains binding to M2B10 and M1H5. None of the truncations, in their soluble or displayed form, was able to be strongly recognized by the neutralizing antibodies, suggesting that the epitopes of M2B10 and M1H5 are discontinuous and conformational.

Yeast surface display in combination with random mutagenesis has been successfully employed for mapping of conformational epitopes for several antigens [210, 212, 216]. The largest antigen displayed in these studies is ~50 kDa. Here, the ~100 kDa RTX_{751} was successfully displayed on yeast surface and recognized by M2B10, M1H5

and 1H6, but not other previous mAbs described by Lee *et al.* [147]. For unknown reason, the c-myc tag at the C-terminal of RTX protein was not detectable by antibody. Instead, we used 1H6 recognizing the C-terminus of ACT as the control for full-length protein and expression level.

Due to the length of the RTX domain, our yeast random mutagenesis library is not meant, nor possible, to cover the entire sequence space. Instead, it provides more details about discontinuous residues of the conformational epitope. The data analysis of high-throughput sequencing is in progress.

Chapter 5 Conclusion and future directions

5.1 CONCLUSIONS

Using phage display technology, we have identified two novel neutralizing antibodies that protect macrophage-like cells from cAMP intoxication by the adenylate cyclase toxin (ACT) of *Bordetella*. M2B10 and M1H5 bind two non-overlapping calcium-dependent conformational epitopes that are different from any previously known anti-ACT monoclonal antibodies. M2B10 does not distinguish ACT from all three *Bordetella* species, while M1H5 preferentially recognize *B. pertussis* ACT. Our data suggest the mode of action for both M2B10 and M1H5 is the disruption of interaction between ACT and its cellular receptor, $\alpha_M\beta_2$ integrin. This is the first report of neutralizing antibodies against toxins from the RTX family using such a mechanism.

The RTX domain of ACT is immunodominant both in mouse and human. It induces neutralizing antibodies in mice at a similar level to that by full-length ACT, yet it is biophysically more stable. Therefore, RTX domain has great potential to become a protective antigen in the next generation acellular pertussis vaccines.

5.2 ONGOING WORK AND RECOMMENDED FUTURE DIRECTIONS

The representative neutralizing antibodies, M2B10 and M1H5, potently neutralize ACT in *in vitro* cell-based assays. However, in order to advance them into the clinic, it is essential to show that they can also provide protection *in vivo*, either by themselves or in combination with neutralizing antibodies against other major toxins of *B. pertussis* (e.g. pertussis toxin). M2B10 broadly neutralizes ACT from *B. pertussis*, *B. bronchiseptica*, and *B. parapertussis*. It would be interesting to see if M2B10 can be used to treat infections by *B. bronchiseptica* and *B. parapertussis* as well.

M2B10 or M1H5 binds the *B. pertussis* cells, but it remains to be determined if they could exert bactericidal activity through antibody-dependent cell-mediated cytotoxicity or complement-mediated killing. This would likely require comparison of the antibodies as different isotypes in *in vitro* or *in vivo* assays.

Although we have shown that RTX domain induced neutralizing antibodies in mice, it remains to be tested in animal models to see if RTX can actually induce protective immunity against bacterial infection. Since RTX domain is likely an addition to, instead of a substitution of, the current acellular vaccines, it would be important to see if its main effect is through induction of anti-ACT neutralizing antibodies, or does it also change the balance of Th1/Th2 response by eliminating the toxicities of ACT on immune cells.

A high resolution crystal structure of ACT alone or co-crystal structure with neutralizing antibodies will be very helpful in understanding the structural basis of stability and immunogenicity of the antigen, which are the basis for designing stable and highly protective antigens.

References

1. Friedman, R.L., *Pertussis: the disease and new diagnostic methods.* Clin Microbiol Rev, 1988. **1**(4): p. 365-76.
2. Cornia, P.B., et al., *Does this coughing adolescent or adult patient have pertussis?* JAMA, 2010. **304**(8): p. 890-6.
3. Chenal-Francisque, V., et al., *Genomic analysis of the adenylate cyclase-hemolysin C-terminal region of Bordetella pertussis, Bordetella parapertussis and Bordetella bronchiseptica.* Res Microbiol, 2009. **160**(5): p. 330-6.
4. Parkhill, J., et al., *Comparative analysis of the genome sequences of Bordetella pertussis, Bordetella parapertussis and Bordetella bronchiseptica.* Nature Genetics, 2003. **35**(1): p. 32-40.
5. Watanabe, M. and M. Nagai, *Whooping cough due to Bordetella parapertussis: an unresolved problem.* Expert Rev Anti Infect Ther, 2004. **2**(3): p. 447-54.
6. Witt, M.A., P.H. Katz, and D.J. Witt, *Unexpectedly limited durability of immunity following acellular pertussis vaccination in preadolescents in a North American outbreak.* Clin Infect Dis, 2012. **54**(12): p. 1730-5.
7. Octavia, S., et al., *Newly emerging clones of Bordetella pertussis carrying prn2 and ptxP3 alleles implicated in Australian pertussis epidemic in 2008-2010.* J Infect Dis, 2012. **205**(8): p. 1220-4.
8. Higgs, R., et al., *Immunity to the respiratory pathogen Bordetella pertussis.* Mucosal Immunol, 2012. **5**(5): p. 485-500.
9. Sheridan, S.L., et al., *Number and order of whole cell pertussis vaccines in infancy and disease protection.* JAMA, 2012. **308**(5): p. 454-6.
10. Warfel, J.M., L.I. Zimmerman, and T.J. Merkel, *Acellular pertussis vaccines protect against disease but fail to prevent infection and transmission in a nonhuman primate model.* Proc Natl Acad Sci U S A, 2014. **111**(2): p. 787-92.
11. Plotkin, S.A., *Complex correlates of protection after vaccination.* Clin Infect Dis, 2013. **56**(10): p. 1458-65.
12. Plotkin, S.A., *Correlates of protection induced by vaccination.* Clin Vaccine Immunol, 2010. **17**(7): p. 1055-65.
13. Dajani, N.A. and D. Scheifele, *How long can we expect pertussis protection to last after the adolescent booster dose of tetanus-diphtheria-pertussis (Tdap) vaccines?* Paediatr Child Health, 2007. **12**(10): p. 873-4.
14. Lim, A., et al., *Protective role of adenylate cyclase in the context of a live pertussis vaccine candidate.* Microbes Infect, 2014. **16**(1): p. 51-60.
15. Polewicz, M., et al., *Novel vaccine formulations against pertussis offer earlier onset of immunity and provide protection in the presence of maternal antibodies.* Vaccine, 2013. **31**(31): p. 3148-55.
16. Cherry, J.D., et al., *Antibody response patterns to Bordetella pertussis antigens in vaccinated (primed) and unvaccinated (unprimed) young children with pertussis.* Clin Vaccine Immunol, 2010. **17**(5): p. 741-7.

17. Berbers, G.A., S.C. de Greeff, and F.R. Mooi, *Improving pertussis vaccination.* Hum Vaccin, 2009. **5**(7): p. 497-503.
18. Carbonetti, N.H., et al., *Pertussis toxin and adenylate cyclase toxin provide a one-two punch for establishment of Bordetella pertussis infection of the respiratory tract.* Infection and immunity, 2005. **73**(5): p. 2698.
19. Goodwin, M. and A. Weiss, *Adenylate cyclase toxin is critical for colonization and pertussis toxin is critical for lethal infection by Bordetella pertussis in infant mice.* Infection and immunity, 1990. **58**(10): p. 3445.
20. Khelef, N., H. Sakamoto, and N. Guiso, *Both adenylate cyclase and hemolytic activities are required by Bordetella pertussis to initiate infection.* Microbial pathogenesis, 1992. **12**(3): p. 227-235.
21. Guiso, N., et al., *Bordetella adenylate cyclase is a virulence associated factor and an immunoprotective antigen.* Microbial pathogenesis, 1989. **7**(5): p. 373-380.
22. Guiso, N., M. Szatanik, and M. Rocancourt, *Protective activity of Bordetella adenylate cyclase-hemolysin against bacterial colonization.* Microbial pathogenesis, 1991. **11**(6): p. 423-431.
23. Farfel, Z., et al., *Antibodies to Bordetella pertussis adenylate cyclase are produced in man during pertussis infection and after vaccination.* Journal of medical microbiology, 1990. **32**(3): p. 173-177.
24. Guo, Q., et al., *Structural basis for the interaction of Bordetella pertussis adenylyl cyclase toxin with calmodulin.* EMBO J, 2005. **24**(18): p. 3190-201.
25. Raptis, A., L. Knipling, and J. Wolff, *Dissociation of catalytic and invasive activities of Bordetella pertussis adenylate cyclase.* Infect Immun, 1989. **57**(6): p. 1725-30.
26. Paccani, S.R., et al., *Suppression of T-lymphocyte activation and chemotaxis by the adenylate cyclase toxin of Bordetella pertussis.* Infect Immun, 2008. **76**(7): p. 2822-32.
27. Henderson, M.W., et al., *Contribution of Bordetella Filamentous Hemagglutinin and Adenylate Cyclase Toxin to Suppression and Evasion of Interleukin-17-Mediated Inflammation.* Infection and immunity, 2012. **80**(6): p. 2061-2075.
28. Rossi Paccani, S., et al., *The adenylate cyclase toxins of Bacillus anthracis and Bordetella pertussis promote Th2 cell development by shaping T cell antigen receptor signaling.* PLoS Pathog, 2009. **5**(3): p. e1000325.
29. Benz, R., et al., *Adenylate cyclase toxin (CyaA) of Bordetella pertussis. Evidence for the formation of small ion-permeable channels and comparison with HlyA of Escherichia coli.* J Biol Chem, 1994. **269**(44): p. 27231-9.
30. Hackett, M., et al., *Hemolytic, but not cell-invasive activity, of adenylate cyclase toxin is selectively affected by differential fatty-acylation in Escherichia coli.* Journal of Biological Chemistry, 1995. **270**(35): p. 20250-20253.
31. Guermonprez, P., et al., *The adenylate cyclase toxin of Bordetella pertussis binds to target cells via the αMβ2 integrin (CD11b/CD18).* The Journal of experimental medicine, 2001. **193**(9): p. 1035.

32. El-Azami-El-Idrissi, M., et al., *Interaction of Bordetella pertussis adenylate cyclase with CD11b/CD18: Role of toxin acylation and identification of the main integrin interaction domain.* J Biol Chem, 2003. **278**(40): p. 38514-21.
33. Basar, T., et al., *Acylation of lysine 983 is sufficient for toxin activity of Bordetella pertussis adenylate cyclase. Substitutions of alanine 140 modulate acylation site selectivity of the toxin acyltransferase CyaC.* J Biol Chem, 2001. **276**(1): p. 348-54.
34. Zaretzky, F.R., M.C. Gray, and E.L. Hewlett, *Mechanism of association of adenylate cyclase toxin with the surface of Bordetella pertussis: a role for toxin-filamentous haemagglutinin interaction.* Mol Microbiol, 2002. **45**(6): p. 1589-98.
35. Perez Vidakovics, M.L., et al., *Adenylate cyclase influences filamentous haemagglutinin-mediated attachment of Bordetella pertussis to epithelial alveolar cells.* FEMS Immunol Med Microbiol, 2006. **48**(1): p. 140-7.
36. Gray, M.C., et al., *Newly secreted adenylate cyclase toxin is responsible for intoxication of target cells by Bordetella pertussis.* Mol Microbiol, 2004. **53**(6): p. 1709-19.
37. Sotomayor Perez, A.C., et al., *Characterization of the regions involved in the calcium-induced folding of the intrinsically disordered RTX motifs from the bordetella pertussis adenylate cyclase toxin.* J Mol Biol, 2010. **397**(2): p. 534-49.
38. Baumann, U., et al., *Three-dimensional structure of the alkaline protease of Pseudomonas aeruginosa: a two-domain protein with a calcium binding parallel beta roll motif.* EMBO J, 1993. **12**(9): p. 3357-64.
39. Eby, J.C., et al., *Selective translocation of the Bordetella pertussis adenylate cyclase toxin across the basolateral membranes of polarized epithelial cells.* Journal of Biological Chemistry, 2010. **285**(14): p. 10662.
40. Martín, C., et al., *Adenylate Cyclase Toxin Promotes Internalisation of Integrins and Raft Components and Decreases Macrophage Adhesion Capacity.* PloS one, 2011. **6**(2): p. e17383.
41. Fiser, R., et al., *Calcium influx rescues adenylate cyclase-hemolysin from rapid cell membrane removal and enables phagocyte permeabilization by toxin pores.* PLoS Pathog, 2012. **8**(4): p. e1002580.
42. Bellalou, J., et al., *Deletions affecting hemolytic and toxin activities of Bordetella pertussis adenylate cyclase.* Infect Immun, 1990. **58**(10): p. 3242-7.
43. Martín, C., et al., *Membrane restructuring by Bordetella pertussis adenylate cyclase toxin, a member of the RTX toxin family.* Journal of bacteriology, 2004. **186**(12): p. 3760-3765.
44. Veneziano, R., et al., *Bordetella pertussis adenylate cyclase toxin translocation across a tethered lipid bilayer.* Proc Natl Acad Sci U S A, 2013. **110**(51): p. 20473-8.
45. Knapp, O., et al., *Pore formation by the Bordetella adenylate cyclase toxin in lipid bilayer membranes: role of voltage and pH.* Biochim Biophys Acta, 2008. **1778**(1): p. 260-9.

46. Rogel, A., R. Meller, and E. Hanski, *Adenylate cyclase toxin from Bordetella pertussis. The relationship between induction of cAMP and hemolysis.* Journal of Biological Chemistry, 1991. **266**(5): p. 3154.
47. Gray, M., et al., *Distinct mechanisms for K+ efflux, intoxication, and hemolysis by Bordetella pertussis AC toxin. Human erythorcytes are resistent to hemolysis by ACT for unknown reason.* Journal of Biological Chemistry, 1998. **273**(29): p. 18260.
48. Schlecht, G., et al., *Antigen targeting to CD11b allows efficient presentation of CD4+ and CD8+ T cell epitopes and in vivo Th1-polarized T cell priming.* The Journal of Immunology, 2004. **173**(10): p. 6089.
49. Osickova, A., et al., *Adenylate cyclase toxin translocates across target cell membrane without forming a pore.* Molecular microbiology, 2010. **75**(6): p. 1550-1562.
50. Basler, M., et al., *Segments crucial for membrane translocation and pore-forming activity of Bordetella adenylate cyclase toxin.* Journal of Biological Chemistry, 2007. **282**(17): p. 12419.
51. Dunne, A., et al., *Inflammasome activation by adenylate cyclase toxin directs Th17 responses and protection against Bordetella pertussis.* The Journal of Immunology, 2010. **185**(3): p. 1711.
52. Gray, M.C., et al., *Translocation-specific conformation of adenylate cyclase toxin from Bordetella pertussis inhibits toxin-mediated hemolysis.* Journal of bacteriology, 2001. **183**(20): p. 5904.
53. Gmira, S., G. Karimova, and D. Ladant, *Characterization of recombinant Bordetella pertussis adenylate cyclase toxins carrying passenger proteins.* Res Microbiol, 2001. **152**(10): p. 889-900.
54. Karimova, G., et al., *Charge-dependent translocation of Bordetella pertussis adenylate cyclase toxin into eukaryotic cells: implication for the in vivo delivery of CD8(+) T cell epitopes into antigen-presenting cells.* Proc Natl Acad Sci U S A, 1998. **95**(21): p. 12532-7.
55. Osika, R., et al., *Delivery of CD8+ T-cell epitopes into major histocompatibility complex class I antigen presentation pathway by Bordetella pertussis adenylate cyclase: delineation of cell invasive structures and permissive insertion sites.* Infect. Immun, 2000. **68**: p. 247-256.
56. Fayolle, C., et al., *In vivo induction of CTL responses by recombinant adenylate cyclase of Bordetella pertussis carrying viral CD8+ T cell epitopes.* J Immunol, 1996. **156**(12): p. 4697-706.
57. Saron, M.F., et al., *Anti-viral protection conferred by recombinant adenylate cyclase toxins from Bordetella pertussis carrying a CD8+ T cell epitope from lymphocytic choriomeningitis virus.* Proc Natl Acad Sci U S A, 1997. **94**(7): p. 3314-9.
58. Loucka, J., et al., *Delivery of a MalE CD4(+)-T-cell epitope into the major histocompatibility complex class II antigen presentation pathway by Bordetella pertussis adenylate cyclase.* Infect Immun, 2002. **70**(2): p. 1002-5.

59. Preville, X., et al., *Eradication of established tumors by vaccination with recombinant Bordetella pertussis adenylate cyclase carrying the human papillomavirus 16 E7 oncoprotein.* Cancer Res, 2005. **65**(2): p. 641-9.
60. Reichert, J.M., *Marketed therapeutic antibodies compendium.* MAbs, 2012. **4**(3): p. 413-5.
61. Wlaschin, K.F. and W.S. Hu, *Fedbatch culture and dynamic nutrient feeding.* Adv Biochem Eng Biotechnol, 2006. **101**: p. 43-74.
62. Maynard, J. and G. Georgiou, *Antibody engineering.* Annu Rev Biomed Eng, 2000. **2**: p. 339-76.
63. Fernandez, P., et al., *A phase 2, randomized, double-blind safety and pharmacokinetic assessment of respiratory syncytial virus (RSV) prophylaxis with motavizumab and palivizumab administered in the same season.* BMC Pediatr, 2010. **10**: p. 38.
64. Stiehm, E.R., M.A. Keller, and G.N. Vyas, *Preparation and use of therapeutic antibodies primarily of human origin.* Biologicals, 2008. **36**(6): p. 363-74.
65. Bakker, A.B., et al., *Novel human monoclonal antibody combination effectively neutralizing natural rabies virus variants and individual in vitro escape mutants.* J Virol, 2005. **79**(14): p. 9062-8.
66. Demarest, S.J., K. Hariharan, and J. Dong, *Emerging antibody combinations in oncology.* MAbs, 2011. **3**(4): p. 338-51.
67. Ben-Kasus, T., et al., *Persistent elimination of ErbB-2/HER2-overexpressing tumors using combinations of monoclonal antibodies: relevance of receptor endocytosis.* Proc Natl Acad Sci U S A, 2009. **106**(9): p. 3294-9.
68. Dechant, M., et al., *Complement-dependent tumor cell lysis triggered by combinations of epidermal growth factor receptor antibodies.* Cancer Res, 2008. **68**(13): p. 4998-5003.
69. Spiridon, C.I., et al., *Targeting multiple Her-2 epitopes with monoclonal antibodies results in improved antigrowth activity of a human breast cancer cell line in vitro and in vivo.* Clin Cancer Res, 2002. **8**(6): p. 1720-30.
70. Nahta, R., M.C. Hung, and F.J. Esteva, *The HER-2-targeting antibodies trastuzumab and pertuzumab synergistically inhibit the survival of breast cancer cells.* Cancer Res, 2004. **64**(7): p. 2343-6.
71. Bostrom, J., et al., *Variants of the antibody herceptin that interact with HER2 and VEGF at the antigen binding site.* Science, 2009. **323**(5921): p. 1610-4.
72. Pedersen, M.W., et al., *Sym004: a novel synergistic anti-epidermal growth factor receptor antibody mixture with superior anticancer efficacy.* Cancer Res, 2010. **70**(2): p. 588-97.
73. Koefoed, K., et al., *Rational identification of an optimal antibody mixture for targeting the epidermal growth factor receptor.* MAbs, 2011. **3**(6): p. 584-95.
74. Spangler, J.B., et al., *Combination antibody treatment down-regulates epidermal growth factor receptor by inhibiting endosomal recycling.* Proc Natl Acad Sci U S A, 2010. **107**(30): p. 13252-7.

75. Skartved, N.J., et al., *Preclinical pharmacokinetics and safety of Sym004: a synergistic antibody mixture directed against epidermal growth factor receptor.* Clin Cancer Res, 2011. **17**(18): p. 5962-72.
76. Volk, W.A., et al., *Neutralization of tetanus toxin by distinct monoclonal antibodies binding to multiple epitopes on the toxin molecule.* Infect Immun, 1984. **45**(3): p. 604-9.
77. de Kruif, J., et al., *Human immunoglobulin repertoires against tetanus toxoid contain a large and diverse fraction of high-affinity promiscuous V(H) genes.* J Mol Biol, 2009. **387**(3): p. 548-58.
78. Lang, A.B., et al., *Immunotherapy with human monoclonal antibodies. Fragment A specificity of polyclonal and monoclonal antibodies is crucial for full protection against tetanus toxin.* J Immunol, 1993. **151**(1): p. 466-72.
79. Nowakowski, A., et al., *Potent neutralization of botulinum neurotoxin by recombinant oligoclonal antibody.* Proc Natl Acad Sci U S A, 2002. **99**(17): p. 11346-50.
80. Cheng, L.W., et al., *Antibody protection against botulinum neurotoxin intoxication in mice.* Infect Immun, 2009. **77**(10): p. 4305-13.
81. Tomic, M., et al., *Recombinant monoclonal antibody based anti-toxin for treatment of type A, B, and E botulism*, in *Public Health Emergency Medical Countermeasures Enterprise* 2011: Washington, DC.
82. Garcia-Rodriguez, C., et al., *Molecular evolution of antibody cross-reactivity for two subtypes of type A botulinum neurotoxin.* Nat Biotechnol, 2007. **25**(1): p. 107-16.
83. Garcia-Rodriguez, C., et al., *Neutralizing human monoclonal antibodies binding multiple serotypes of botulinum neurotoxin.* Protein Eng Des Sel, 2011. **24**(3): p. 321-31.
84. Kramer, R.A., et al., *The human antibody repertoire specific for rabies virus glycoprotein as selected from immune libraries.* Eur J Immunol, 2005. **35**(7): p. 2131-45.
85. Goudsmit, J., et al., *Comparison of an anti-rabies human monoclonal antibody combination with human polyclonal anti-rabies immune globulin.* J Infect Dis, 2006. **193**(6): p. 796-801.
86. Bakker, A.B., et al., *First administration to humans of a monoclonal antibody cocktail against rabies virus: safety, tolerability, and neutralizing activity.* Vaccine, 2008. **26**(47): p. 5922-7.
87. Lowy, I., et al., *Treatment with monoclonal antibodies against Clostridium difficile toxins.* N Engl J Med, 2010. **362**(3): p. 197-205.
88. ter Meulen, J., et al., *Human monoclonal antibody combination against SARS coronavirus: synergy and coverage of escape mutants.* PLoS Med, 2006. **3**(7): p. e237.
89. Galun, E., et al., *Clinical evaluation (phase I) of a combination of two human monoclonal antibodies to HBV: safety and antiviral properties.* Hepatology, 2002. **35**(3): p. 673-9.

90. Eren, R., et al., *Preclinical evaluation of two neutralizing human monoclonal antibodies against hepatitis C virus (HCV): a potential treatment to prevent HCV reinfection in liver transplant patients.* J Virol, 2006. **80**(6): p. 2654-64.
91. Armbruster, C., et al., *Passive immunization with the anti-HIV-1 human monoclonal antibody (hMAb) 4E10 and the hMAb combination 4E10/2F5/2G12.* J Antimicrob Chemother, 2004. **54**(5): p. 915-20.
92. Trkola, A., et al., *In vivo efficacy of human immunodeficiency virus neutralizing antibodies: estimates for protective titers.* J Virol, 2008. **82**(3): p. 1591-9.
93. Doria-Rose, N.A., et al., *HIV-1 neutralization coverage is improved by combining monoclonal antibodies that target independent epitopes.* J Virol, 2012. **86**(6): p. 3393-7.
94. Klitgaard, J.L., et al., *Reduced susceptibility of recombinant polyclonal antibodies to inhibitory anti-variable domain antibody responses.* J Immunol, 2006. **177**(6): p. 3782-90.
95. Coljee, V.W., *Staphylococcus aureus specific human recombinant polyclonal antibodies and uses thereof*. 2010.
96. Zondervan, Q., et al., *Human recombinant antibody (Ab) cocktails protect against Methicillin Resistant Staphylococcus aureus (MRSA) infection in mice*, in *Interscience Conference on Antimicrobial Agents and Chemotherapy*. 2010: Boston, MA.
97. Bruss, J.B. and G.R. Siber, *Protective effects of pertussis immunoglobulin (P-IGIV) in the aerosol challenge model.* Clin Diagn Lab Immunol, 1999. **6**(4): p. 464-70.
98. Bruss, J.B., et al., *Treatment of severe pertussis: a study of the safety and pharmacology of intravenous pertussis immunoglobulin.* Pediatr Infect Dis J, 1999. **18**(6): p. 505-11.
99. Granstrom, M., et al., *Specific immunoglobulin for treatment of whooping cough.* Lancet, 1991. **338**(8777): p. 1230-3.
100. Halperin, S.A., et al., *Is pertussis immune globulin efficacious for the treatment of hospitalized infants with pertussis? No answer yet.* Pediatr Infect Dis J, 2007. **26**(1): p. 79-81.
101. Sato, H. and Y. Sato, *Protective activities in mice of monoclonal antibodies against pertussis toxin.* Infect Immun, 1990. **58**(10): p. 3369-74.
102. Sutherland, J.N. and J.A. Maynard, *Characterization of a key neutralizing epitope on pertussis toxin recognized by the monoclonal antibody 1B7.* Biochemistry, 2009. **48**(50): p. 11982-11993.
103. Lee, S.J., et al., *Epitope mapping of monoclonal antibodies against Bordetella pertussis adenylate cyclase toxin.* Infect Immun, 1999. **67**(5): p. 2090-5.
104. Maynard, J.A., et al., *Protection against anthrax toxin by recombinant antibody fragments correlates with antigen affinity.* Nature Biotechnology, 2002. **20**: p. 597-601.
105. Binley, J.M., et al., *Human antibody responses to HIV type 1 glycoprotein 41 cloned in phage display libraries suggest three major epitopes are recognized and*

give evidence for conserved antibody motifs in antigen binding. AIDS Res Hum Retroviruses, 1996. **12**(10): p. 911-24.
106. Yu, X., et al., *Neutralizing antibodies derived from the B cells of 1918 influenza pandemic survivors.* Nature, 2008. **455**(7212): p. 532-6.
107. Tiller, T., et al., *Efficient generation of monoclonal antibodies from single human B cells by single cell RT-PCR and expression vector cloning.* J Immunol Methods, 2008. **329**(1-2): p. 112-24.
108. Smith, K., et al., *Rapid generation of fully human monoclonal antibodies specific to a vaccinating antigen.* Nat Protoc, 2009. **4**(3): p. 372-84.
109. Jiang, N., et al., *Lineage structure of the human antibody repertoire in response to influenza vaccination.* Sci Transl Med, 2013. **5**(171): p. 171ra19.
110. Cheung, W.C., et al., *A proteomics approach for the identification and cloning of monoclonal antibodies from serum.* Nat Biotechnol, 2012. **30**(5): p. 447-52.
111. Wine, Y., et al., *Molecular deconvolution of the monoclonal antibodies that comprise the polyclonal serum response.* Proc Natl Acad Sci U S A, 2013. **110**(8): p. 2993-8.
112. Krause, J.C., et al., *Epitope-specific human influenza antibody repertoires diversify by B cell intraclonal sequence divergence and interclonal convergence.* J Immunol, 2011. **187**(7): p. 3704-11.
113. Poulsen, T.R., et al., *Limits for antibody affinity maturation and repertoire diversification in hypervaccinated humans.* J Immunol, 2011. **187**(8): p. 4229-35.
114. Poulsen, T.R., et al., *Kinetic, affinity, and diversity limits of human polyclonal antibody responses against tetanus toxoid.* J Immunol, 2007. **179**(6): p. 3841-50.
115. Foote, J. and H.N. Eisen, *Kinetic and affinity limits on antibodies produced during immune responses.* Proc Natl Acad Sci U S A, 1995. **92**(5): p. 1254-6.
116. Batista, F.D. and M.S. Neuberger, *Affinity dependence of the B cell response to antigen: a threshold, a ceiling, and the importance of off-rate.* Immunity, 1998. **8**(6): p. 751-9.
117. Meijer, P.J., et al., *Isolation of human antibody repertoires with preservation of the natural heavy and light chain pairing.* J Mol Biol, 2006. **358**(3): p. 764-72.
118. Andersen, P.S., et al., *Extensive restrictions in the VH sequence usage of the human antibody response against the Rhesus D antigen.* Mol Immunol, 2007. **44**(4): p. 412-22.
119. Lauritsen, K.J. and T. Nguyen, *Combination products regulation at the FDA.* Clin Pharmacol Ther, 2009. **85**(5): p. 468-70.
120. Meng, Q., et al., *Domain-based assays of individual antibody concentrations in an oligoclonal combination targeting a single protein.* Anal Biochem, 2012. **421**(2): p. 351-61.
121. Freeberg, J., et al., *Development of a Lyophilized Formulation for Anti-BoNT A Drug Product XOMA 3AB*, in *Interagency Botulism Research Coordinating Committee Meeting* 2010: Atlanta, GA.

122. Rasmussen, S.K., et al., *Recombinant antibody mixtures; optimization of cell line generation and single-batch manufacturing processes.* BMC Proc, 2011. **5 Suppl 8**: p. O2.
123. Wang, X.Z., V.W. Coljee, and J.A. Maynard, *Back to the future: recombinant polyclonal antibody therapeutics.* Curr Opin Chem Eng, 2013. **2**(4): p. 405-415.
124. Kohler, G. and C. Milstein, *Continuous cultures of fused cells secreting antibody of predefined specificity.* Nature, 1975. **256**(5517): p. 495-7.
125. Shankar, G., et al., *Scientific and regulatory considerations on the immunogenicity of biologics.* Trends Biotechnol, 2006. **24**(6): p. 274-80.
126. Boylston, A.W., *Hybridoma technology in the biosciences and medicine by Timothy A. Springer, Plenum Publishing Corporation 1985, US$ 75.00 (xxv + 602 pages) ISBN 0 306 41996 3.* Immunol Today, 1986. **7**(4): p. 120.
127. Rahman, Q.K., et al., *Breaking the non-responsiveness of C57BL/6 mice to the malarial antigen EB200--the role of carrier and adjuvant molecules.* Scand J Immunol, 2003. **58**(4): p. 395-403.
128. Verch, T., V. Yusibov, and H. Koprowski, *Expression and assembly of a full-length monoclonal antibody in plants using a plant virus vector.* J Immunol Methods, 1998. **220**(1-2): p. 69-75.
129. Mazor, Y., et al., *Isolation of engineered, full-length antibodies from libraries expressed in Escherichia coli.* Nat Biotechnol, 2007. **25**(5): p. 563-5.
130. Frenzel, A., M. Hust, and T. Schirrmann, *Expression of recombinant antibodies.* Front Immunol, 2013. **4**: p. 217.
131. Okamoto, T., et al., *Optimal construction of non-immune scFv phage display libraries from mouse bone marrow and spleen established to select specific scFvs efficiently binding to antigen.* Biochem Biophys Res Commun, 2004. **323**(2): p. 583-91.
132. Sidhu, S.S. and F.A. Fellouse, *Synthetic therapeutic antibodies.* Nat Chem Biol, 2006. **2**(12): p. 682-8.
133. Filpula, D., *Antibody engineering and modification technologies.* Biomol Eng, 2007. **24**(2): p. 201-15.
134. Hoogenboom, H.R., *Selecting and screening recombinant antibody libraries.* Nat Biotechnol, 2005. **23**(9): p. 1105-16.
135. Lonberg, N., *Human antibodies from transgenic animals.* Nat Biotechnol, 2005. **23**(9): p. 1117-25.
136. Smith, G.P., *Filamentous fusion phage: novel expression vectors that display cloned antigens on the virion surface.* Science, 1985. **228**(4705): p. 1315-7.
137. McCafferty, J., et al., *Phage antibodies: filamentous phage displaying antibody variable domains.* Nature, 1990. **348**(6301): p. 552-4.
138. Carmen, S. and L. Jermutus, *Concepts in antibody phage display.* Brief Funct Genomic Proteomic, 2002. **1**(2): p. 189-203.
139. Lonberg, N., *Fully human antibodies from transgenic mouse and phage display platforms.* Curr Opin Immunol, 2008. **20**(4): p. 450-9.

140. Paschke, M., *Phage display systems and their applications.* Appl Microbiol Biotechnol, 2006. **70**(1): p. 2-11.
141. Ellgaard, L. and A. Helenius, *Quality control in the endoplasmic reticulum.* Nat Rev Mol Cell Biol, 2003. **4**(3): p. 181-91.
142. Boder, E.T. and K.D. Wittrup, *Yeast surface display for screening combinatorial polypeptide libraries.* Nat Biotechnol, 1997. **15**(6): p. 553-7.
143. Hewlett, E.L., et al., *Extracytoplasmic adenylate cyclase of Bordetella pertussis.* Proc Natl Acad Sci U S A, 1976. **73**(6): p. 1926-30.
144. Hewlett, E.L., et al., *Adenylate cyclase toxin from Bordetella pertussis. Identification and purification of the holotoxin molecule.* J Biol Chem, 1989. **264**(32): p. 19379-84.
145. Eby, J.C., et al., *Quantification of the adenylate cyclase toxin of Bordetella pertussis in vitro and during respiratory infection.* Infect Immun, 2013. **81**(5): p. 1390-8.
146. Betsou, F., P. Sebo, and N. Guiso, *The C-terminal domain is essential for protective activity of the Bordetella pertussis adenylate cyclase-hemolysin.* Infection and immunity, 1995. **63**(9): p. 3309.
147. Lee, S.J., et al., *Epitope mapping of monoclonal antibodies against Bordetella pertussis adenylate cyclase toxin.* Infection and immunity, 1999. **67**(5): p. 2090.
148. Krebber, A., et al., *Reliable cloning of functional antibody variable domains from hybridomas and spleen cell repertoires employing a reengineered phage display system.* J Immunol Methods, 1997. **201**(1): p. 35-55.
149. Hayhurst, A., et al., *Isolation and expression of recombinant antibody fragments to the biological warfare pathogen Brucella melitensis.* J Immunol Methods, 2003. **276**(1-2): p. 185-96.
150. Maynard, J., et al., *High-level bacterial secretion of single-chain alphabeta T-cell receptors.* J Immunol Methods, 2005. **306**(1-2): p. 51-67.
151. Wilkins, M.R., et al., *Protein identification and analysis tools in the ExPASy server.* Methods Mol Biol, 1999. **112**: p. 531-52.
152. Karimova, G. and D. Ladant, *cAMP assays.* CSH Protoc, 2007. **2007**: p. pdb prot4739.
153. Ohmura, N., S.J. Lackie, and H. Saiki, *An immunoassay for small analytes with theoretical detection limits.* Anal Chem, 2001. **73**(14): p. 3392-9.
154. Betsou, F., P. Sebo, and N. Guiso, *CyaC-mediated activation is important not only for toxic but also for protective activities of Bordetella pertussis adenylate cyclase-hemolysin.* Infection and immunity, 1993. **61**(9): p. 3583.
155. Basler, M., et al., *Pore-forming and enzymatic activities of Bordetella pertussis adenylate cyclase toxin synergize in promoting lysis of monocytes.* Infect Immun, 2006. **74**(4): p. 2207-14.
156. Saggy, I., et al., *Antibody isolation from immunized animals: comparison of phage display and antibody discovery via V gene repertoire mining.* Protein Eng Des Sel, 2012. **25**(10): p. 539-49.

157. Rose, T., et al., *Interaction of calcium with Bordetella pertussis adenylate cyclase toxin. Characterization of multiple calcium-binding sites and calcium-induced conformational changes.* J Biol Chem, 1995. **270**(44): p. 26370-6.
158. Hewlett, E.L., et al., *Adenylate cyclase toxin from Bordetella pertussis. Conformational change associated with toxin activity.* J Biol Chem, 1991. **266**(26): p. 17503-8.
159. Gray, M.C., et al., *Translocation-specific conformation of adenylate cyclase toxin from Bordetella pertussis inhibits toxin-mediated hemolysis.* J Bacteriol, 2001. **183**(20): p. 5904-10.
160. Fedele, G., et al., *Lipopolysaccharides from Bordetella pertussis and Bordetella parapertussis differently modulate human dendritic cell functions resulting in divergent prevalence of Th17-polarized responses.* J Immunol, 2008. **181**(1): p. 208-16.
161. Bowley, D.R., et al., *Antigen selection from an HIV-1 immune antibody library displayed on yeast yields many novel antibodies compared to selection from the same library displayed on phage.* Protein Eng Des Sel, 2007. **20**(2): p. 81-90.
162. Bumba, L., et al., *Bordetella adenylate cyclase toxin mobilizes its beta2 integrin receptor into lipid rafts to accomplish translocation across target cell membrane in two steps.* PLoS Pathog, 2010. **6**(5): p. e1000901.
163. Karst, J.C., et al., *Identification of a region that assists membrane insertion and translocation of the catalytic domain of Bordetella pertussis CyaA toxin.* J Biol Chem, 2012. **287**(12): p. 9200-12.
164. Demarest, S.J., et al., *Neutralization of Clostridium difficile toxin A using antibody combinations.* MAbs, 2010. **2**(2): p. 190-8.
165. Chen, Z., et al., *Efficient neutralization of anthrax toxin by chimpanzee monoclonal antibodies against protective antigen.* J Infect Dis, 2006. **193**(5): p. 625-33.
166. Aoki, K.R., L.A. Smith, and M.Z. Atassi, *Mode of action of botulinum neurotoxins: current vaccination strategies and molecular immune recognition.* Crit Rev Immunol, 2010. **30**(2): p. 167-87.
167. Mills, K.H., *Immunity to Bordetella pertussis.* Microbes Infect, 2001. **3**(8): p. 655-77.
168. Hewlett, E.L., et al., *Pertussis pathogenesis--what we know and what we don't know.* J Infect Dis, 2014. **209**(7): p. 982-5.
169. Cherry, J.D., *Pertussis: challenges today and for the future.* PLoS Pathog, 2013. **9**(7): p. e1003418.
170. Smallridge, W.E., et al., *Different effects of whole-cell and acellular vaccines on Bordetella transmission.* J Infect Dis, 2014. **209**(12): p. 1981-8.
171. Guiso, N., M. Szatanik, and M. Rocancourt, *Protective activity of Bordetella adenylate cyclase-hemolysin against bacterial colonization.* Microb Pathog, 1991. **11**(6): p. 423-31.
172. Guiso, N., et al., *Bordetella adenylate cyclase is a virulence associated factor and an immunoprotective antigen.* Microb Pathog, 1989. **7**(5): p. 373-80.

173. Hormozi, K., R. Parton, and J. Coote, *Adjuvant and protective properties of native and recombinant Bordetella pertussis adenylate cyclase toxin preparations in mice.* FEMS Immunol Med Microbiol, 1999. **23**(4): p. 273-82.
174. Ross, P.J., et al., *Adenylate cyclase toxin from Bordetella pertussis synergizes with lipopolysaccharide to promote innate interleukin-10 production and enhances the induction of Th2 and regulatory T cells.* Infect Immun, 2004. **72**(3): p. 1568-79.
175. Mountzouros, K.T., A. Kimura, and J.L. Cowell, *A bactericidal monoclonal antibody specific for the lipooligosaccharide of Bordetella pertussis reduces colonization of the respiratory tract of mice after aerosol infection with B. pertussis.* Infect Immun, 1992. **60**(12): p. 5316-8.
176. Shahin, R.D., et al., *Analysis of protective and nonprotective monoclonal antibodies specific for Bordetella pertussis lipooligosaccharide.* Infect Immun, 1994. **62**(2): p. 722-5.
177. Cheung, G.Y., et al., *Effect of different forms of adenylate cyclase toxin of Bordetella pertussis on protection afforded by an acellular pertussis vaccine in a murine model.* Infect Immun, 2006. **74**(12): p. 6797-805.
178. Betsou, F., P. Sebo, and N. Guiso, *The C-terminal domain is essential for protective activity of the Bordetella pertussis adenylate cyclase-hemolysin.* Infect Immun, 1995. **63**(9): p. 3309-15.
179. Goyard, S., et al., *Identification of a common domain in calmodulin-activated eukaryotic and bacterial adenylate cyclases.* Biochemistry, 1989. **28**(5): p. 1964-7.
180. Monneron, A., et al., *Immunological relatedness between Bordetella pertussis and rat brain adenylyl cyclases.* Biochemistry, 1988. **27**(2): p. 536-9.
181. Gallay, J., et al., *Insight into the activation mechanism of Bordetella pertussis adenylate cyclase by calmodulin using fluorescence spectroscopy.* European Journal of Biochemistry, 2004. **271**(4): p. 821-833.
182. Powthongchin, B. and C. Angsuthanasombat, *High level of soluble expression in Escherichia coli and characterisation of the CyaA pore-forming fragment from a Bordetella pertussis Thai clinical isolate.* Arch Microbiol, 2008. **189**(2): p. 169-74.
183. Pojanapotha, P., et al., *Bordetella pertussis CyaA-RTX subdomain requires calcium ions for structural stability against proteolytic degradation.* Protein Expr Purif, 2011. **75**(2): p. 127-32.
184. Blenner, M.A., et al., *Calcium-induced folding of a beta roll motif requires C-terminal entropic stabilization.* J Mol Biol, 2010. **400**(2): p. 244-56.
185. Karst, J.C., et al., *Calcium, acylation and molecular confinement favor folding of Bordetella pertussis adenylate cyclase CyaA toxin into a monomeric and cytotoxic form.* J Biol Chem, 2014.
186. Bauche, C., et al., *Structural and functional characterization of an essential RTX subdomain of Bordetella pertussis adenylate cyclase toxin.* J Biol Chem, 2006. **281**(25): p. 16914-26.

187. Chenal, A., et al., *RTX calcium binding motifs are intrinsically disordered in the absence of calcium: implication for protein secretion.* J Biol Chem, 2009. **284**(3): p. 1781-9.
188. Masin, J., et al., *Acylation of lysine 860 allows tight binding and cytotoxicity of Bordetella adenylate cyclase on CD11b-expressing cells.* Biochemistry, 2005. **44**(38): p. 12759-66.
189. Cheung, G.Y.C., et al., *Effect of different forms of adenylate cyclase toxin of Bordetella pertussis on protection afforded by an acellular pertussis vaccine in a murine model.* Infection and immunity, 2006. **74**(12): p. 6797.
190. Goldstein, D.A., *Serum Calcium.* Clinical Methods: The History, Physical, and Laboratory Examinations. 3rd edition. Boston: Butterworths, 1990.
191. Sutherland, J.N., et al., *Antibodies recognizing protective pertussis toxin epitopes are preferentially elicited by natural infection versus acellular immunization.* Clin Vaccine Immunol, 2011. **18**(6): p. 954-62.
192. Witt, M.A., et al., *Reduced risk of pertussis among persons ever vaccinated with whole cell pertussis vaccine compared to recipients of acellular pertussis vaccines in a large US cohort.* Clin Infect Dis, 2013. **56**(9): p. 1248-54.
193. Watanabe, M., B. Connelly, and A.A. Weiss, *Characterization of serological responses to pertussis.* Clin Vaccine Immunol, 2006. **13**(3): p. 341-8.
194. Brézin, C., et al., *Protective effects of anti-Bordetella pertussis adenylate cyclase antibodies against lethal respiratory infection of the mouse.* FEMS Microbiology Letters, 1987. **42**(1): p. 75-80.
195. Confer, D.L. and J.W. Eaton, *Phagocyte impotence caused by an invasive bacterial adenylate cyclase.* Science, 1982. **217**(4563): p. 948-50.
196. Weingart, C.L., et al., *Neutralizing antibodies to adenylate cyclase toxin promote phagocytosis of Bordetella pertussis by human neutrophils.* Infection and immunity, 2000. **68**(12): p. 7152.
197. Weingart, C.L. and A.A. Weiss, *Bordetella pertussis virulence factors affect phagocytosis by human neutrophils.* Infection and immunity, 2000. **68**(3): p. 1735.
198. Eby, J.C., et al., *Role of CD11b/CD18 in the process of intoxication by the adenylate cyclase toxin of Bordetella pertussis.* Infect Immun, 2012. **80**(2): p. 850-9.
199. Gueirard, P. and N. Guiso, *Virulence of Bordetella bronchiseptica: role of adenylate cyclase-hemolysin.* Infect Immun, 1993. **61**(10): p. 4072-8.
200. Khelef, N., et al., *Bordetella pertussis and Bordetella parapertussis: two immunologically distinct species.* Infect Immun, 1993. **61**(2): p. 486-90.
201. Angkawidjaja, C., et al., *Crystal structure of a family I.3 lipase from Pseudomonas sp. MIS38 in a closed conformation.* FEBS Lett, 2007. **581**(26): p. 5060-4.
202. Lupardus, P.J., et al., *Small molecule-induced allosteric activation of the Vibrio cholerae RTX cysteine protease domain.* Science, 2008. **322**(5899): p. 265-8.

203. John M. Walker, R.R., *Molecular Biomethods Handbook. 2nd Ed.* 2008: p. 683-696.
204. Rosen, O. and J. Anglister, *Epitope Mapping of Antibody–Antigen Complexes by Nuclear Magnetic Resonance Spectroscopy*, in *Epitope Mapping Protocols*, M. Schutkowski and U. Reineke, Editors. 2009, Humana Press. p. 37-57.
205. Hoofnagle, A.N., K.A. Resing, and N.G. Ahn, *Protein analysis by hydrogen exchange mass spectrometry.* Annu Rev Biophys Biomol Struct, 2003. **32**: p. 1-25.
206. Hilpert, K., D.F. Winkler, and R.E. Hancock, *Peptide arrays on cellulose support: SPOT synthesis, a time and cost efficient method for synthesis of large numbers of peptides in a parallel and addressable fashion.* Nat Protoc, 2007. **2**(6): p. 1333-49.
207. Irving, M.B., O. Pan, and J.K. Scott, *Random-peptide libraries and antigen-fragment libraries for epitope mapping and the development of vaccines and diagnostics.* Curr Opin Chem Biol, 2001. **5**(3): p. 314-24.
208. Weiss, G.A., et al., *Rapid mapping of protein functional epitopes by combinatorial alanine scanning.* Proc Natl Acad Sci U S A, 2000. **97**(16): p. 8950-4.
209. Cochran, J.R., et al., *Domain-level antibody epitope mapping through yeast surface display of epidermal growth factor receptor fragments.* J Immunol Methods, 2004. **287**(1-2): p. 147-58.
210. Levy, R., et al., *Fine and domain-level epitope mapping of botulinum neurotoxin type A neutralizing antibodies by yeast surface display.* J Mol Biol, 2007. **365**(1): p. 196-210.
211. Doolan, K.M. and D.W. Colby, *Conformation-dependent epitopes recognized by prion protein antibodies probed using mutational scanning and deep sequencing.* J Mol Biol, 2015. **427**(2): p. 328-40.
212. Van Blarcom, T., et al., *Precise and efficient antibody epitope determination through library design, yeast display and next-generation sequencing.* J Mol Biol, 2015. **427**(6 Pt B): p. 1513-34.
213. Benatuil, L., et al., *An improved yeast transformation method for the generation of very large human antibody libraries.* Protein Eng Des Sel, 2010. **23**(4): p. 155-9.
214. Podnar, J., H. Deiderick, and S. Hunicke-Smith, *Next-generation sequencing fragment library construction.* Curr Protoc Mol Biol, 2014. **107**: p. 7 17 1-7 17 16.
215. Kondo, A. and M. Ueda, *Yeast cell-surface display--applications of molecular display.* Appl Microbiol Biotechnol, 2004. **64**(1): p. 28-40.
216. Chao, G., J.R. Cochran, and K.D. Wittrup, *Fine epitope mapping of anti-epidermal growth factor receptor antibodies through random mutagenesis and yeast surface display.* J Mol Biol, 2004. **342**(2): p. 539-50.
217. Scarselli, M., et al., *Rational design of a meningococcal antigen inducing broad protective immunity.* Sci Transl Med, 2011. **3**(91): p. 91ra62.

218. McLellan, J.S., et al., *Structure-based design of a fusion glycoprotein vaccine for respiratory syncytial virus.* Science, 2013. **342**(6158): p. 592-8.